2016

Real and Reactive Power Control of Induction Motor Drives

Juan Rafael Nunez
Louisiana State University and Agricultural and Mechanical College

REAL AND REACTIVE POWER CONTROL OF INDUCTION MOTOR DRIVES

A Thesis

Submitted to the Graduate Faculty of the
Louisiana State University and
Agricultural and Mechanical College
in partial fulfillment of the
requirements for the degree of
Master of Science in Electrical Engineering

in

The Department of Electrical & Computer Engineering

by
Juan Rafael Nunez Forestieri
B.S., Escuela Superior Politecnica del Litoral, 2004
December 2016

ACKNOWLEDGEMENTS

First and foremost, I would like to thank God for providing me with the strength and spiritual perseverance to complete this work.

I would like to express my gratitude to Dr. Mehdi Farasat for his guidance and patience. His valuable advice and support throughout my research enriched my knowledge and enhanced my scientific motivation.

I am deeply indebted to my committee members, Dr. Shahab Mehraeen and Dr. Guoxiang Gu. I would like to express my thankfulness to them for their comments and support for my dissertation. I would also like to acknowledge the faculty and staff of the School of Electrical Engineering, with special recognition to Beth Cochran for her continuous support since the first day I enrolled as a graduate student.

My love and sincere appreciation to my parents, I owe them much more than a few lines can express. Thanks to my sister and her little angel Rafaella, for their perfectly timed distractions. I would like to thank my family for their priceless words of support, in especial to my uncle Daniel.

I dedicate this dissertation to my parents, Rafael and Pilar, who are
the heart and soul of my being. God will do the miracle mother,
soon.

TABLE OF CONTENTS

LIST OF TABLES

LIST OF FIGURES

ABSTRACT

Induction motors are considered the workhorse in the majority of industrial applications. Their rugged, low-maintenance, and efficient designs keep finding new forms of use nowadays.

In this work, power control strategies of induction motor drives based on principles of Direct Torque Control and Model Predictive Control are investigated. The proposed methods control the real and reactive power flow into/out of the machine by selecting and applying proper voltage space phasors to the stator. First, the impact of voltage space phasors on real and reactive power variations is explored. Based on these observations, two methods to choose the appropriate voltage space phasors are proposed based on: six-sector and twelve-sector direct power control, and model predictive power control. Methods to calculate reference and motor powers are then introduced. The presence of high currents during the motor start-up period is analyzed and solutions to limit them are proposed. Finally, simulations using ®Matlab ™Simulink are carried out to test the performance of the control strategies under different operating conditions, including presence of motor parameter variations.

CHAPTER 1:
INTRODUCTION

In the past, DC machines were the preferred choice for variable speed drives. Nevertheless, these types of machines have some disadvantages when compared with induction motors (IM). Among the disadvantages are: high maintenance costs and difficulty to operate in dusty and explosive environments. With the advances in the field of power electronics switching devices, and development of low cost microprocessors in recent decades, producing economical and efficient variable frequency power sources has become possible. As a consequence, DC drives have been progressively replaced by AC machines equipped with AC drives.

Nowadays, many industrial applications not only require operation at wide speed ranges, but demand precise control of torque and position, with fast response and acceptable dynamic performance. Some applications even require operation with different types of loads. Majority of these requirements can be met with different configurations of AC drives. In Fig 1.1, a classification of induction motor strategies methods is shown [17].

The most simple variable frequency control method is scalar based. In this method the stator voltage (or current) and frequency are the parameters to be adjusted. The steady-state characteristics of the machine are employed in the control scheme to set the stator flux magnitude for different speed and torque set points. Since this method does not offer good dynamic performance, it is mainly used in applications where fast changes in the speed and torque are not important. Such applications include pumps, blowers, or fans [16]-[17]. In applications where accurate control of the torque developed by the motor is required, high-

performance control strategies (vector based) are the preferred alternative. Among the well-known vector based control techniques are Field-Oriented Control and Direct Torque Control.

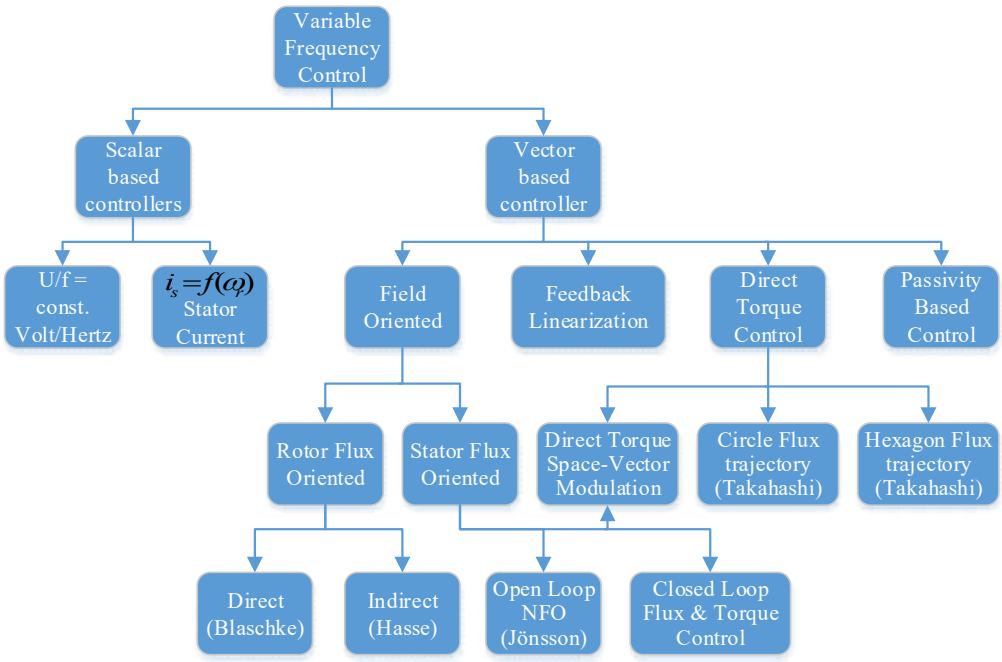

Figure 1.1 General Classification of IM control strategies.

Fiel-Oriented Control (FOC) of IM was developed in the late 60's by Hasse and early 70's by Blaschke, independetly from each other [3]. The main idea of FOC is to make the IM imitate the separately excited DC machine in the sense of variable torque source [16]. To achieve this goal, the machine equations are transformed to a reference frame rotating in synchronism with the rotor flux (Rotor Flux Oriented) and the stator current is decomposed into two components: the *flux-current* (direct-axis) and the *torque-current* (quadrature-axis). The flux-current, and as a consequence, the rotor flux is kept constant at their rated values, while the torque is adjusted by means of the torque-current. Since the introduction of FOC, it has been subject to numerous studies and refinements, especially with regards to improving the robustness

of this method agaisnt motor parameters variations. FOC has acceptable dynamic performance and has become an industry standard.

Direct Torque Control (DTC) of IM was introduced by Depenbrock, and Takahashi and Noguchi in the early 80's [3]. The principle of DTC considers that the magnitude of the stator flux and torque can be varied by choosing the appropiate voltage space phasor generated by an inverter. The magnitude and position of the stator flux phasor can be obtained by integrating the stator voltage phasor. Depending on the required changes on flux and torque magnitudes, the proper voltage phasor is selected using an optimal switching table [11]. DTC is considered a simple control method with fast response to load torque changes, and in constrant with FOC, DTC has low sensitivity to parameter variations. Due to its simplicity and robustness, DTC is considered a promising alternative to FOC.

In recent years, with the production of more powerful and fast microprocessors the idea of Model Predictive Control (MPC), which was introduced in the 1960s, has been applied to high-performance AC motor drives. MPC uses a model of the system to be controlled, here the model of induction motor, to pre-calculate the future values of the model states, and these predictions are then evaluated through a cost function. The sequence (switching states of the inverter) that minimizes the cost function is then used to determine the optimal future control actions. This strategy is considered simple and intuitive. Non-linearites and hard constrains can be included in the MPC control scheme [10]. Among the control strategies of IM implemented based on model predictive concepts is Model Predictive Torque Control (MPTC), which features fast dynamic response. In MPTC the same idea of DTC is employed. However, the voltage phasors are not selected from a switching table, rather a switching sequence, hence a voltage phasor that minimizes the cost function is selected and applied.

In this thesis, two high-performance induction motor control strategies, i.e direct power control and model predictive power control are presented. In constrast to their classical counterpart techniques, DTC and MPTC, where the controlled variables are stator flux and electromagnetic torque, the real and reactive power absorbed by the motor are controlled here.

In the following chapter, the models of the induction machine and the voltage source inverter are introduced. These two elements are pilars to develop the analysis throughout this work. Chapter 3 presents the concepts on which classical DTC and MPTC are based. These ideas are employed to develop the principles of the proposed control strategies. The first section of chapter 4 deals with the concepts regarding the control of real and reactive power injected/absorbed by the stator of the induction motor. Later discussion will be devoted to analysis of real and reactive power variations with respect to the applied stator voltage space phasors. Based on these studies, equations employed in the proposed control strategy are derived. Finally, the structure of the control method and a current limitation technique during the start-up period of the motor is developed. In the second section of chapter 4, stator real and reactive power flow control based on model predictive control principle is discussed. As MPC offers the possibility of including constraints in the cost function, current limitation during the start-up period of the motor becomes feasible. In chapter 5, the performance and robustness of the proposed control strategies against motor parameter variations are studied. Several simulations with accurate and erroneous knowledge of motor parameters are carried out based on the presented methods in chapter 4. Conclusions and future study plans ate provided in Chapter 6.

CHAPTER 2:
MODELING OF INDUCTION MOTOR AND VOLTAGE SOURCE INVERTER

2.1 Dynamic Model of Induction Motor

The dynamic behavior of an induction motor is traditionally represented by a set of equations expressed in a system of orthogonal axis, or *qd0* axis [5]. In this system, all three-phase variables (voltages, currents, flux linkages, etc.) corresponding to each of the machine windings are transformed to a reference frame ("fictitious windings") rotating at an arbitrary angular speed, ω. A scheme of this transformation is shown in Fig. 2.1. The angular displacement, θ, and the angular speed, ω, of the reference frame are related according to equation (2.1).

$$\omega = \frac{d\theta}{dt} \tag{2.1}$$

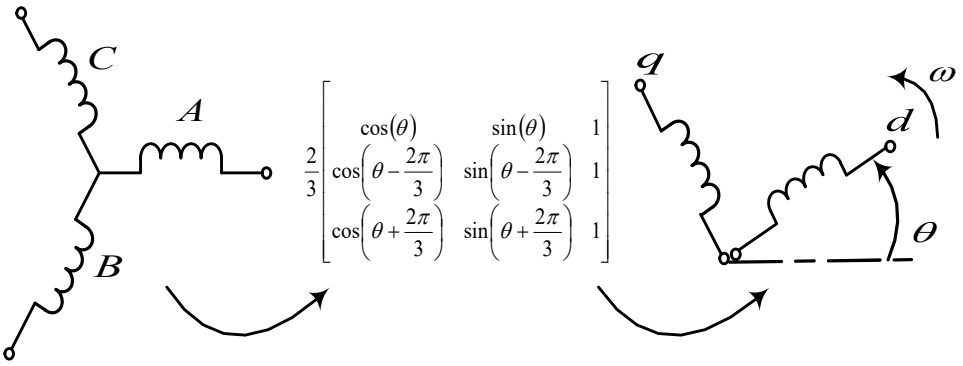

Figure 2.1 ABC to qd0 transformation scheme.

Assumptions made in deriving the state equations of IM are as follows [3]:

- Each phase winding of the machine, stator and rotor, generate a sinusoidal magneto-motive force in space, all with the same wave length. This means that only the fundamental waves are considered and harmonics of higher orders are neglected.
- A constant air-gap along the circumference of the motor is present, and as a consequence the machine is magnetically symmetric.
- Saturation of the magnetic circuits is not considered.
- The power source delivers three-phase balanced voltages, and as a result the zero voltages, currents and flux linkages are set equal to zero.
- The rotor of the motor is of the squirrel-cage type, thus the rotor voltages are set to zero.

The stator and rotor voltage equations written in terms of *qd0* components in the stationary reference frame, ω=0, are as following [1]:

$$v_{qs}^{s} = R_s i_{qs}^{s} + p\lambda_{qs}^{s} \tag{2.2}$$

$$v_{ds}^{s} = R_s i_{ds}^{s} + p\lambda_{ds}^{s} \tag{2.3}$$

$$v_{0s} = R_s i_{0s} + p\lambda_{0s} \tag{2.4}$$

$$0 = R'_r i'^{s}_{qr} - \omega_r \lambda'^{s}_{dr} + p\lambda'^{s}_{qr} \tag{2.5}$$

$$0 = R'_r i'^{s}_{dr} + \omega_r \lambda'^{s}_{qr} + p\lambda'^{s}_{dr} \tag{2.6}$$

$$0 = R'_r i'_{0r} + p\lambda'_{0r} \tag{2.7}$$

D-Q flux linkage equations and electromagnetic torque are expressed as follows:

$$\lambda_{qs}^{s} = L_{ls} i_{qs}^{s} + L_m\left(i_{qs}^{s} + i'^{s}_{qr}\right) \tag{2.8}$$

$$\lambda_{ds}^{s} = L_{ls} i_{ds}^{s} + L_m(i_{ds}^{s} + i'^{s}_{dr}) \tag{2.9}$$

$$\lambda_{0s} = L_{ls} i_{0s} \tag{2.10}$$

$$\lambda'^{s}_{qr} = L'_{lr} i'^{s}_{qr} + L_m\left(i_{qs}^{s} + i'^{s}_{qr}\right) \tag{2.11}$$

$$\lambda'^{s}_{dr} = L'_{lr} i'^{s}_{dr} + L_m (i^{s}_{ds} + i'^{s}_{dr}) \tag{2.12}$$

$$\lambda'_{0r} = L'_{lr} i'_{0r} \tag{2.13}$$

$$T_e = \frac{3}{2}\frac{P}{2}\left(\lambda^{s}_{ds} i^{s}_{qs} - \lambda^{s}_{qs} i^{s}_{ds}\right) \tag{2.14}$$

$$T_e = J\frac{2}{P} p\omega_r + T_L \tag{2.15}$$

In the above equations, v^{s}_{qs}, i^{s}_{qs}, λ^{s}_{qs}, and v^{s}_{ds}, i^{s}_{ds}, λ^{s}_{ds} represent the q-d voltages, currents and flux-linkages of the stator. v'^{s}_{qr}, i'^{s}_{qr}, λ'^{s}_{qr}, and v'^{s}_{dr}, i'^{s}_{dr}, λ'^{s}_{dr} are the q-d voltages, currents and flux-linkages of the rotor referred to the stator. R_s, L_{ls}, R'_r, L'_{lr}, L_m are the resistance and leakage inductance of the stator, resistance and leakage inductance of the rotor referred to the stator, and the magnetizing inductance, respectively. T_e and P represent the electromagnetic torque and the number of poles of the motor. $v_{0s}, i_{0s}, \lambda_{0s}$, and v'_{0r}, i'_{0r}, λ'_{0r} are the stator and rotor zero voltages, currents, and flux-linkages, respectively. p represents $\frac{d}{dt}$, ω_r the rotor speed, J the inertia of both the motor and the load, and T_L is the torque of the load connected to the shaft of the motor.

To simplify the analysis presented in the following chapters, the Space Phasor model of the induction motor in the stationary reference frame is generated from the *qd0* model, since it is based on the same assumptions. For the Space Phasor model the following equations are considered for the stator and rotor windings [4]:

$$\boldsymbol{V}^{s}_{s} = v^{s}_{ds} + j v^{s}_{qs} \tag{2.16}$$

$$\boldsymbol{I}^{s}_{s} = i^{s}_{ds} + j i^{s}_{qs} \tag{2.17}$$

$$\boldsymbol{\lambda}^{s}_{s} = \lambda^{s}_{ds} + j\lambda^{s}_{qs} \tag{2.18}$$

$$\boldsymbol{I}'^{s}_{r} = i'^{s}_{dr} + j i'^{s}_{qr} \tag{2.19}$$

$$\boldsymbol{\lambda}'^{s}_{r} = \lambda'^{s}_{dr} + j\lambda'^{s}_{qr} \tag{2.20}$$

In the above equations, $\boldsymbol{V}_s^s$, $\boldsymbol{I}_s^s$, $\boldsymbol{\lambda}_s^s$, $\mathbf{I'}_\mathrm{r}^s$, $\boldsymbol{\lambda}_\mathrm{r}^{\prime s}$ are space phasors of stator and rotor voltages, currents, and flux-linkages. As an example, assuming phase A in the stator axis as the reference, $\boldsymbol{\lambda}_s^s$ can be interpreted as a space phasor that rotates at a speed ω, and its amplitude represents the peak of the field distribution. Figure 2.2 depicts the description given for $\boldsymbol{\lambda}_s^s$ in the stationary reference frame. In the figure ω_e is the angular frequency of the source.

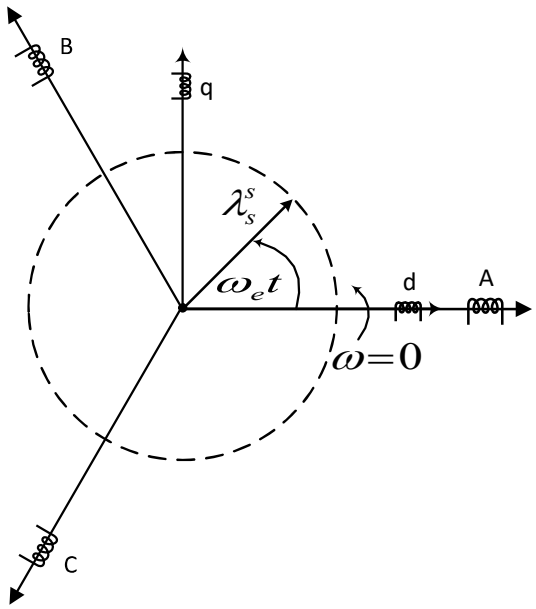

Figure 2.2 Flux linkage space phasor representation.

Based on the expressions (2.2)-(2.14) and (2.16)-(2.20), the voltages, flux-linkages, and torque equations of the induction motor in the stationary reference frame can be written as follows [4]:

$$\boldsymbol{V}_s^s = R_s \boldsymbol{I}_s^s + p\boldsymbol{\lambda}_s^s \tag{2.21}$$

$$0 = R_r \boldsymbol{I}_r^{\prime s} + p\boldsymbol{\lambda}_r^{\prime s} - j\omega_r \boldsymbol{\lambda}_r^{\prime s} \tag{2.22}$$

$$\boldsymbol{\lambda}_s^s = L_s \boldsymbol{I}_s^s + L_m \boldsymbol{I}_r^{\prime s} \tag{2.23}$$

$$\boldsymbol{\lambda}_r^{\prime s} = L_r' \boldsymbol{I}'^s_r + L_m \boldsymbol{I}_s^s \tag{2.24}$$

$$T_e = \frac{3}{2}\frac{P}{2}\frac{L_m}{L_s L_r'}(\boldsymbol{\lambda}_r'^s \times \boldsymbol{\lambda}_s^s) \tag{2.25}$$

where $L_s = L_{ls} + L_m$ and $L_r' = L_{lr}' + L_m$. The "×" in (2.25) represents the cross product of the stator and rotor flux linkage phasors.

The equivalent circuit of the induction motor based on equations (2.21)-(2.25) is drawn and shown in Fig. 2.3.

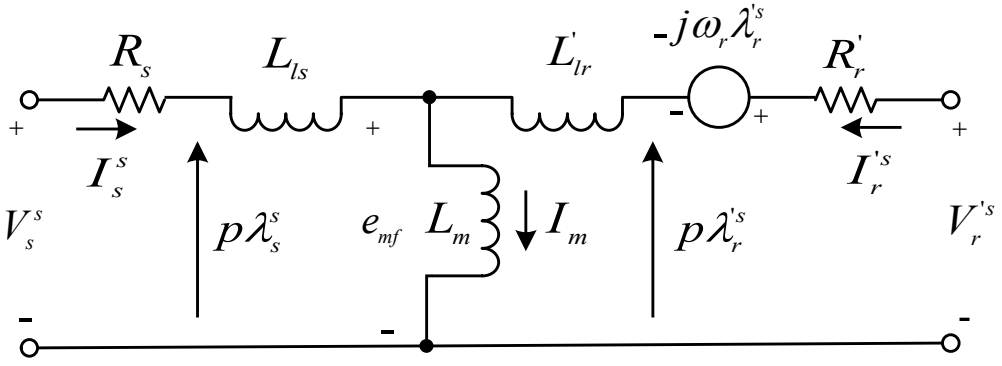

Figure 2.3 Induction Motor equivalent circuit in the stationary reference frame.

2.2 Voltage Source Inverter Model

The voltage source inverter (VSI) that will be considered in this work is a generic three-phase two level type, which can generate six active switches. Topology of the inverter is shown in Fig. 2.4. The inverter uses either MOSFETs (low-power applications) or IGBTs (medium- and large-power) as the switching devices. Anti-parallel diodes offer freewheel paths that are required when the load is inductive. The inverter is supplied from a DC-link capacitor whose voltage is regulated by a front-end rectifier [6].

It is possible to visualize each inverter-leg having two ideal ON/OFF switches which cannot be turned on at the same time. Furthermore, making the restriction that each phase of the

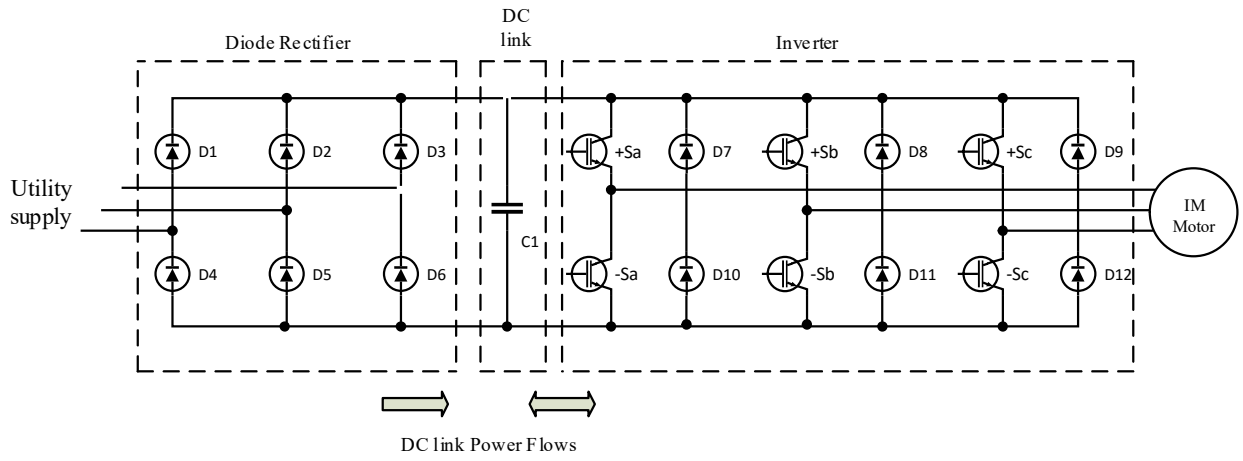

Figure 2.4 Basic arrangement of an IM drive.

load must always be either connected to the positive or negative terminal of the DC-link, there will be only eight possible combinations of the states of the switches. These states correspond to a set of space voltage phasors, six of which are non-zero or active and two are zero. The set of space phasors is defined in equation 2.26, where V_{dc} is the DC-link voltage [2].

$$V_k = \begin{cases} \frac{2}{3} V_{dc} e^{j(k-1)\pi/3} & k = 1,2,\dots,6 \\ 0 & k = 7,8 \end{cases} \tag{2.26}$$

The voltage space phasors are shown in Fig. 2.5.

In chapters 3 and 4 direct torque control, model predictive torque control, and real and reactive power control strategies are discussed. Information presented in this chapter is employed in explaining the principles of the aforementioned control methods.

It is important to point out that the stationary reference frame will be used throughout this work. In addition, the motor will be considered to operate within the constant torque region.

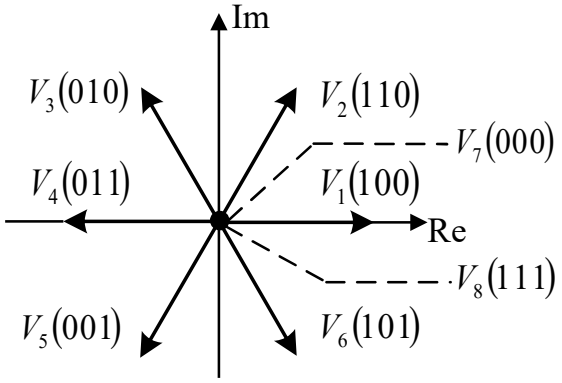

Figure 2.5 Inverter output voltages represented as space phasors.

CHAPTER 3:
DIRECT TORQUE CONTROL AND MODEL PREDICTIVE TORQUE CONTROL OF INDUCTION MOTORS

3.1 Direct Torque Control

Direct Torque Control (DTC) is one of the well-known high-performance induction motor (and other AC motors) control strategies. In this control strategy, the stator flux-linkage and the electromagnetic torque of an induction motor fed by a voltage source inverter are controlled indirectly by selecting and applying voltage phasors determined from a predefined switching table. The purpose in DTC is to keep flux and torque errors within preset hysteresis bands, generate fast torque response, and keep the switching and harmonic losses as low as possible [2].

The electromagnetic torque developed by a symmetrical induction machine in space phasor form is given by equation (2.25). If this expression is further expanded using the definition of vector cross product, then the electromagnetic torque can be expressed as in (3.1), where $|\boldsymbol{\lambda}_s^s|$, $|\boldsymbol{\lambda}_r'^s|$, and ρ are the magnitude of the stator flux-linkage space phasor, rotor flux-linkage space phasor, and the angle between these two space phasors, respectively.

$$T_e = \frac{3}{2}\frac{P}{2}\frac{L_m}{L_s L_r'}|\boldsymbol{\lambda}_r'^s||\boldsymbol{\lambda}_s^s|\, si \tag{3.1}$$

From (3.1) it can be notice that the torque is a function of the amplitudes of the rotor flux-linkage space phasor, stator flux-linkage space phasor, and the phase displacement between them. Assuming that it is possible to keep the magnitudes of the stator and rotor flux linkages constant (typically at their rated values), it follows from (3.1) that fast torque changes can be obtained by adjusting the angle ρ according to the required direction accordingly [2].

If the voltage drop across the stator resistance is neglected in (2.21), the stator voltage space phasor can be written as:

$$\boldsymbol{V}_s^s = p\boldsymbol{\lambda}_s^s \tag{3.2}$$

For very short sampling periods of time, Δt, it is possible to compute the change in the stator flux-linkage space phasor, $\Delta\boldsymbol{\lambda}_s^s$, from (3.2). The stator flux-linkage space phasor within the sampling period is given by:

$$\Delta\boldsymbol{\lambda}_s^s = \boldsymbol{V}_s^s \Delta t \tag{3.3}$$

In other words, (3.3) implies that it is possible to change the magnitude and position of the stator flux-linkage by applying any of the six active voltage space phasors for Δt period of time.

The rotor time-constant, L_r/R_r, of a typical small induction motor can have a value around 0.25 s. For larger motors this constant can be even larger [6]. Therefore, it is reasonable to assume that the rotor flux-linkage changes slowly compared to the stator flux-linkage. Consequently the rotor flux-linkage can be assumed constant during the sampling period. By controlling the magnitude and position of the stator flux-linkage, and with the magnitude of the rotor flux-linkage constant, it is possible to control fast torque changes [2]. Figure 3.1 shows how the magnitude and position of the stator flux-linkage, and as a consequence the electromagnetic torque, can be controlled.

In Fig 3.1 it is assumed that a reduction in the electromagnetic torque and a reduction in the stator flux linkage magnitude are required to keep both values within the bands of the hysteresis controllers. Therefore, an appropriate voltage phasor should be selected and applied within the sample time to produce the desired changes. In order to determine the required active space phasor, the *q*-*d* plane is dived into six sectors (60 degrees each). Any of the zero voltage

phasors will keep the magnitude and position of the stator flux-linkage voltage phasor almost constant, and a reduction in the torque will be achieved (ρ will decrease). In the case of Fig 3.1, the original $\boldsymbol{\lambda}_s$ is assumed to be located in sector 1, thus the best alternative to reduce both the magnitude of $\boldsymbol{\lambda}_s$, and the angle between $\boldsymbol{\lambda}_s$ and $\boldsymbol{\lambda}_r$ (as a consequence a torque reduction) is applying voltage space phasor $\boldsymbol{V}_5$ ($\boldsymbol{\lambda}_5 = \boldsymbol{V}_5 \Delta t$ as in the figure). A block diagram of a typical inverter-fed induction machine with DTC is shown in Fig 3.2, and the optimal switching table is provided in Table 3.1.

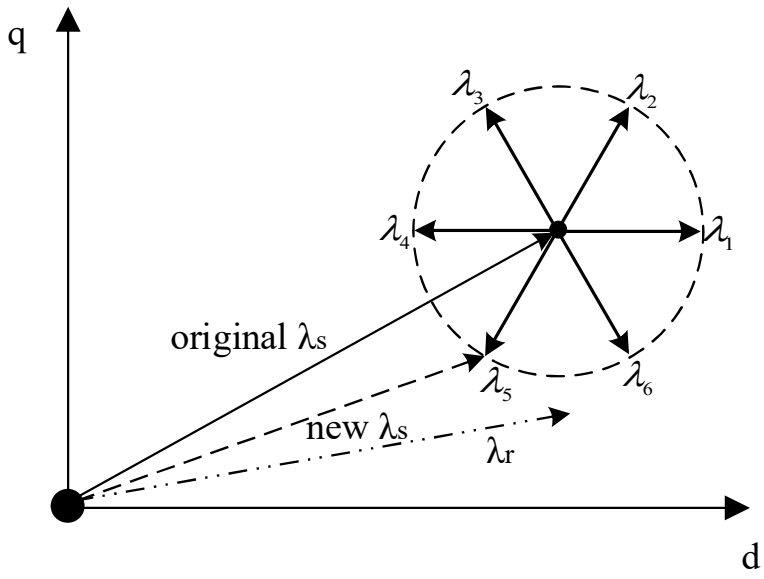

Figure 3.1 Control of stator flux-linkage space phasor by applying stator voltage space phasors [6].

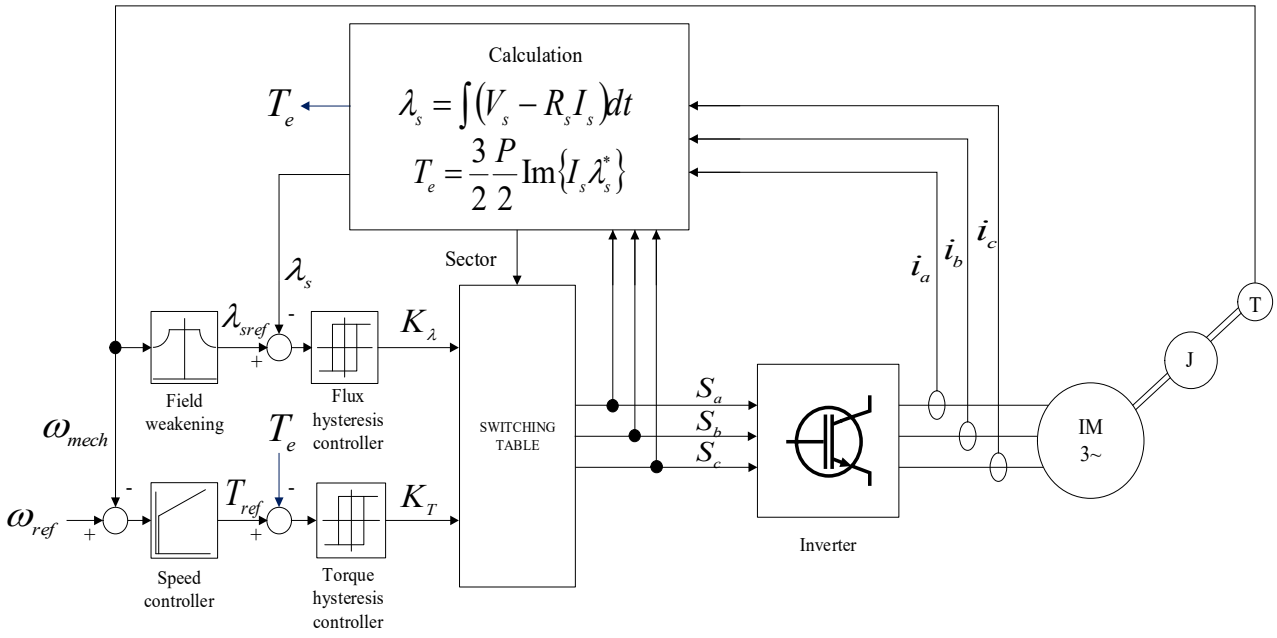

Figure 3.2 Block diagram of DTC scheme [3].

Table 3.1 DTC Optimal switching table [2].

K_T	$K\lambda$	Sector 1	Sector 2	Sector 3	Sector 4	Sector 5	Sector 6
1	1	V_2	V_3	V_4	V_5	V_6	V_1
	0	V_7	V_8	V_7	V_8	V_7	V_8
	-1	V_6	V_1	V_2	V_3	V_4	V_5
0	1	V_3	V_4	V_5	V_6	V_1	V_2
	0	V_8	V_7	V_8	V_7	V_8	V_7
	-1	V_5	V_6	V_1	V_2	V_3	V_4

3.2 Model Predictive Control (MPC)

Predictive control employs a model of the system to predict the future behavior of the system. The predicted information is used by the controller to determine the optimal future control actions that minimize an appropriate cost function [7]-[10].

Predictive control contemplates a wide spectrum of controllers, such as: deadbeat, hysteresis based, trajectory based, and model predictive, which can be further divided into MPC with continuous control set and MPC with finite control set [10]. In this work, MPC with finite control set is considered and adopted to induction motor drives.

The idea of MPC, which is based on optimal control theory, was conceived in the 1960s. Due to the high number of mathematical calculations required for the prediction and optimization of system behavior, MPC was only applied in process engineering (late 1970s) where the time constants are long enough to allow the required computations. Application of MPC in power electronics and drives has gained interest of researchers in the last decade with the evolution of powerful and fast microprocessors [8]-[10].

In MPC, the future behavior of the system variables is predicted over a time horizon using a system model. The predictions are then assessed based on a cost function, and the optimal future control actions that minimized the cost function are determined. This process (pre-calculation, optimization, and control) is repeated at each sample time [7].

Generally, the control objectives determine the form of the cost function [8]. A simple cost function can be defined as the error between the predicted and reference values of a controlled variable, such as torque, flux, power, current, and etc. It is noteworthy to mention that MPC is not restricted to a single variable. Multiple variables, perturbations, saturations, system

constrains, among others, can be considered in the predictive model and cost function. Suitable weighted factors can be employed to aggregate multiple variables in the cost function. Advantages of MPC over classical control methods, such as the linear control scheme in which the cascade structure is used, are [10]:

- Easy implementation,
- Non-linearities can be considered and included in the model,
- Adjustments for dead times can be achieved,
- Constrains can be treated in a simple manner,
- Not limited to single controlled variables,
- Can be applied to a wide variety of systems.

Some drawbacks of MPC are [10]:

- Higher number of computations in comparison to classic controllers.
- Adaptive algorithms have to be considered if the parameters of the system are subject to variations in time.

Model of the system used to predict its future behavior needs to be defined prior to any computations. A linear system can be expressed by a state space model. Given the discrete-time nature of MPC, a discrete-time state-model should be selected as follows:

$$\boldsymbol{x}[k+1] = A\boldsymbol{x}[k] + B\boldsymbol{u}[k] \tag{3.4}$$

$$\boldsymbol{y}[k] = C\boldsymbol{x}[k] + D\boldsymbol{u}[k] \tag{3.5}$$

Since the system model in this work (inverter/induction motor) is first-order, all the derivatives will be approximated using a simple numerical approach called Euler's forward method:

$$\frac{\boldsymbol{dx}}{\boldsymbol{dt}} = \frac{\boldsymbol{x}[k+1]-\boldsymbol{x}[k]}{T_S} \tag{3.6}$$

In addition to model of the system, a cost function should be defined as well. Generally, this function is dependent on the target reference and predicted controlled variables, that is [7]:

$$g_i = f\{x^*[k], x_{pi}[k+1]\} \quad \text{for } i = 1,2,\ldots n. \tag{3.7}$$

where n represents a finite number of control actuations, $x^*[k]$ is the target reference value, and $x_{pi}[k+1]$ represents the predictions. It is assumed that within the sample time, T_s, which is considered small enough compared with the dynamic response of the system (inverter/induction motor), the reference value is constant. To control the system, the cost function is evaluated with the n predictions, and as a result n costs are obtained. The control action that produces the minimum value of the cost function, $\min\{g_i\}$ for $i = 1,2,\ldots n.$, is selected [7]. A generic block diagram of MPC is shown in Fig 3.3.

3.3 Model Predictive Torque Control

Model predictive torque Control (MPTC) shares the same principles with DTC. In MPTC, the future values of stator flux and electromagnetic torque are calculated based on a discrete-time state-space model of the system (motor). Using the eight possible stator voltage space phasors, seven predictions of stator flux and electromagnetic torque are generated. The cost function, which considers the reference values and predictions, is evaluated and the voltage phasor that minimizes the cost function is selected. The cost function has the following form [7]:

$$g_T = \left|T_{ref} - T_e\right| + \varphi_\lambda \left|\left|\lambda_{ref}\right| - \left|\lambda_s\right|\right| \tag{3.8}$$

where φ_λ is a weighting factor that normalizes the magnitude relation between torque and flux. In general, it is possible to consider this weighting factor as the ratio between the rated torque and rated stator flux [10]:

$$\varphi_\lambda = \frac{|T_m(rated)|}{|\lambda_s(rated)|} \tag{3.9}$$

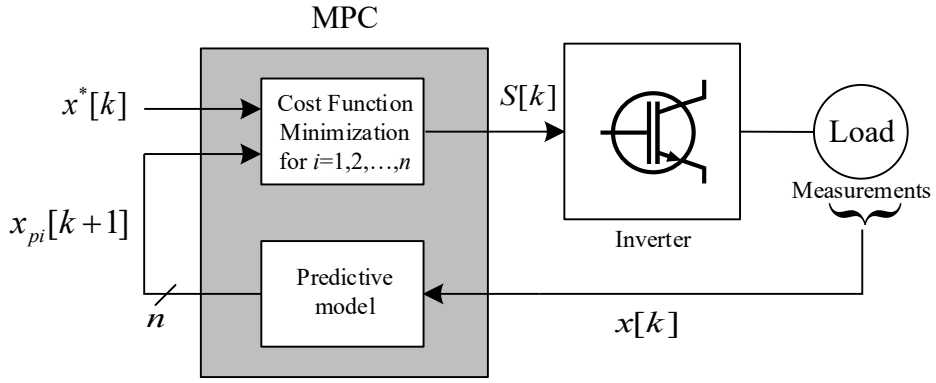

Figure 3.3 Generic MPC block diagram [7].

Fig.3.4 depicts the general block diagram of MPTC.

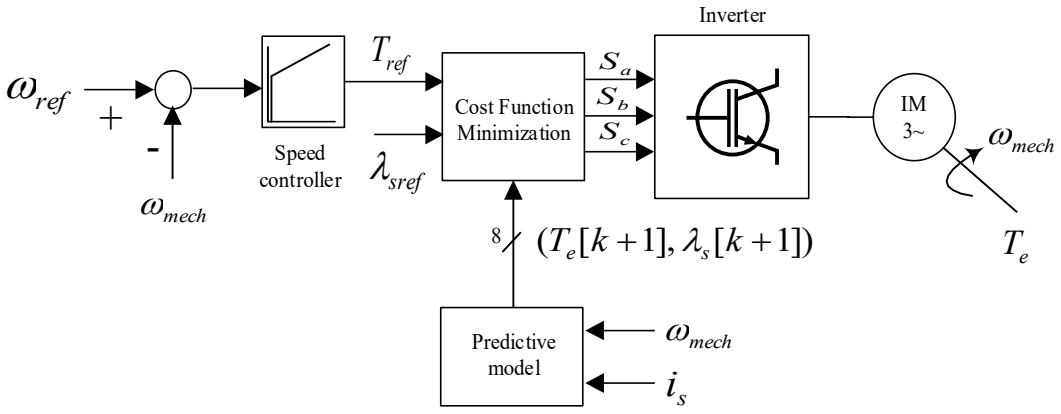

Figure 3.4 MPTC block diagram [9].

CHAPTER 4:
REAL AND REACTIVE POWER CONTROL OF INDUCTION MOTORS

4.1 Introduction

The principle of power control was implemented in the mid 80's in reactive power compensator applications. However, its application in the field of electric drives has gained some attention in recent years [11]. Direct Power Control (DPC) and Instantaneous Power Control (IPC) are among the control strategies with applications in electric drives. These methods share some similar attributes with DTC [11]-[12]. For example, DPC employs an optimal switching table to select the rotor voltage space phasor that needs to be applied to the rotor side of a wound-rotor induction motor if a change in the real or reactive power absorbed by the stator is required; in IPC, as in DTC, the stationary reference frame is used, to simplify its implementation [11].

The first section of this chapter is devoted to describe the concepts of controlling the real and reactive power injected/absorbed by the stator of a squirrel-cage induction motor (SCIM). Variations of real and reactive power with the application of stator voltage space phasor are analyzed, and the basic equations needed for the control strategy are introduced. Finally, the structure of the control method and a current limitation technique during the starting period of the machine is developed. In the second section, application of model predictive control principles to stator real and reactive power control is discussed. As MPC provides possibility of treating constraints, current limitation during the starting period of the motor is achieved in a simple, yet effective, manner.

4.2 Real and Reactive Power Control

This section explores stator real and reactive power control of a SCIM fed from a voltage source inverter. The concepts presented in chapter 2 and chapter 3 will be used to support the presented theory. It is assumed that positive direction of power flow is into the machine.

4.2.1 Real Power Control

The stator active power absorbed by the motor can be expressed as the dot product of voltage and current space phasors [12]

$$P_s = \frac{3}{2}\boldsymbol{V}_s^s \cdot \boldsymbol{I}_s^s \tag{4.1}$$

Combining (2.21) with (4.1), P_s can be written as

$$P_s = \frac{3}{2}(R_s\boldsymbol{I}_s^s + p\boldsymbol{\lambda}_s^s) \cdot \boldsymbol{I}_s^s \tag{4.2}$$

Neglecting the voltage drop $R_s\boldsymbol{I}_s^s$, (4.2) is reduced to

$$P_s = \frac{3}{2}(p\boldsymbol{\lambda}_s^s) \cdot \boldsymbol{I}_s^s \tag{4.3}$$

In steady state, p can be replaced by $j(\omega_e - \omega)$, where ω_e is the angular frequency of the source and ω is the angular speed of the reference frame. Since the stationary reference frame is selected, ω is equal to zero. Then (4.3) can be re-written as:

$$P_s = \frac{3}{2}(j\omega_e\boldsymbol{\lambda}_s^s) \cdot \boldsymbol{I}_s^s \tag{4.4}$$

According to (2.24), the rotor current space phasor is given by

$$\boldsymbol{I'}_r^s = \frac{\boldsymbol{\lambda}_r'^s - L_m\boldsymbol{I}_s^s}{L_r'} \tag{4.5}$$

Substituting (4.5) into (2.23) and after some mathematical manipulations, the stator current space phasor can be calculated as

$$\boldsymbol{I}_s^s = \frac{\boldsymbol{\lambda}_s^s}{\sigma L_s} - \frac{L_m \boldsymbol{\lambda}_r'^s}{\sigma L_s L_r'} \tag{4.6}$$

where $\sigma = \frac{(L_s L_r' - L_m{}^2)}{L_s L_r'}$ is the leakage factor.

The vector diagram shown in Fig. 4.1, illustrates the relation between stator and rotor flux-linkage space phasors in the stationary reference frame $(q^s - d^s)$.

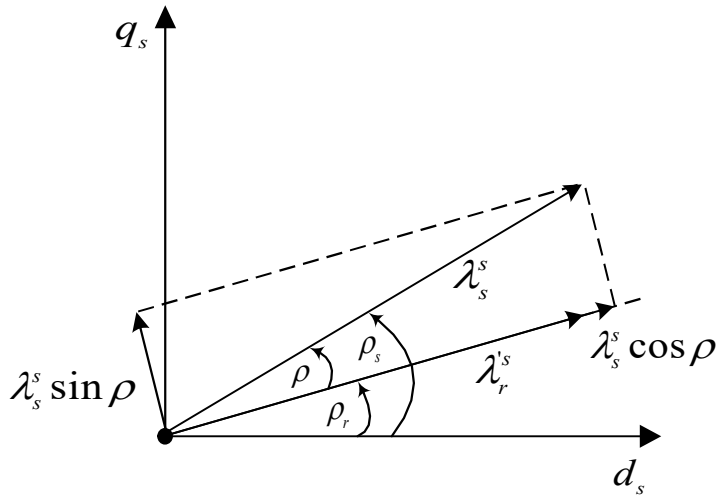

Figure 4.1 Stator and rotor flux-linkage space phasors.

By considering that $\boldsymbol{\lambda}_s^s = |\lambda_s^s| e^{j\rho_s}$ and $\boldsymbol{\lambda}_r'^s = |\lambda_r'^s| e^{j\rho_r}$, it is possible to express (4.6) in the following form:

$$\boldsymbol{I}_s^s = \frac{|\lambda_s^s| e^{j\rho_s}}{\sigma L_s} - \frac{L_m |\lambda_r'^s| e^{j\rho_r}}{\sigma L_s L_r'} \tag{4.7}$$

Substituting (4.7) in (4.4) yields

$$P_s = \frac{3}{2}(j\omega_e|\lambda_s^s|e^{j\rho_s}) \cdot \left(\frac{|\lambda_s^s|e^{j\rho_s}}{\sigma L_s} - \frac{L_m|\lambda'^s_r|e^{j\rho_r}}{\sigma L_s L_r'}\right) \quad (4.8)$$

Performing the dot product and arranging the terms, (4.8) can be simplified as

$$P_s = \frac{3}{2}\frac{L_m}{\sigma L_s L_r'}\omega_e|\lambda'^s_r||\lambda_s^s|sin\rho \; ; \rho = \rho_s - \rho_r \quad (4.9)$$

Rate of change of real power with respect to time is

$$\frac{dP_s}{dt} = \frac{3}{2}\frac{L_m}{\sigma L_s L_r'}\omega_e|\lambda'^s_r|\frac{d|\lambda_s^s|sin\rho}{dt} \quad (4.10)$$

As mentioned earlier, rotor flux-linkage space phasor changes slowly in comparison with stator flux-linkage. In a short sample time, the magnitude rotor flux-linkage space phasor remains constant, and according to (4.9) fast variations of real power can be obtained by changing the term $|\lambda_s^s|\sin\rho$, which corresponds to the component of stator flux-linkage space phasor in quadrature with rotor flux-linkage space phasor.

It is important to point out that the initial position of stator flux-linkage space phasor and its amplitude do not have any direct effect on the active power variations.

4.2.2 Reactive Power Control

The reactive power drawn from the source is associated to instantaneous variations of magnitude of flux space phasor. The reactive power controls the flux in the motor, and is a key element to maintain it. It is also a very important variable to prevent the occurrence of real power positive feedback during the regenerative braking mode of the motor [11].

The magnetizing inductance, L_m, determines the magnetizing current which is required to build up the desired flux in the machine. The reactive power in the motor (neglecting the stator

and rotor leakage inductances) is the power absorbed by the magnetizing inductance. Using the equivalent circuit in Fig. 2.3, the stator reactive power is given by the product of the back-electromotive force and the magnetizing current

$$Q_s = e_{mf}\boldsymbol{I}_m \tag{4.11}$$

where e_{mf} is the back-electromotive force, and I_m is the magnetizing current.

In (4.11), $\boldsymbol{I}_m = \frac{\boldsymbol{\lambda}_m}{L_m}$. Hence

$$Q_s = e_{mf}\frac{\boldsymbol{\lambda}_m}{L_m} \tag{4.12}$$

From Fig. 2.3, $e_{mf} = p\boldsymbol{\lambda}_s^s - L_{ls}\boldsymbol{I}_s^s$. If the term $L_{ls}\boldsymbol{I}_s^s$ is neglected, which is reasonable since stator leakage flux is very small compared to stator flux-linkage, and p is substituted by $j\omega_e$, the back-electromotive force can be calculated as $e_{mf} = j\omega_e\lambda_s^s$. The reactive power in (4.12) is then given by

$$Q_s = j\omega_e\lambda_s^s\frac{\boldsymbol{\lambda}_m}{L_m} \tag{4.13}$$

Magnetizing flux is related to stator flux-linkage as

$$\boldsymbol{\lambda}_s^s = L_{ls}\boldsymbol{I}_s^s + \boldsymbol{\lambda}_m \tag{4.14}$$

By neglecting the term $L_{ls}\boldsymbol{I}_s^s$ in (4.14), $\boldsymbol{\lambda}_s^s \approx \boldsymbol{\lambda}_m$. Therefore, (4.13) can be written as

$$Q_s = \frac{\omega_e}{L_m}|\lambda_s^s|^2 \tag{4.15}$$

Differentiating (4.15) with respect to time results in the following

$$\frac{dQ_s}{dt} = 2\frac{\omega_e}{L_m}\frac{d|\lambda_s^s|}{dt} \tag{4.16}$$

According to (4.16), reactive power control can be achieved by changing the magnitude of stator flux-linkage. This confirm the strong correlation between the reactive power and the flux in the machine.

4.3 Effect of Voltage Space Phasors

In section 3.1 it was explained that the direction of rotation of stator flux depends on the direction of the applied voltage space phasor, and its speed of rotation is in direct proportion to the amplitude of the voltage space phasor. As a result, by properly selecting the voltage space phasor, the rotation of the stator flux can be controlled. It is important to point out, that the selection of voltage phasors is dependent on the location of the stator flux space phasor. Therefore, the q_s- d_s plane is divided into six sectors, as shown in Fig. 4.2.

The impact of each of the six active and two zero voltage space phasors on the active and reactive power variations are analyzed in the following sub-sections.

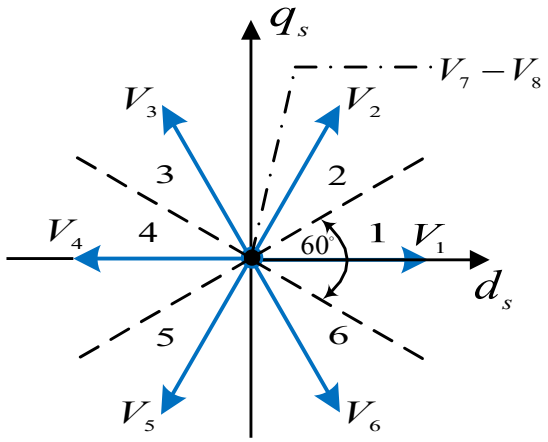

Figure 4.2 Voltage space phasors and six-sector division.

4.3.1 Six-Sector Analysis

As described in sub-sections 4.21 and 4.2.2, real and reactive power control can be accomplished by changing $|\boldsymbol{\lambda}_s^s| sin\rho$ in (4.10), and $|\boldsymbol{\lambda}_s^s|$ in (4.16), respectively.

To analyze the effect of voltage space phasors on real and reactive powers, it will be assumed that the stator flux-linkage space phasor is located in sector 2, and an increase in the amount of real power, and a reduction in reactive power is required. The original position and magnitude of $\boldsymbol{\lambda}_s$ is shown in Fig 4.3. The best alternative to increase the quadrature component of $\boldsymbol{\lambda}_s$ with respect to $\boldsymbol{\lambda}_r$, $|\boldsymbol{\lambda}_s^s| sin\rho$, and decrease the magnitude of $\boldsymbol{\lambda}_s$ is the voltage space phasor $\boldsymbol{V}_4$ ($\boldsymbol{\lambda}_4 = \boldsymbol{V}_4 \Delta t$).

The impact on real and reactive power changes are studied for each active voltage space phasor and the results are summarized in Table 4.1.

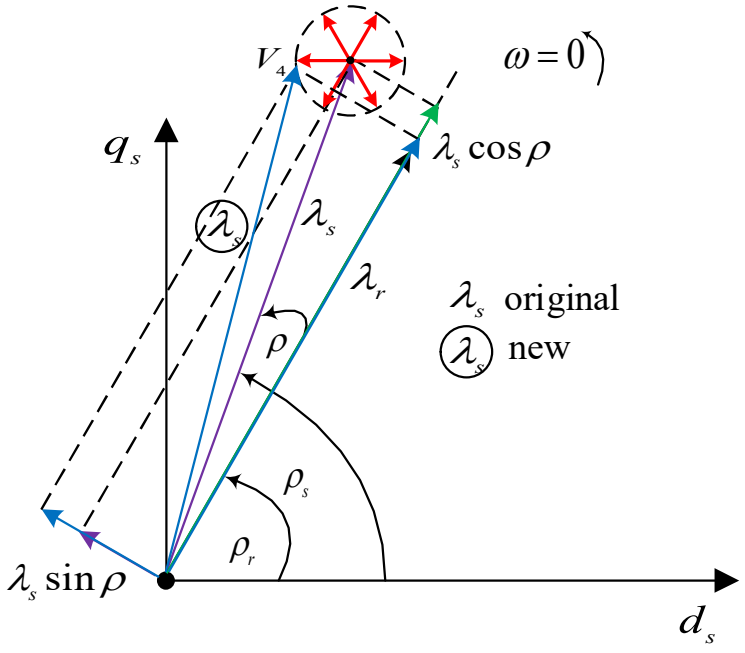

Figure 4.3 Selection of appropriate voltage space phasors.

Table 4.1 Impact of active voltage space phasors on real and reactive power (six-sector).

		Sector					
		1	2	3	4	5	6
V_1	P_s	↑↓	↓	↓	↑↓	↑	↑
	Q_s	↑	↑	↓	↓	↓	↑
V_2	P_s	↑	↑↓	↓	↓	↑↓	↑
	Q_s	↑	↑	↑	↓	↓	↓
V_3	P_s	↑	↑	↑↓	↓	↓	↑↓
	Q_s	↓	↑	↑	↑	↓	↓
V_4	P_s	↑↓	↑	↑	↑↓	↓	↓
	Q_s	↓	↓	↑	↑	↑	↓
V_5	P_s	↓	↑↓	↑	↑	↑↓	↓
	Q_s	↓	↓	↓	↑	↑	↑
V_6	P_s	↓	↓	↑↓	↑	↑	↑↓
	Q_s	↑	↓	↓	↓	↑	↑

The stator flux-linkage space phasor always leads the rotor flux-linkage space phasor when the induction machine is working as a motor. The impact of zero voltage space phasors is to stall the stator flux without affecting its magnitude. Since λ'^{s}_{r} keeps rotating in the positive direction (counter-clockwise for the case in Fig 4.3), the angle ρ decreases when zero voltage phasors are applied. A decrease in the angle ρ, results in a reduction of $|\lambda^{s}_{s}|sin\rho$, and as a consequence, the real power absorbed by the motor decreases.

The impact of zero voltage space phasors on the reactive power is found to be insignificant. Due to the presence of the stator resistance, a slight reduction in the reactive power is observed when zero voltage space phasors are applied. The effect of zero voltage phasors on real and reactive power variations are summarized in Table 4.2.

Table 4.2 Impact of zero voltage space phasors on real and reactive power (six-sector).

	Sector
	1--6
P_s	↓
Q_s	↓

4.3.2 Twelve-Sector Analysis

In Table 4.1 there are voltage phasors that can increase or decrease the real power in the same sector (V_1 and V_4 in sector 1 for example). As a result, not all the voltage phasors are used in each sector. In addition, when a power variation is required, whether this change is small or significant, the same voltage phasor is applied. Therefore, high ripple will appear on motor real and reactive powers.

In order to address this issue, the $q_s - d_s$ plane in Fig 4.2 is divided into twelve sectors, as shown in Fig 4.4. The analysis performed for the real and reactive powers in the six sectors case (sub-section 4.3.1) is still valid for the twelve sectors. It should be mentioned that, since in the twelve sector case all voltage phasors are used, a criterion of "small" and "large" change is introduced.

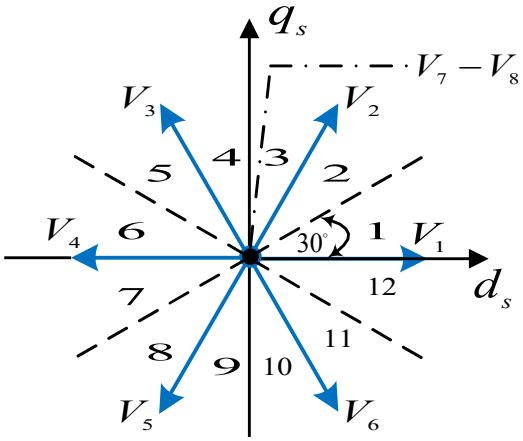

Figure 4.4 Voltage space phasors and twelve-sector division.

Similar analysis to those performed for a six-sector case are carried out for a twelve-sector case, and the effect of active and zero voltage phasors on real and reactive power variations are observed. Tables 4.3 and 4.4 summarize these results.

4.4 Power Control Strategy

Prior to presenting the power control strategy, discussions on computing the reference real and reactive powers along with absorbed real and reactive powers are provided.

Table 4.3 Impact of active voltage space phasors on real and reactive power (twelve-sector).

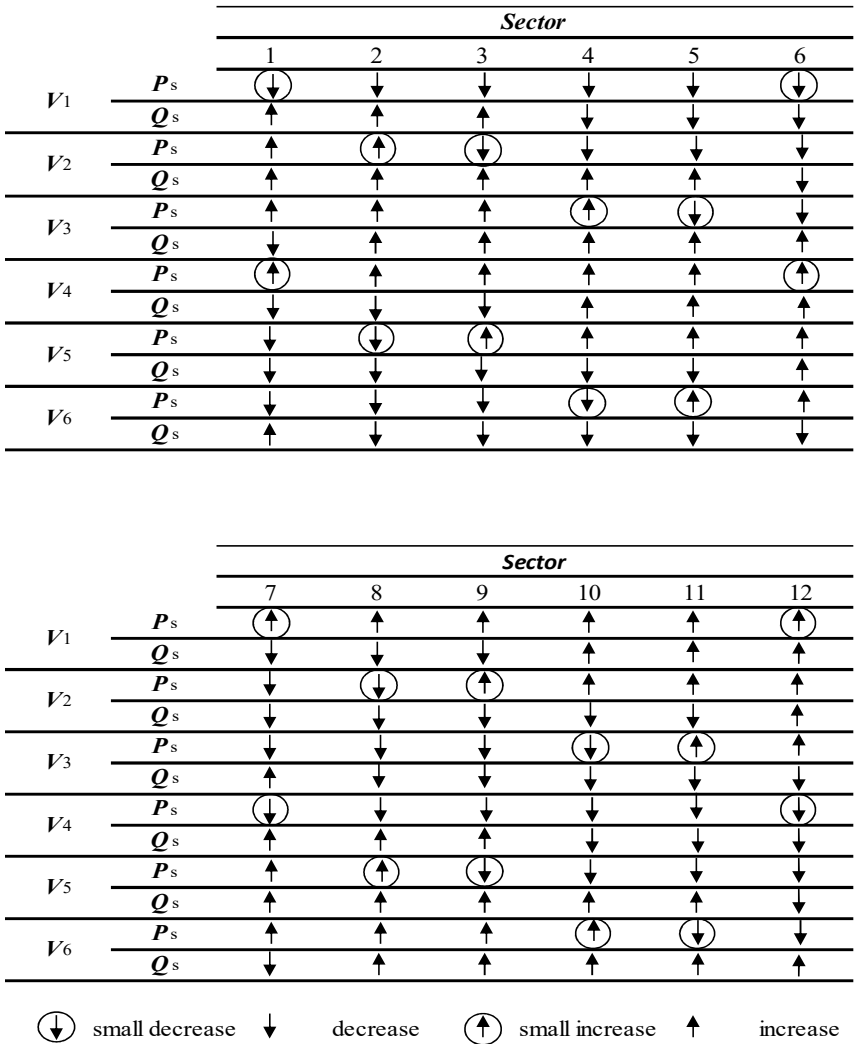

Table 4.4 Impact of zero voltage space phasors on real and reactive power (twelve sector).

	Sector
	1--12
P_s	↓
Q_s	⊕

4.4.1 Power Reference Generation

Fig 4.5 depicts the power flow diagram of an SCIM, which is developed based on the equivalent circuit shown in Fig. 2.3.

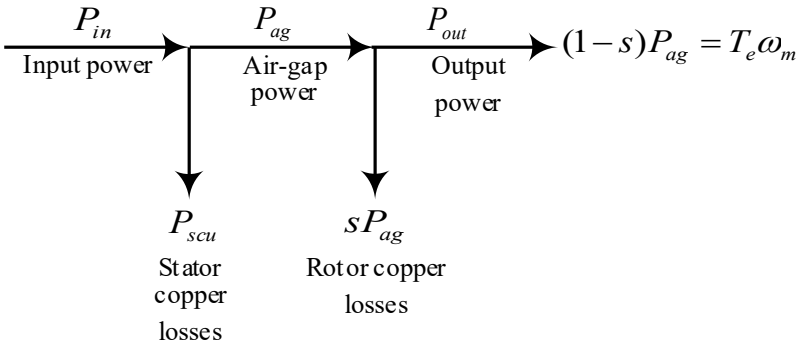

Figure 4.5 SCIM power flow diagram.

In this diagram, *s* represents the slip and is defined as $s = (w_e - w_r)/w_r$, where w_e is the synchronous speed and w_r is the rotor speed in radians per second. The rotor mechanical speed in radians per second, w_m, is related to w_r by the number of pole pairs of the machine: $w_r = \frac{P}{2} w_m$. Based on these considerations, and using the expression for the output power given in Fig 4.5, the reference real power can be calculated as follows:

$$P_{sref} = \frac{2}{P} \frac{T_{ref}}{\omega_e} \tag{4.17}$$

where T_{ref} is the reference electromagnetic torque. It is noteworthy to mention that this power corresponds to the air-gap power, P_{ag}.

Based on the carried out analysis for the reactive power in sub-section 4.2.2, it is possible to use (4.13) and (4.14) to obtain an expression for the reference reactive power. In that study, the stator leakage inductance, L_{ls}, was neglected. However, the stator leakage inductance will be considered in obtaining reference reactive power since at high values of slip the air-gap flux does not remain constant. This is due to the fact that at high-slip conditions, the effect of leakage fluxes is higher compared to low-slip conditions [6]. The reduction in the air-gap flux at high values of slip affects the reactive power absorbed by the motor. Consequently, the leakage inductance is considered in these calculations.

By substituting (4.14) in (4.13), the reference reactive power can be calculated as follows

$$Q_{sref} = \frac{\omega_e}{L_m}\left(\boldsymbol{\lambda}^s_{sref} - L_{ls}|\boldsymbol{I}^s_s|\right)^2 \tag{4.18}$$

where $\boldsymbol{\lambda}^s_{sref}$ is the reference stator flux-linkage of the motor. In general $\boldsymbol{\lambda}^s_{sref}$ is set to the rated value. $|\boldsymbol{I}^s_s|$ is the magnitud of the measured stator current space phasor.

4.4.2 Consumed real and reactive power

Two methods are proposed for calculating the consumed real power of an SCIM.

In ***method 1***, the real power is estimated using the electromagnetic torque and the synchronous speed. The estimated electromagnetic torque is given by (2.14). The synchronous speed can be calculated as follows

$$\omega_e = \frac{d\rho_r}{dt} \tag{4.19}$$

where ρ_r is the angle of the rotor flux-linkage space phasor.

The angle ρ_r can be calculated by taking the inverse tangent of rotor flux q-and-d axis components ratio

$$\rho_r = tan^{-1}\frac{\lambda'^s_{qr}}{\lambda'^s_{dr}} \tag{4.20}$$

Substituting (4.20) in (4.19) and rearranging the terms, the synchronous speed is given by

$$\omega_e = \frac{\lambda'^s_{dr} p\lambda'^s_{qr} - \lambda'^s_{qr} p\lambda'^s_{dr}}{\lambda'^{s\,2}_{dr} + \lambda'^{s\,2}_{qr}} \tag{4.21}$$

where p is the $\frac{d}{dt}$ operator.

Based on (4.17), and using (2.14) and (4.21), the consumed real power can be calculated as follows

$$P_s = \frac{2}{P}\frac{T_e}{\omega_e} \tag{4.22}$$

The consumed real power in ***method 2*** is calculating using stator voltages and currents, and the calculated reactive power. The apparent stator power in space phasor form can be expressed as

$$S_s = \frac{3}{2}\boldsymbol{V}_s\boldsymbol{I}_s^* \tag{4.23}$$

where $\boldsymbol{I}_s^*$ is the complex conjugate of the stator current space phasor.

In general, the real power can be obtained from the relation $P = Scos\varphi$, where $cos\varphi$ is the power factor. The angle φ is given by:

$$\varphi = sin^{-1}\frac{Q_s}{S_s} \tag{4.24}$$

where Q_s is the reactive power.

Based on Fig 4.5, the consumed real power can be expressed as the difference between P_{in} and P_{scu}

$$P_s = |S_s| \cos\varphi - \frac{3}{2} R_s |\boldsymbol{I}_s|^2 \tag{4.25}$$

The consumed reactive power is calculated by using the estimated stator flux-linkage, measured stator current and the synchronous speed. The estimated stator flux-linkage can be obtained from (2.21). Integrating both sides of (2.21) and rearranging the terms, the stator flux-linkage space phasor is given by:

$$\boldsymbol{\lambda}_s^s = \int (\boldsymbol{V}_s^s - R_s \boldsymbol{I}_s^s) dt \tag{4.26}$$

Substituting (4.26) into (4.19), the estimated consumed reactive power can be obtained as follows

$$Q_s = \frac{\omega_e}{L_m} (|\boldsymbol{\lambda}_s^s| - L_{ls} |\boldsymbol{I}_s^s|)^2 \tag{4.27}$$

4.4.3 Switching Tables

In order to determine the inverter switching states, the power states, and the position of the stator flux-linkage space phasor are employed as inputs to switching tables 4.5 (for six-sector) and 4.6 (for twelve-sector), and the appropriate voltage phasors are identified. These switching tables are established based on the discussions provided in sub-sections 4.3.1 and 4.32. The real power state, K_p, and the reactive power state, K_q, are obtained from three-level hysteresis controller for the six-sector case, and four–level hysteresis controller for the twelve sector case.

In the six-sector case, if a real or reactive power increase is required, their respective power state will adopt a value of 1. If a reduction in real or reactive power is needed, their respective power state will adopt a value of -1. If no change in the real or reactive power is required, their respective power state will adopt a value of 0. The real and reactive power conditions for the hysteresis controllers are defined as follows

$$K_f = 1 \text{ if } |\boldsymbol{f}_s| \leq \left|\boldsymbol{f}_{sref}\right| - |\Delta \boldsymbol{f}_s| \tag{4.28}$$

$$K_f = -1 \text{ if } |\boldsymbol{f}_s| \geq \left|\boldsymbol{f}_{sref}\right| + |\Delta \boldsymbol{f}_s| \tag{4.29}$$

$$K_f = 0 \text{ if } -\left|\Delta \boldsymbol{f}_s\right| \leq \left|\boldsymbol{f}_{sref}\right| - \left|\boldsymbol{f}_s\right| \leq \left|\Delta \boldsymbol{f}_s\right| \tag{4.30}$$

where $\boldsymbol{f}$ can be replaced by $\boldsymbol{P}$ or $\boldsymbol{Q}$. $\Delta \boldsymbol{f}$ represents the width of the hysteresis band dived by 2.

For the twelve-sector case, same approach can be followed to define the real and reactive power conditions for the hysteresis controllers. However, a difference should be made regarding the size of the increment/reduction that is required (sub-section 4.3.2). In this case, the power states will adopt a value of 2 when an increase for either the real or reactive power is needed. If a small increase is required the power states will adopt a value of 1. If a decrease is required, the power states will adopt a value of -2. If a small decrease is needed, the power states will adopt a value of -1. If no change is required, then the respective power states will adopt a value of 0. The conditions for the twelve-sector case are defined as follows

$$K_f = 2 \text{ if } |\boldsymbol{f}_s| < \left|\boldsymbol{f}_{sref}\right| - |\Delta \boldsymbol{f}_s| \tag{4.31}$$

$$K_f = 1 \text{ if } |\Delta \boldsymbol{f}_s| \geq \left|\boldsymbol{f}_{sref}\right| - |\boldsymbol{f}_s| > 0 \tag{4.32}$$

$$K_f = -1 \text{ if } -\left|\Delta \boldsymbol{f}_s\right| \leq \left|\boldsymbol{f}_{sref}\right| - \left|\boldsymbol{f}_s\right| < 0 \tag{4.33}$$

$$K_f = -2 \text{ if } |\boldsymbol{f}_s| > |\boldsymbol{f}_{sref}| + |\Delta \boldsymbol{f}_s| \tag{4.34}$$

$$K_f = 0 \text{ if } |\boldsymbol{f}_{sref}| - |\boldsymbol{f}_s| = 0 \tag{4.35}$$

Table 4.5 Switching Table (Six-sector).

		Sector					
		1	2	3	4	5	6
Kq =1	***Kp*** =1	$\boldsymbol{V}2$	$\boldsymbol{V}3$	$\boldsymbol{V}4$	$\boldsymbol{V}5$	$\boldsymbol{V}6$	$\boldsymbol{V}1$
	Kp =0	$\boldsymbol{V}1$	$\boldsymbol{V}2$	$\boldsymbol{V}3$	$\boldsymbol{V}4$	$\boldsymbol{V}5$	$\boldsymbol{V}6$
	Kp = -1	$\boldsymbol{V}6$	$\boldsymbol{V}1$	$\boldsymbol{V}2$	$\boldsymbol{V}3$	$\boldsymbol{V}4$	$\boldsymbol{V}5$
Kq =0	***Kp*** =1	$\boldsymbol{V}3$	$\boldsymbol{V}4$	$\boldsymbol{V}5$	$\boldsymbol{V}6$	$\boldsymbol{V}1$	$\boldsymbol{V}2$
	Kp =0	$\boldsymbol{V}7$	$\boldsymbol{V}8$	$\boldsymbol{V}7$	$\boldsymbol{V}8$	$\boldsymbol{V}7$	$\boldsymbol{V}8$
	Kp = -1	$\boldsymbol{V}5$	$\boldsymbol{V}6$	$\boldsymbol{V}1$	$\boldsymbol{V}2$	$\boldsymbol{V}3$	$\boldsymbol{V}4$
Kq = -1	***Kp*** =1	$\boldsymbol{V}3$	V4	$\boldsymbol{V}5$	$\boldsymbol{V}6$	$\boldsymbol{V}1$	$\boldsymbol{V}2$
	Kp =0	$\boldsymbol{V}4$	$\boldsymbol{V}5$	$\boldsymbol{V}6$	$\boldsymbol{V}1$	V2	$\boldsymbol{V}3$
	Kp = -1	$\boldsymbol{V}5$	$\boldsymbol{V}6$	$\boldsymbol{V}1$	$\boldsymbol{V}2$	$\boldsymbol{V}3$	$\boldsymbol{V}4$

Table 4.6 Switching Table (Twelve-sector).

		Sector											
		1	2	3	4	5	6	7	8	9	10	11	12
Kq =1	***Kp*** =2	$\boldsymbol{V}2$	$\boldsymbol{V}3$	$\boldsymbol{V}3$	$\boldsymbol{V}4$	$\boldsymbol{V}4$	$\boldsymbol{V}5$	$\boldsymbol{V}5$	$\boldsymbol{V}6$	$\boldsymbol{V}6$	$\boldsymbol{V}1$	$\boldsymbol{V}1$	$\boldsymbol{V}2$
	Kp =1	$\boldsymbol{V}2$	$\boldsymbol{V}2$	$\boldsymbol{V}3$	$\boldsymbol{V}3$	$\boldsymbol{V}4$	$\boldsymbol{V}4$	$\boldsymbol{V}5$	$\boldsymbol{V}5$	$\boldsymbol{V}6$	$\boldsymbol{V}6$	$\boldsymbol{V}1$	$\boldsymbol{V}1$
	Kp =0	$\boldsymbol{V}1$	$\boldsymbol{V}2$	$\boldsymbol{V}2$	$\boldsymbol{V}3$	$\boldsymbol{V}3$	$\boldsymbol{V}4$	$\boldsymbol{V}4$	$\boldsymbol{V}5$	$\boldsymbol{V}5$	$\boldsymbol{V}6$	$\boldsymbol{V}6$	$\boldsymbol{V}1$
	Kp = -1	$\boldsymbol{V}1$	$\boldsymbol{V}1$	$\boldsymbol{V}2$	$\boldsymbol{V}2$	$\boldsymbol{V}3$	$\boldsymbol{V}3$	$\boldsymbol{V}4$	$\boldsymbol{V}4$	$\boldsymbol{V}5$	$\boldsymbol{V}5$	$\boldsymbol{V}6$	$\boldsymbol{V}6$
	Kp = -2	$\boldsymbol{V}6$	$\boldsymbol{V}1$	$\boldsymbol{V}1$	$\boldsymbol{V}2$	$\boldsymbol{V}2$	$\boldsymbol{V}3$	$\boldsymbol{V}3$	$\boldsymbol{V}4$	$\boldsymbol{V}4$	$\boldsymbol{V}5$	$\boldsymbol{V}5$	$\boldsymbol{V}6$
Kq =0	***Kp*** =2	$\boldsymbol{V}3$	$\boldsymbol{V}4$	$\boldsymbol{V}4$	$\boldsymbol{V}5$	$\boldsymbol{V}5$	$\boldsymbol{V}6$	$\boldsymbol{V}6$	$\boldsymbol{V}1$	$\boldsymbol{V}1$	$\boldsymbol{V}2$	$\boldsymbol{V}2$	$\boldsymbol{V}3$
	Kp =1	$\boldsymbol{V}4$	$\boldsymbol{V}4$	$\boldsymbol{V}5$	$\boldsymbol{V}5$	$\boldsymbol{V}6$	$\boldsymbol{V}6$	$\boldsymbol{V}1$	$\boldsymbol{V}1$	$\boldsymbol{V}2$	$\boldsymbol{V}2$	$\boldsymbol{V}3$	$\boldsymbol{V}3$
	Kp =0	$\boldsymbol{V}7$	$\boldsymbol{V}8$	$\boldsymbol{V}7$	$\boldsymbol{V}8$	$\boldsymbol{V}7$	$\boldsymbol{V}8$	$\boldsymbol{V}7$	$\boldsymbol{V}8$	$\boldsymbol{V}7$	$\boldsymbol{V}8$	$\boldsymbol{V}7$	$\boldsymbol{V}8$
	Kp = -1	$\boldsymbol{V}5$	$\boldsymbol{V}5$	$\boldsymbol{V}6$	$\boldsymbol{V}6$	$\boldsymbol{V}1$	$\boldsymbol{V}1$	$\boldsymbol{V}2$	$\boldsymbol{V}2$	$\boldsymbol{V}3$	$\boldsymbol{V}3$	$\boldsymbol{V}4$	$\boldsymbol{V}4$
	Kp = -2	$\boldsymbol{V}5$	$\boldsymbol{V}6$	$\boldsymbol{V}6$	$\boldsymbol{V}1$	$\boldsymbol{V}1$	$\boldsymbol{V}2$	$\boldsymbol{V}2$	$\boldsymbol{V}3$	$\boldsymbol{V}3$	$\boldsymbol{V}4$	$\boldsymbol{V}4$	$\boldsymbol{V}5$
Kq = -1	***Kp*** =2	$\boldsymbol{V}3$	$\boldsymbol{V}4$	$\boldsymbol{V}4$	$\boldsymbol{V}5$	$\boldsymbol{V}5$	$\boldsymbol{V}6$	$\boldsymbol{V}6$	$\boldsymbol{V}1$	$\boldsymbol{V}1$	$\boldsymbol{V}2$	$\boldsymbol{V}2$	$\boldsymbol{V}3$
	Kp =1	$\boldsymbol{V}4$	$\boldsymbol{V}4$	$\boldsymbol{V}5$	$\boldsymbol{V}5$	$\boldsymbol{V}6$	$\boldsymbol{V}6$	$\boldsymbol{V}1$	$\boldsymbol{V}1$	$\boldsymbol{V}2$	$\boldsymbol{V}2$	$\boldsymbol{V}3$	$\boldsymbol{V}3$
	Kp =0	$\boldsymbol{V}4$	$\boldsymbol{V}5$	$\boldsymbol{V}5$	$\boldsymbol{V}6$	$\boldsymbol{V}6$	$\boldsymbol{V}1$	$\boldsymbol{V}1$	$\boldsymbol{V}2$	$\boldsymbol{V}2$	$\boldsymbol{V}3$	$\boldsymbol{V}3$	$\boldsymbol{V}4$
	Kp = -1	$\boldsymbol{V}5$	$\boldsymbol{V}5$	$\boldsymbol{V}6$	$\boldsymbol{V}6$	$\boldsymbol{V}1$	$\boldsymbol{V}1$	$\boldsymbol{V}2$	$\boldsymbol{V}2$	$\boldsymbol{V}3$	$\boldsymbol{V}3$	$\boldsymbol{V}4$	$\boldsymbol{V}4$
	Kp = -2	$\boldsymbol{V}5$	$\boldsymbol{V}6$	$\boldsymbol{V}6$	$\boldsymbol{V}1$	$\boldsymbol{V}1$	$\boldsymbol{V}2$	$\boldsymbol{V}2$	$\boldsymbol{V}3$	$\boldsymbol{V}3$	$\boldsymbol{V}4$	$\boldsymbol{V}4$	$\boldsymbol{V}5$

As mentioned earlier, zero voltage space phasors almost stall the rotation of stator flux-linkage. Based on this consideration, zero voltage space phasors are employed only when both real and reactive power states are zero.

4.4.4 Direct Power Control

A block diagram of the proposed control strategy is shown in Fig 4.6. The stator currents are measured and transformed into the stationary q-d reference frame. The voltages can be measured and then transformed into the stationary q-d reference frame, or they can be calculated by using the switching states, S_a, S_b, and S_c, and the DC-link voltaje, V_{dc}

$$\begin{bmatrix} v_{qs}^{s} \\ v_{ds}^{s} \end{bmatrix} = \frac{2}{3} V_{dc} \begin{bmatrix} 1 & -0.5 & -0.5 \\ 0 & \sqrt{3}/2 & -\sqrt{3}/2 \end{bmatrix} \begin{bmatrix} S_a \\ S_b \\ S_c \end{bmatrix} \tag{4.36}$$

The stator real and reactive powers are calculated using the machine model given in sub-section 2.1. To generate the reference active and reactive powers, the synchronous speed, magnitude of the stator current space phasor, reference value of the stator flux, and the reference torque are used. The reference torque is obtained from a speed controller. The calculated powers are compared to their respective reference values by the hysteresis controllers and the power states K_p and K_q are obtained. Both power states, along with the position (sector) of the estimated stator flux-linkage space phasor are fed to the switching table to obtain the proper switching states.

4.4.5 Starting Current Limitation

High values of stator current appear during the motor start-up period. These high currents can cause severe damage to power switching devices and motor insulation. Consequently, a

method to limit the starting currents based on the principles of power control strategy is proposed.

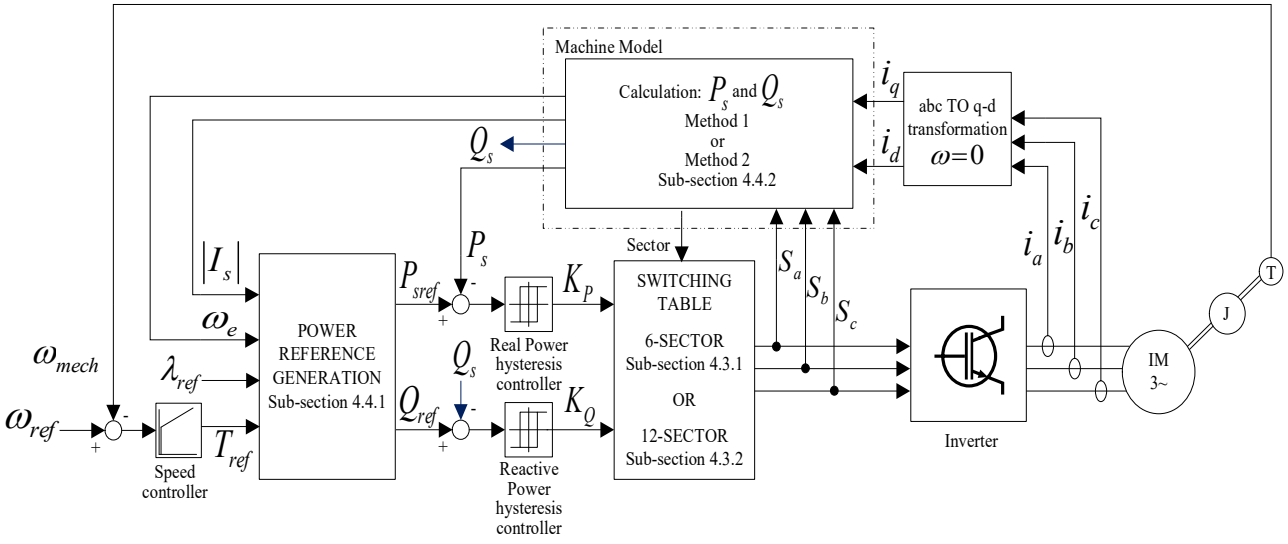

Figure 4.6 Block diagram of direct power control.

If (2.21) and (2.22) are combined and the stator current is solved in terms of stator and rotor flux-linkages, the following expression is obtained

$$\sigma \boldsymbol{I}_s^s = \frac{1}{\boldsymbol{L}_s} (\boldsymbol{\lambda}_s^s - \frac{L_m}{\boldsymbol{L}_s} \boldsymbol{\lambda}_r'^s) \tag{4.37}$$

where σ represents the leakage factor defined in sub-section 4.2.1.

Considering that σ is very small, a flux transient, i.e difference between $\boldsymbol{\lambda}_s^s$ and $\boldsymbol{\lambda}_r'^s$, can generate a fast variation of the stator current magnitude [14]-[15].

During the motor start-up period, the control strategy selects the switching states that produce fast variations of stator flux linkage to build up the flux, and to meet the real and reactive power references. Since rotor flux-linkage changes slowly compared to stator flux-

linkage (due to rotor time constant), a considerably discrepancy between the stator and rotor flux-linkage space phasors takes place. This in turn, results in high stator currents at start-up stage.

The previous analysis suggests that high starting currents occur mainly to the fact that, apart from the residual flux that exists in the stator, the machine requires to build-up the stator flux almost from zero. In other words, the machine can be considered practically "demagnetized". A method to limit the stator current amplitude can be contemplated in the sense of providing the machine with the stator flux already existent, and then apply the power reference commands.

The pre-magnetizing stage considered in the strategy builds-up the stator flux by applying an arbitrary active voltage space phasor until the flux magnitude reaches the reference (rated) value. Application of an active voltage space phasor generates a quick increment in the stator flux magnitude and, as a result, fast variations of stator occur. In order to control these current variations, a zero voltage space phasor is applied when the magnitude of the stator current reaches its pre-defined limit, $\boldsymbol{I}_{smax}^{s}$. Once the pre-magnetizing period has been completed, a command is given, and the power control strategy takes over and starts the machine normally. It is important to point out that the power commands are not applied during the pre-magnetizing stage. Fig 4.7 shows a block diagram of the proposed control method, including the current limitation strategy. Here, ϕ can assume a value of either 0 or 1, and it controls the switching between the pre-magnetizing stage and the power control strategy.

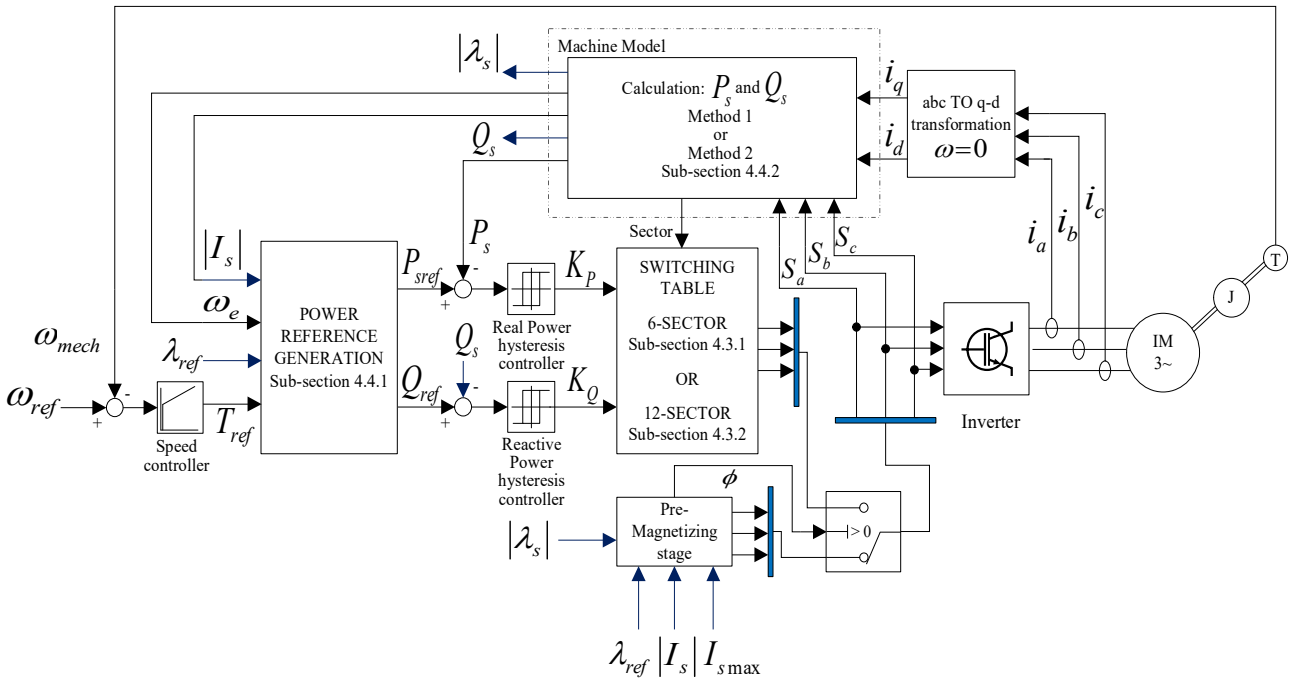

Figure 4.7 Block diagram of direct power control with starting current limitation.

4.5 Model Predictive Power Control (MPPC)

As already mentioned, a fundamental element in the structure of MPC is the model of the system to be controlled. Here, the model that represents the SCIM is considered. From the equations of the machine given by (2.21)-(2.24), two state variables are selected: the stator current space phasor, $\boldsymbol{I}_s^s$, and the rotor flux-linkage state phasor, $\boldsymbol{\lambda}_r'^s$. The stator current is specifically selected as a state variable as it can be measured and, some unwanted stator dynamics, like impacts on stator inductance, stator resistance, and back-electromotive force can be avoided [10]. The equations of the SCIM in state-space form in the stationary reference frame are given by [9]:

$$\tau_\sigma p\boldsymbol{I}_s^s + \boldsymbol{I}_s^s = \frac{\boldsymbol{V}_s^s}{R_\sigma} + \frac{k_r}{R_\sigma}\left(\frac{1}{\tau_r} - j\omega_r\right)\boldsymbol{\lambda}_r'^s \tag{4.38}$$

$$\tau_r p\boldsymbol{\lambda}_r'^s + \boldsymbol{\lambda}_r'^s = L_m \boldsymbol{I}_s^s + j\omega_r \tau_r \boldsymbol{\lambda}_r'^s \tag{4.39}$$

where $k_r = \frac{L_m}{L_r'}$, $R_\sigma = R_s + {k_r}^2 R_r$, $\sigma = \frac{(L_s L_r' - {L_m}^2)}{L_s L_r'}$, $\tau_\sigma = \sigma \frac{L_s}{R_\sigma}$, and $\tau_r = \frac{L_r'}{R_r}$.

4.5.1 MPPC Scheme

Principles presented in section 4.2 and 4.3 regarding the impact of voltage space phasors on real and reactive power variations are still valid in MPPC. However, this method does not use a switching table to select the proper voltage space phasor. Instead, MPPC predicts the future values of real and reactive power for each of the eight voltage space phasors, and selects the one that results in the minimum cost function value. The cost function aggregates the real and reactive power errors. Fig 4.8 shows a block diagram of the proposed MPPC strategy.

The measured stator currents are transformed into the stationary *q-d* reference frame, and fed to the *estimation* block. Since the actual values of stator flux-linkage, rotor flux-linkage, and synchronous speed cannot be measured, they are estimated as well. The estimated values of stator flux-linkage, rotor flux-linkage, and synchronous speed are employed in the *prediction* block, where the values of real and reactive powers at the instant k+1 are predicted. The real and reactive power predictions are calculated for each of the eight voltage space phasors. Finally, the *minimization* block, which receives all the power predictions and the reference powers, selects the switching state that minimizes the cost function.

Synchronous speed is calculated using (4.21). Stator and rotor flux-linkages can be estimated using the machine model given in (2.21)-(2.24), and (3.6) [10]

$$\boldsymbol{\lambda}_s^s[k] = \boldsymbol{\lambda}_s^s[k-1] + T_s \boldsymbol{V}_s^s[k] - R_s T_s \boldsymbol{I}_s^s[k] \tag{4.40}$$

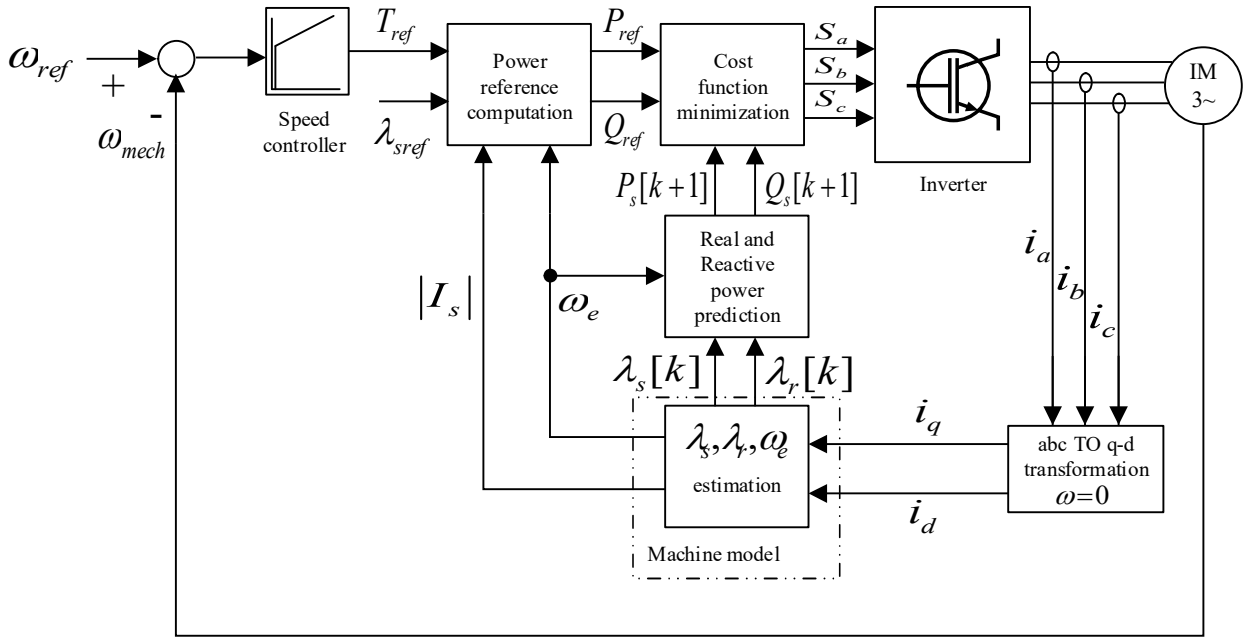

Figure 4.8 Block diagram of MPPC scheme.

$$\boldsymbol{\lambda'}_r^s[k] = \frac{L'_r}{L_m}\boldsymbol{\lambda}_s^s[k] + \boldsymbol{I}_s^s[k]\left(L_m - \frac{L'_r L_s}{L_m}\right) \tag{4.41}$$

Real and reactive power predictions can be obtained using (4.22) and (4.27), respectively. In (4.22), the predicted value of electromagnetic torque is required. In (4.27), the predicted value of the stator flux linkage is required. To predict the stator flux-linkage, for the next sampling time, (4.40) is employed. Since the future value of the stator flux-linkage is required in prediction, (4.40) is adjusted as following

$$\boldsymbol{\lambda}_s^s[k+1] = \boldsymbol{\lambda}_s^s[k] + T_s\boldsymbol{V}_s^s[k] - R_s T_s \boldsymbol{I}_s^s[k] \tag{4.42}$$

Writing (2.14) in space phasor format, yields

$$T_e = \frac{3}{2}\frac{P}{2} Im(\boldsymbol{I}_S^s\, \boldsymbol{\lambda}_S^{s*}) \tag{4.43}$$

where $\boldsymbol{\lambda}_s^{s*}$ represents the complex conjugate of predicted stator flux-linkage space phasor.

Thus, using (4.43) and the predicted values of stator current and flux-linkage, the predicted electromagnetic torque can be obtained as follows:

$$T_e[k+1] = \frac{3}{2}\frac{P}{2} Im(\boldsymbol{I}_s^s[k+1]\boldsymbol{\lambda}_s^{s*}[k+1]) \tag{4.44}$$

The predicted value of stator current can be obtained by discretizing (4.38) using Euler's forward method [10]:

$$\boldsymbol{I}_s^s[k+1] = \left(1+\frac{T_s}{\tau_\sigma}\right)\boldsymbol{I}_s^s[k] + \frac{T_s}{\tau_\sigma + T_s}\left\{\frac{1}{R_\sigma}\left[\left(\frac{k_r}{\tau_r} - k_r j\omega_r\right)\boldsymbol{\lambda}'^s_r[k] + \boldsymbol{V}_s^s[k]\right]\right\} \tag{4.45}$$

After stator flux-linkage and stator current predictions are determined, it is possible to obtain the real and reactive power predictions

$$P_s[k+1] = \frac{2}{P}\frac{T_e[k+1]}{\omega_e} \tag{4.46}$$

$$Q_s[k+1] = \frac{\omega_e}{L_m}\left(|\boldsymbol{\lambda}_s^s[k+1]| - L_{ls}|\boldsymbol{I}_s^s[k+1]|\right)^2 \tag{4.47}$$

It is important to notice that the predictions of P_s and Q_s are obtained for each of the eight voltage space phasors. Hence, seven predictions for the real and reactive powers are obtained (predictions for $\boldsymbol{V}_7$ and $\boldsymbol{V}_8$ are the same).

The switching states that minimize a cost function, which considers the reference and predicted values, and contains the control criterion to reduce the power errors, are selected. The cost function for MPPC is formulated as follows

$$g_p = \left|P_{sref} - P_s[k+1]\right| + \varphi_Q\left|\left|Q_{sref}\right| - |Q_s[k+1]|\right| \tag{4.48}$$

where φ_Q represents the weighting which normalizes the magnitude relation between the real and reactive powers.

4.5.2 Starting Current Limitation

As explained in sub-section 4.4.5, high stator currents appear during the machine start-up period, which can cause damage to power switches devices.

Flexibility offered by the model predictive control method regarding the inclusion of hard constrains in the cost function, can be taken advantage of to limit the high current during the motor start-up stage. The modified cost function that takes this constrain into consideration can be expressed as

$$g_p = \left|P_{sref} - P_s[k+1]\right| + \varphi_Q \left|\left|Q_{sref}\right| - \left|Q_s[k+1]\right|\right| + K_{Islim} \tag{4.49}$$

where K_{Islim} is defined as:

$$K_{Islim} = \begin{cases} \infty & if \quad |\boldsymbol{I}_s[k+1]| > \boldsymbol{I}_{smax} \\ 0 & if \quad |\boldsymbol{I}_s[k+1]| \leq \boldsymbol{I}_{smax} \end{cases} \tag{4.50}$$

The main objective of this modified cost function is to discard any voltage space phasor that produces a current that exceeds the pre-selected stator current limit, $\boldsymbol{I}_{smax}$. Hence, if a voltage space phasor creates a stator current higher than $\boldsymbol{I}_{smax}$, the term K_{Islim} will make the cost function become very large, and this voltage space phasor will not be considered. If, on the other hand, the voltage space phasor produce a stator current with a magnitude equal or lower than $\boldsymbol{I}_{smax}$, the term K_{Islim} will assume a value of zero, and the cost function will take the form of (4.48), and the voltage space phasor will be considered for the minimization of the power errors.

CHAPTER 5:
SIMULATION RESULTS

To verify performance of the proposed control strategies, several simulations studies were carried out in ®Matlab ™Simulink environment. The parameters of the motor are listed in Table 5.1 [16]. The reference speed is set to $300\ rad/s$. At t = 1.01 s, t = 1.5 s, and t = 2 load torques of 35 N-m, 80 N-m and -90 N-m are applied, respectively.

Table 5.1 Parameters of the simulated induction motor.

Rated Power [hp]	Stator Voltage [V]	Rs [ohm]	Rr [ohm]	Ls [H]	Lr [H]	Lm [H]
30	230	0.294	0.156	0.0424	0.0417	0.041
J [Kg*m2]	f [Hz]	Pp	wm [rpm]	Tn [N.m]	In [A]	Stator flux [Wb]
0.4	60	3	1168	183	39.5	0.58

5.1 Six-Sector Direct Power Control

- *Method 1*

In this case study, consumed real power is calculated using method 1, presented in sub-section 4.4.2.

As can be seen in Fig 5.1, the motor reaches the reference speed in 1 second. The estimated power follows the reference value and fast responses of real power, reactive power, and electromagnetic torque are observed when the load torque steps are applied. Fig 5.2 shows three-phase stator currents and the harmonic spectrum of a phase current. In addition, the stator current space phasor is also shown in Fig 5.2. As already mentioned in sub-section 4.4.5, during motor start-up period high stator currents are present. To limit the high starting current, the

strategy presented in sub-section 4.4.5 is used. The impact of inclusion of the overcurrent protection can be seen in Fig 5.3.

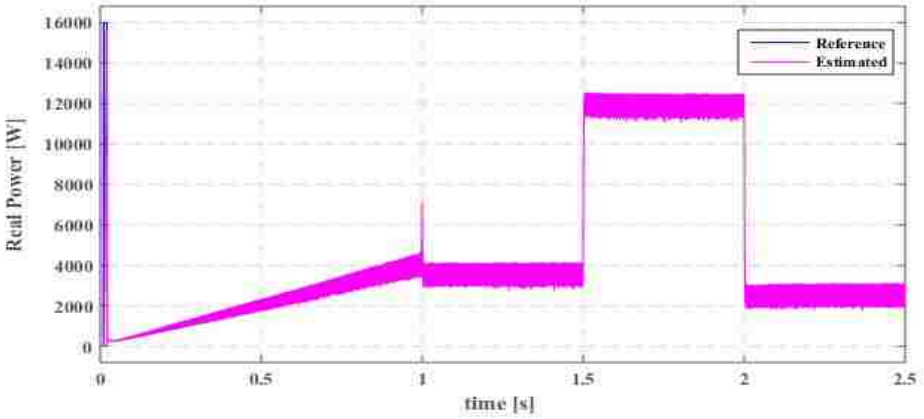

(a)

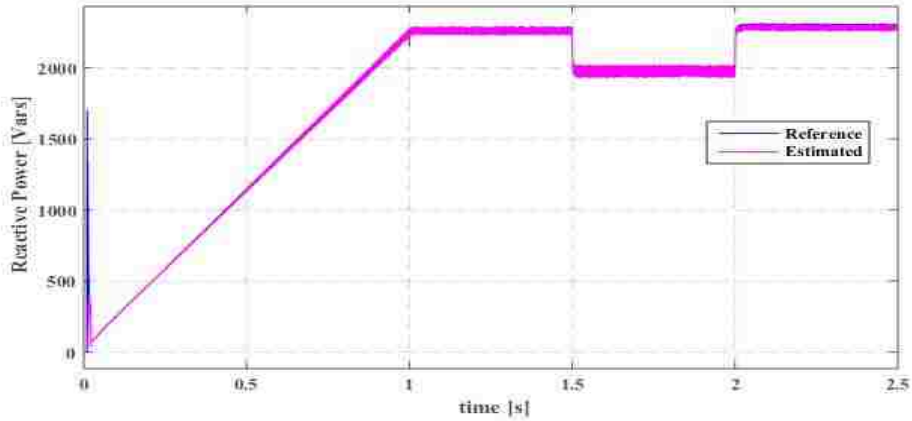

(b)

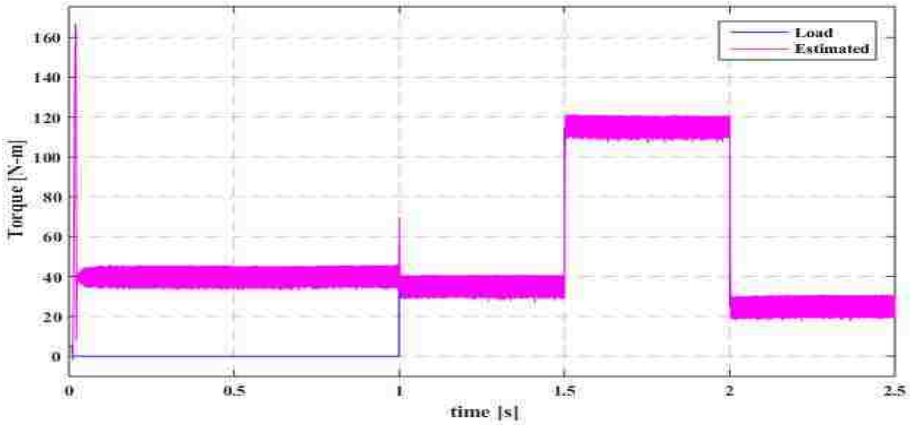

(c)

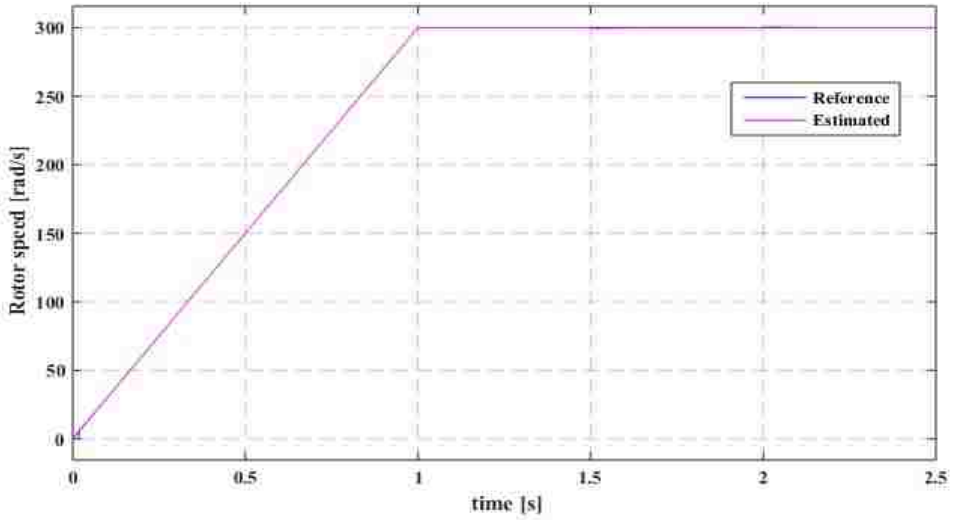

(d)

Figure 5.1 (a) Real Power [W], (b) Reactive Power [Vars], (c) Load and Electromagnetic torque [N-m], (d) Rotor speed [rad/s]. (six-sector, Method 1)

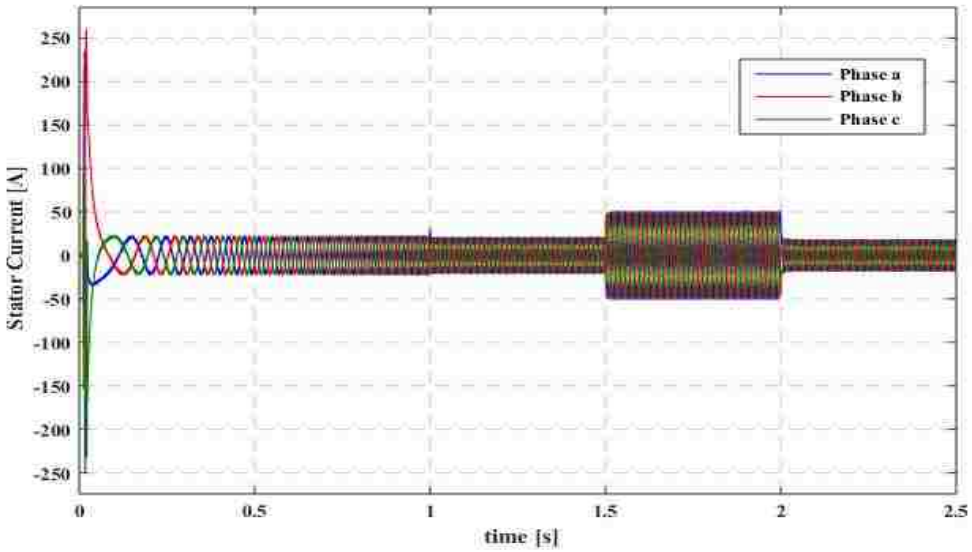

(a)

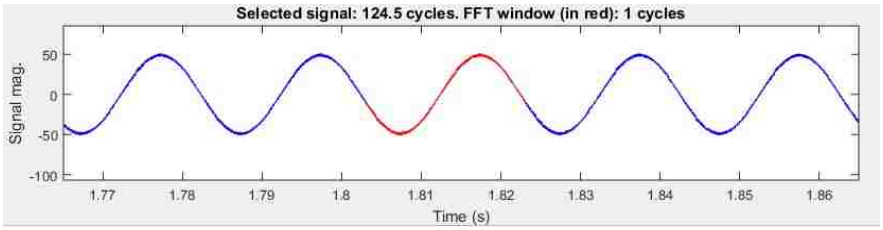

(b)

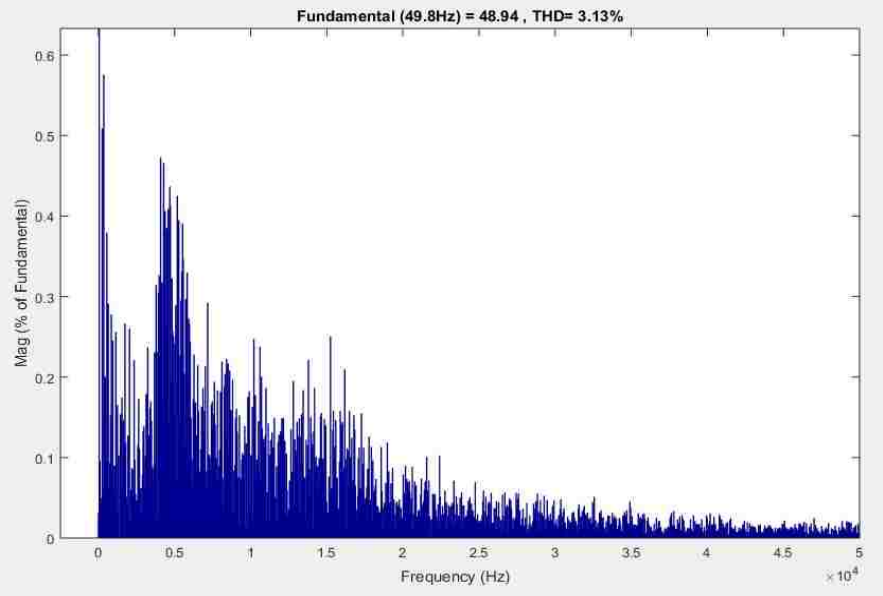

(c)

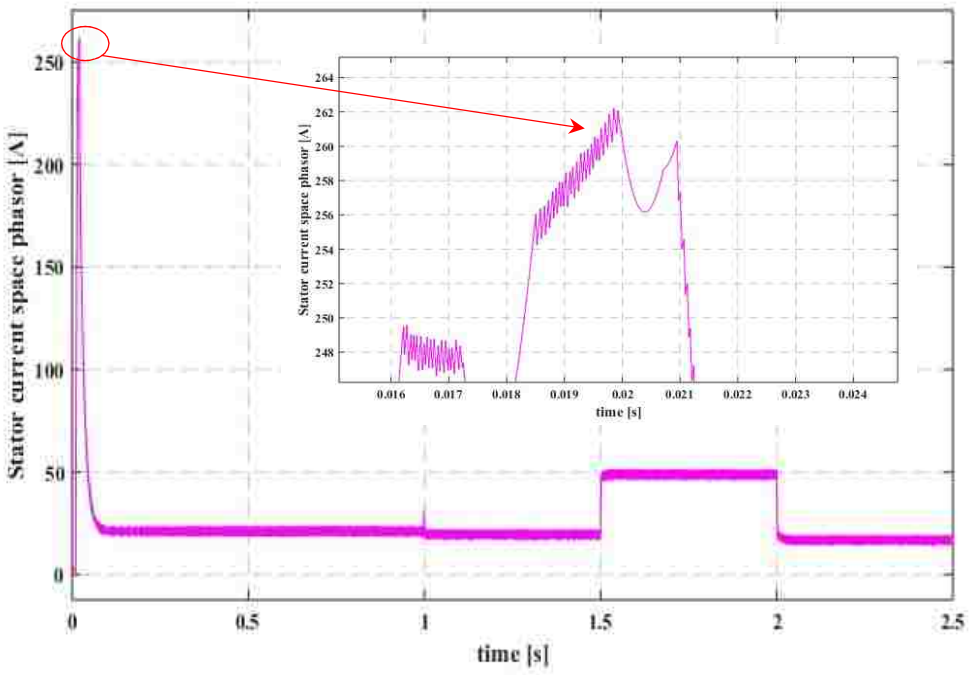

(d)

Figure 5.2 (a) Three-phase stator currents [A], (b)-(c) Harmonic spectrum of phase stator current, (d) Stator current space phasor showing overcurrent during motor start-up period [A]. (six-sector, Method 1)

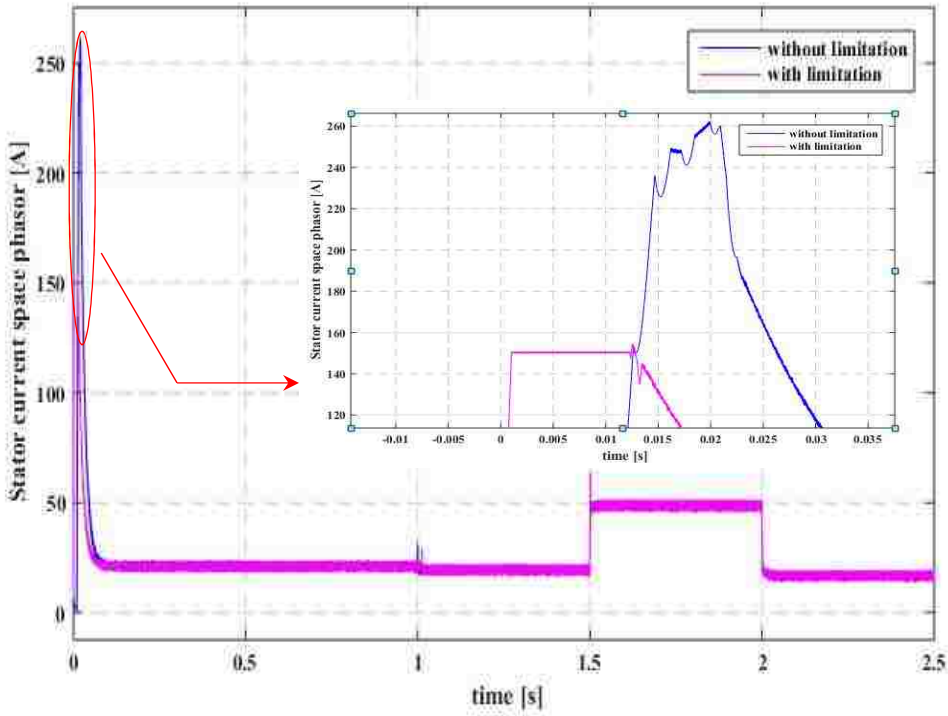

Figure 5.3 Stator current with overcurrent limitation strategy during motor start-up stage. (six-sector, Method 1)

- *Method 2*

Simulation results employing method 2 to calculate the consumed real power are shown in Figs 5.4-5.6. In the second method, the real power is calculated using measured voltages and currents. This constitutes the major advantage of the second method over the first one, since the only two quantities that need to be estimated in order to calculate the real power are stator flux and synchronous speed, whereas in method 1 electromagnetic torque is also required. This method also offers an excellent dynamic response of real and reactive power to load step changes. As in method 1, motor reaches the reference speed in 1 second, and current limitation strategy can also be included.

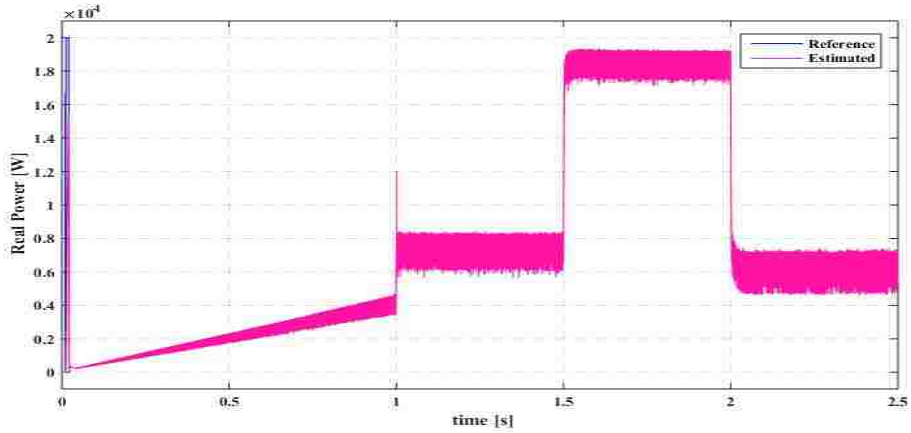
×10^4
Real Power [W]
time [s]
Reference
Estimated

(a)

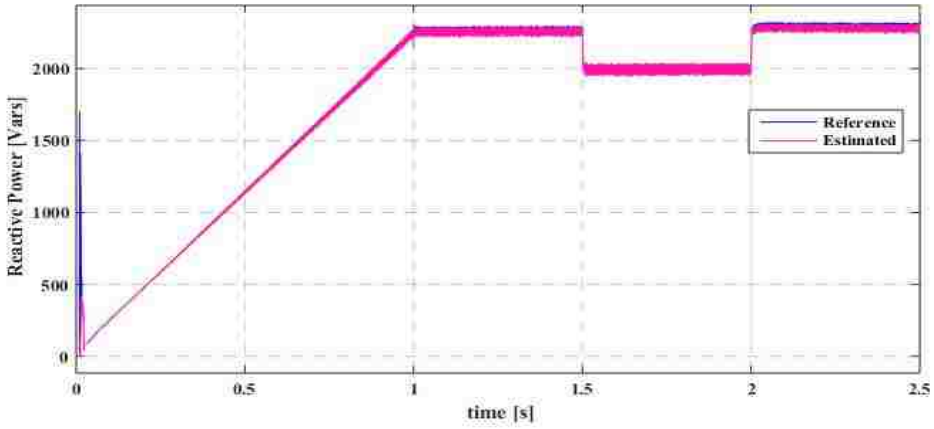
Reactive Power [Vars]
time [s]
Reference
Estimated

(b)

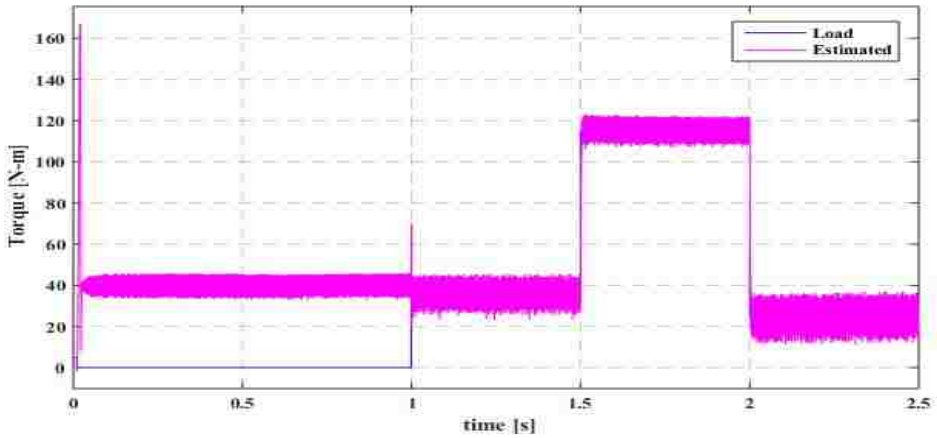
Torque [N-m]
time [s]
Load
Estimated

(c)

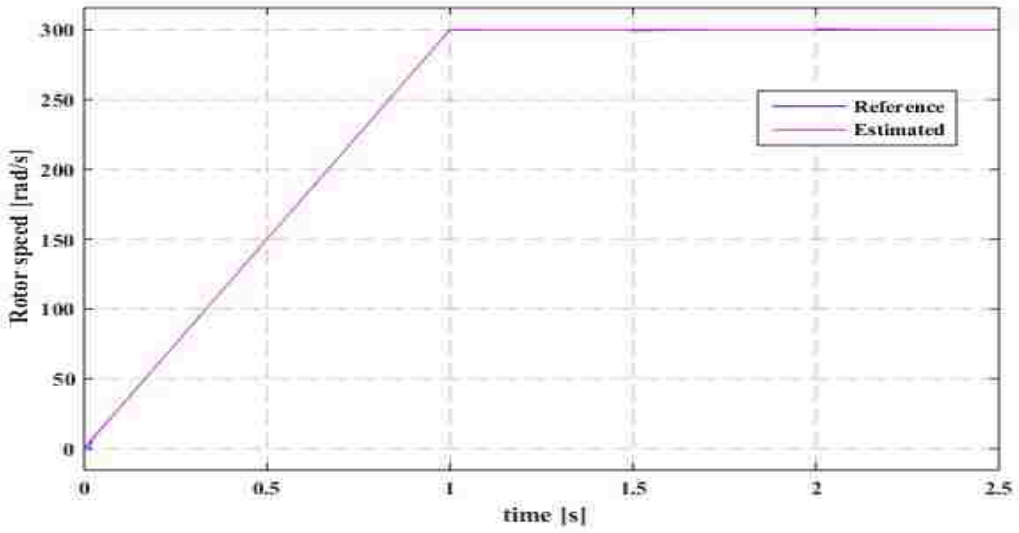

(d)

Figure 5.4 (a) Real Power [W], (b) Reactive Power [Vars], (c) Load and electromagnetic torque [N-m], (d) Rotor speed [rad/s]. (six-sector, Method 2)

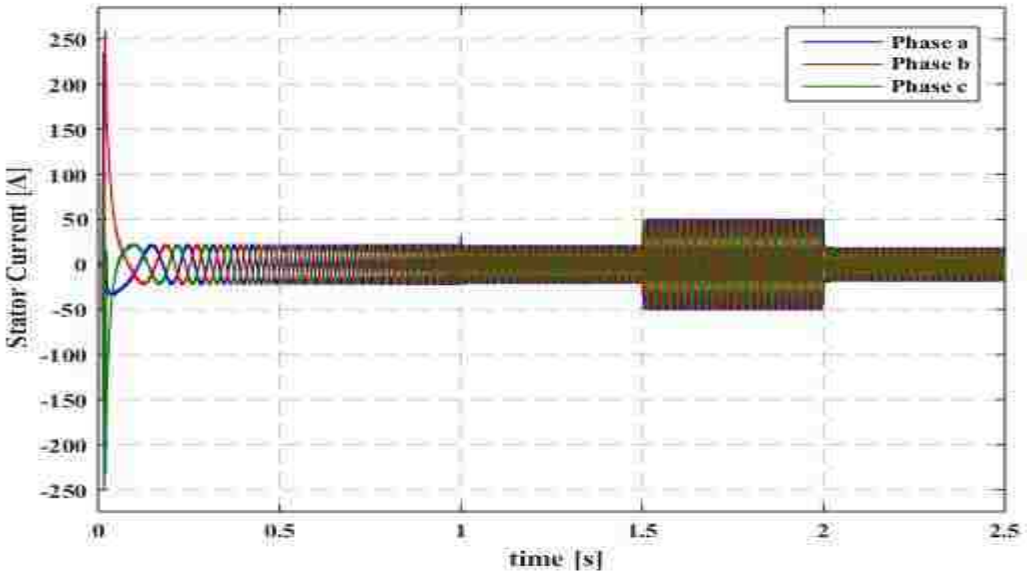

(a)

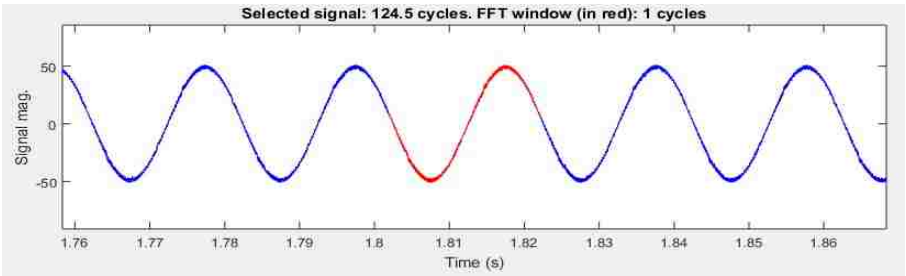

(b)

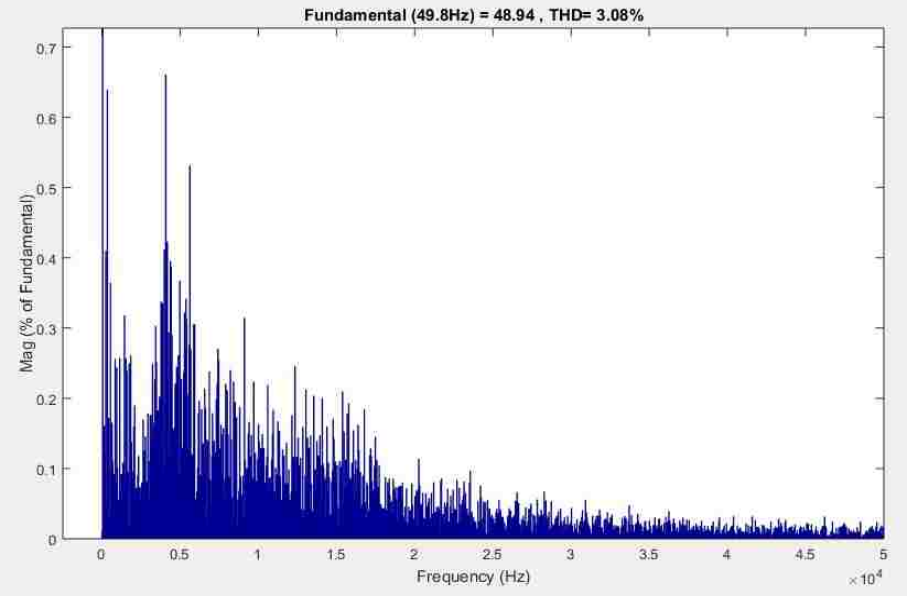

(c)

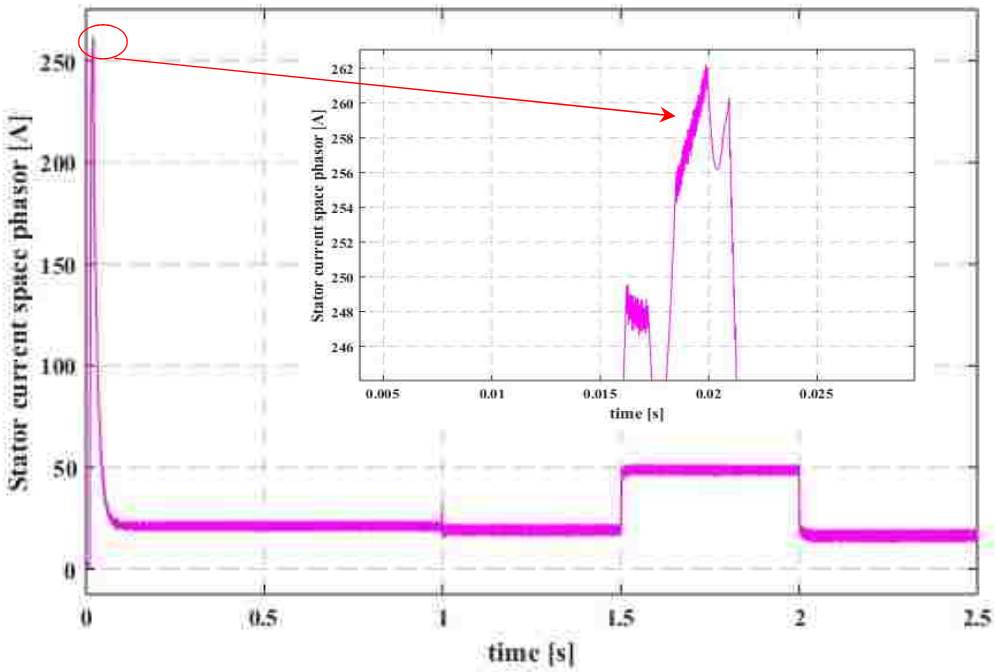

(d)

Figure 5.5 (a) Three-phase stator currents [A], (b)-(c) Harmonic spectrum of phase stator current, (d) Stator current space phasor showing overcurrent during motor start-up period [A]. (six-sector, Method 2)

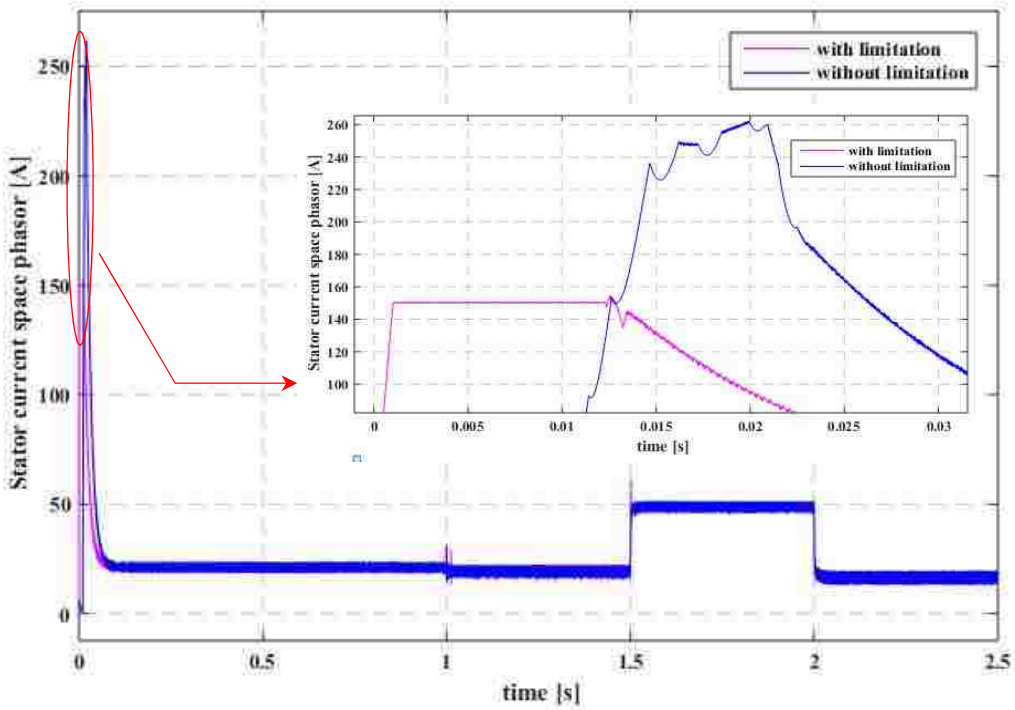

Figure 5.6 Stator current with overcurrent limitation strategy during motor start-up stage. (six-sector, Method 2)

5.2 Twelve-Sector Direct Power Control

- *Method 1*

Motor performance with twelve-sector control strategy, method 1, under the same load conditions as of the six-sector method is shown in Figs 5.7-5.9. Motor is started at no-load and it reaches the reference speed in 1 second. The twelve-sector strategy develops fast responses of real power, reactive power, and electromagnetic torque when the load torque steps are applied. A stator current of 280 A is produced during the motor start-up period. The overcurrent protection is applied thanks to which the stator current is limited to 150 A.

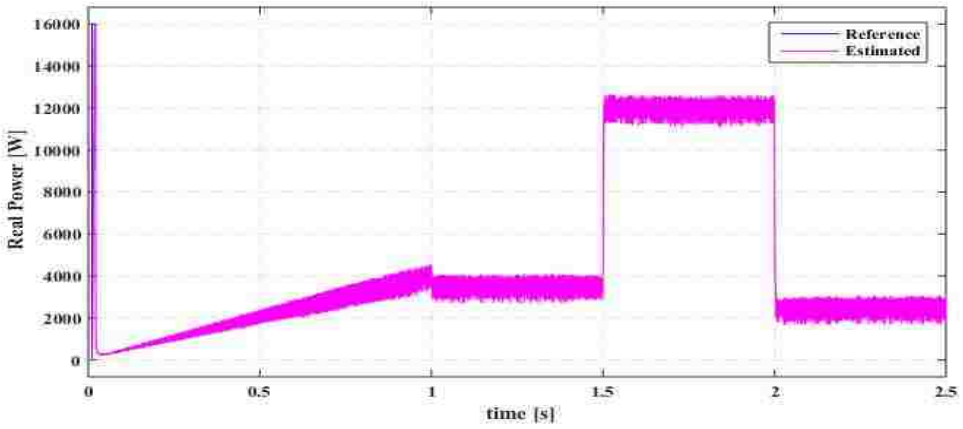
Real Power [W]
time [s]
Reference
Estimated

(a)

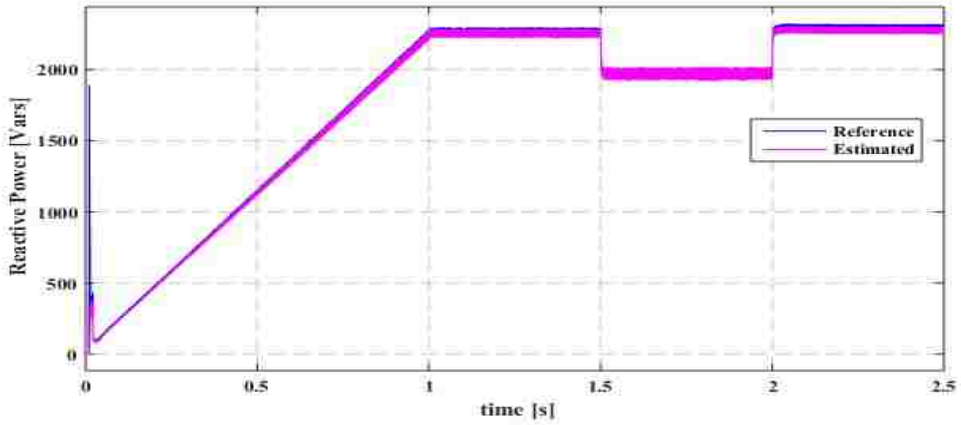
Reactive Power [Vars]
time [s]
Reference
Estimated

(b)

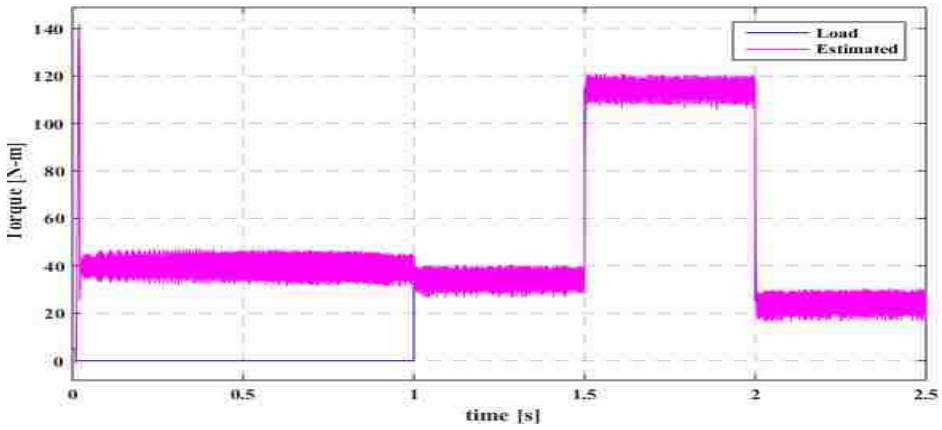
Torque [N-m]
time [s]
Load
Estimated

(c)

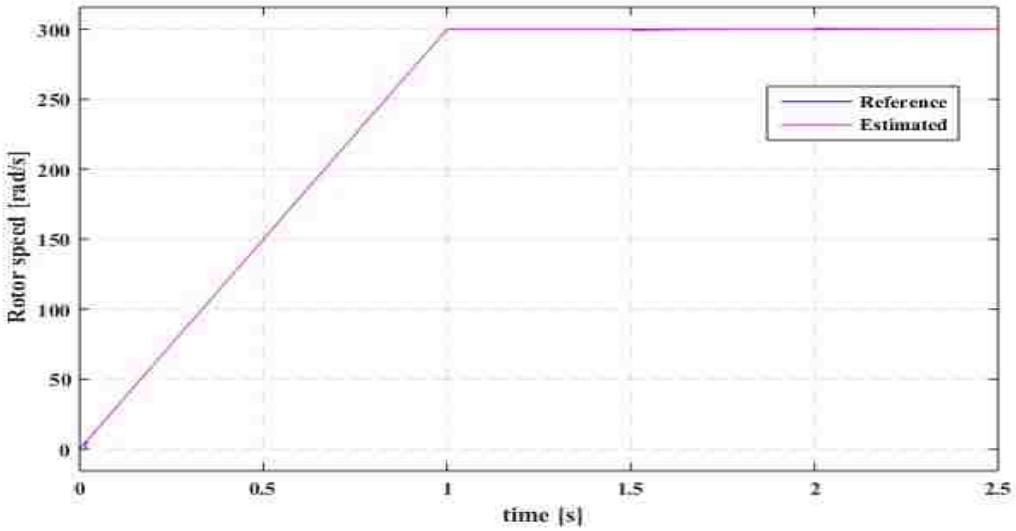

(d)

Figure 5.7 (a) Real Power [W], (b) Reactive Power [Vars], (c) Load and electromagnetic torque [N-m], (d) Rotor speed [rad/s]. (twelve-sector, Method 1)

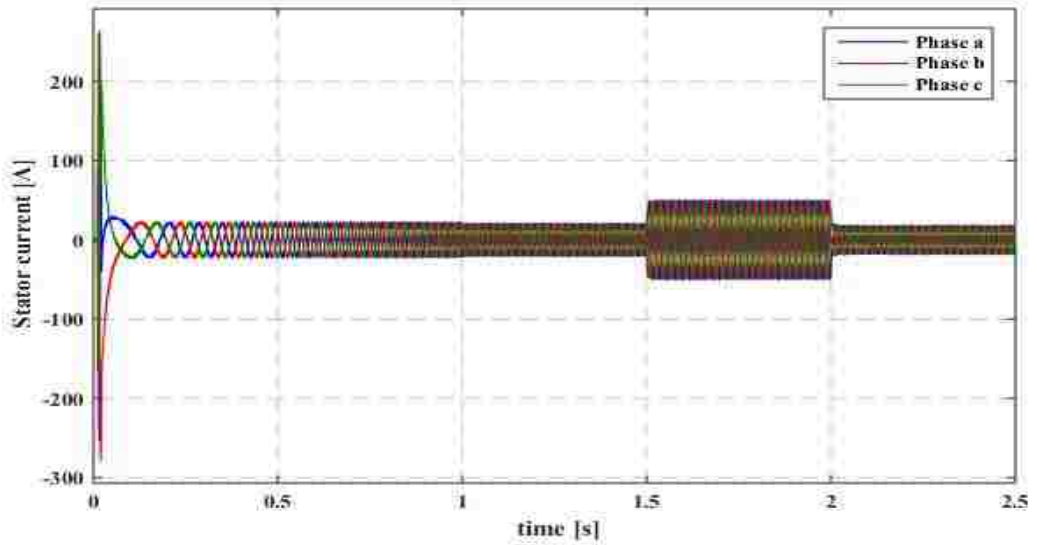

(a)

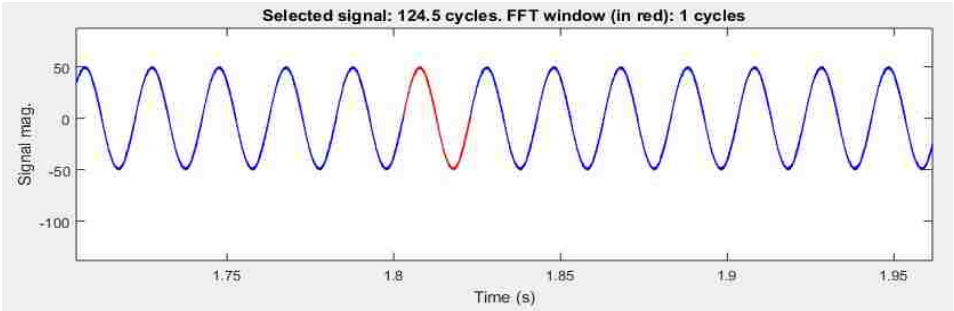

(b)

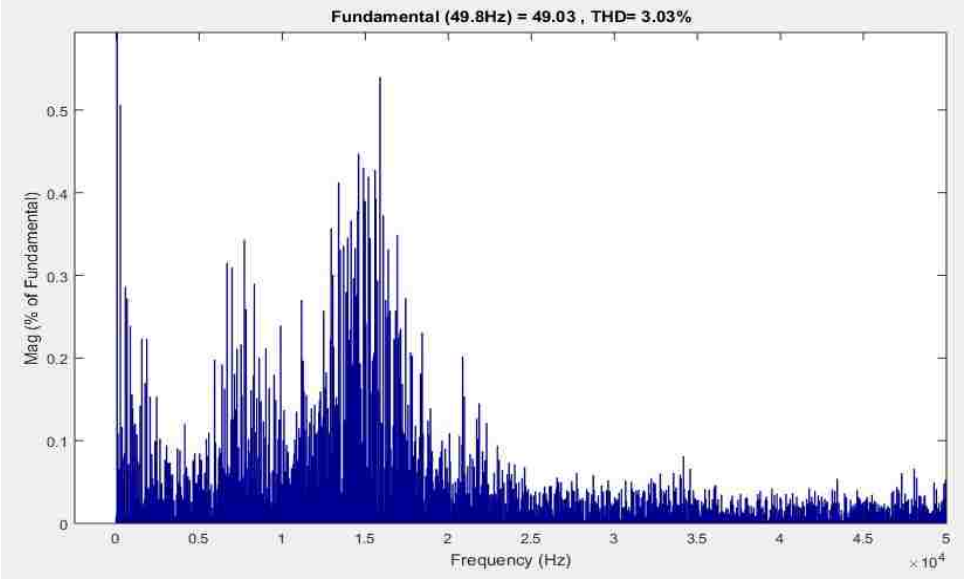

(c)

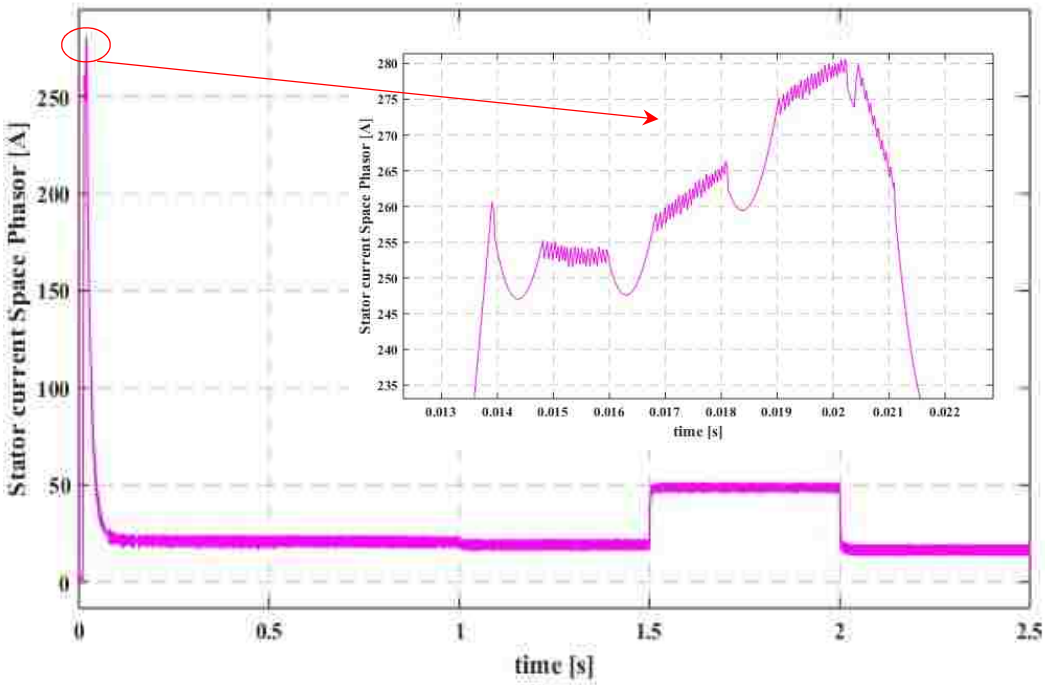

(d)

Figure 5.8 (a) Three-Phase stator currents [A], (b)-(c) Harmonic spectrum of phase stator current, (d) Stator current space phasor showing overcurrent during motor start-up period [A]. (twelve-sector, Method 1)

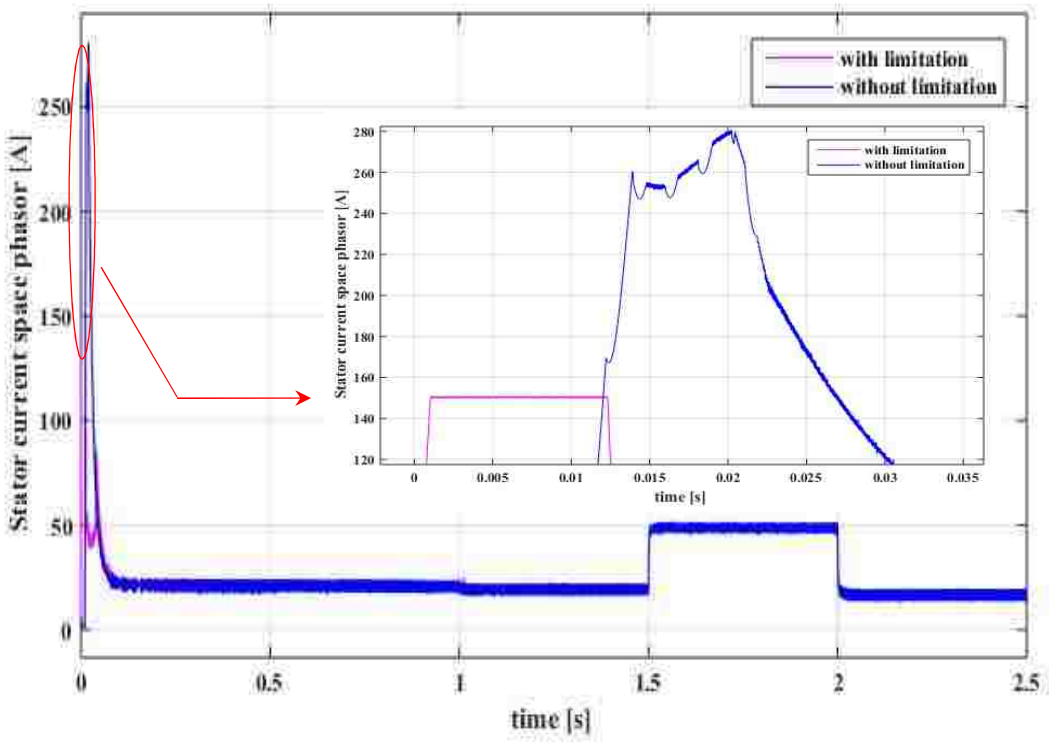

Figure 5.9 Stator current with overcurrent limitation strategy during motor start-up stage. (twelve-sector, Method 1)

A comparative study of the six-sector and twelve-sector strategies in terms of real power and torque ripples is carried out and the results are shown in Fig 5.10. It can be concluded that the twelve-sector method outperforms the six-sector method and results in reduced real power and torque ripples.

- *Method 2*

Motor is operated with the same speed and load-torque profile and the results are illustrated in Figs 5.11-5.13. As in the previous cases, this method also offers excellent dynamic responses of real power, reactive power, and electromagnetic torque with virtually no overshoot when load torque steps are applied.

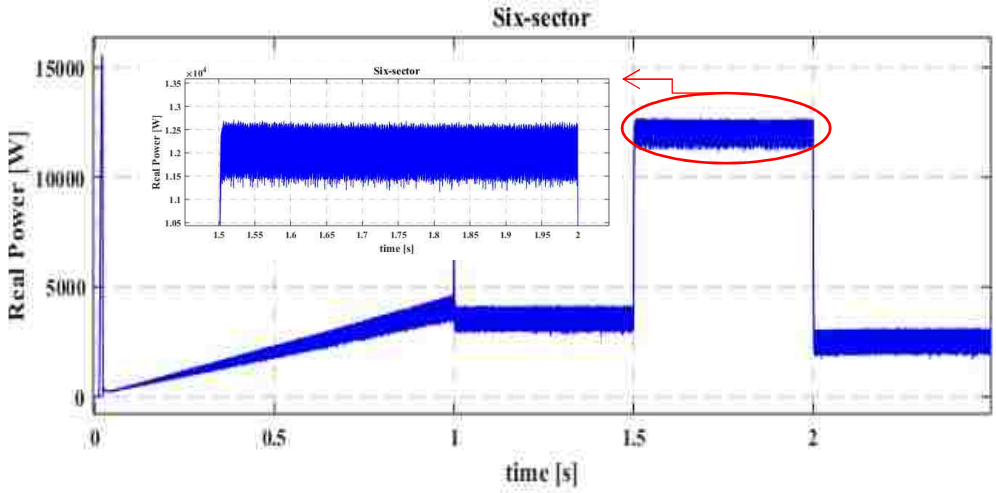
Six-sector
Real Power [W]
time [s]
Six-sector
Real Power [W]
time [s]

(a)

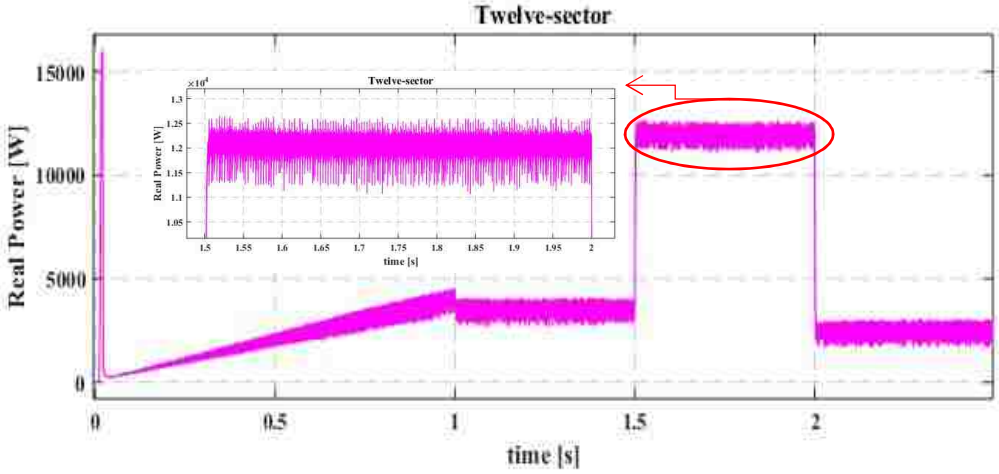
Twelve-sector
Real Power [W]
time [s]
Twelve-sector
Real Power [W]
time [s]

(b)

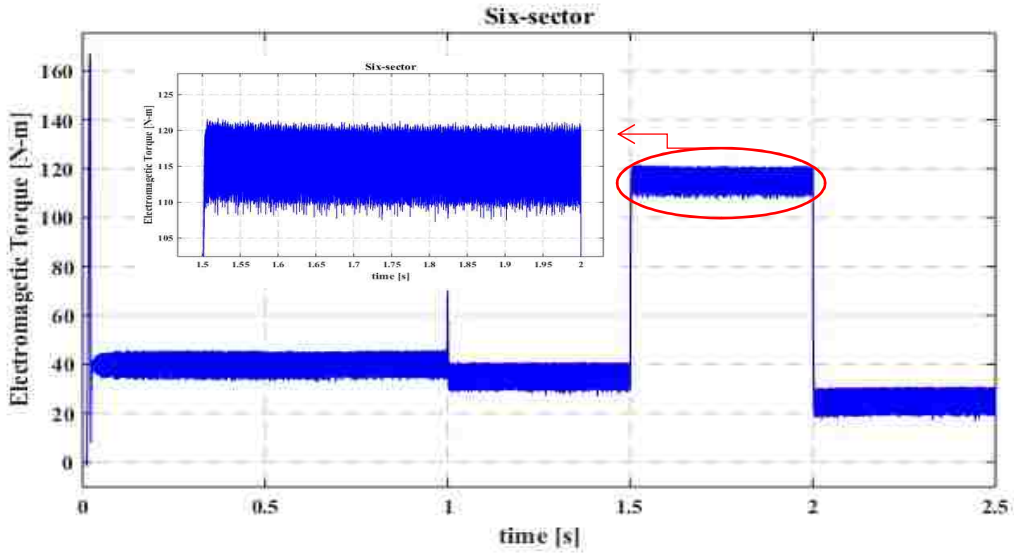
Six-sector
Electromagetic Torque [N-m]
time [s]
Six-sector
Electromagetic Torque [N-m]
time [s]

(d)

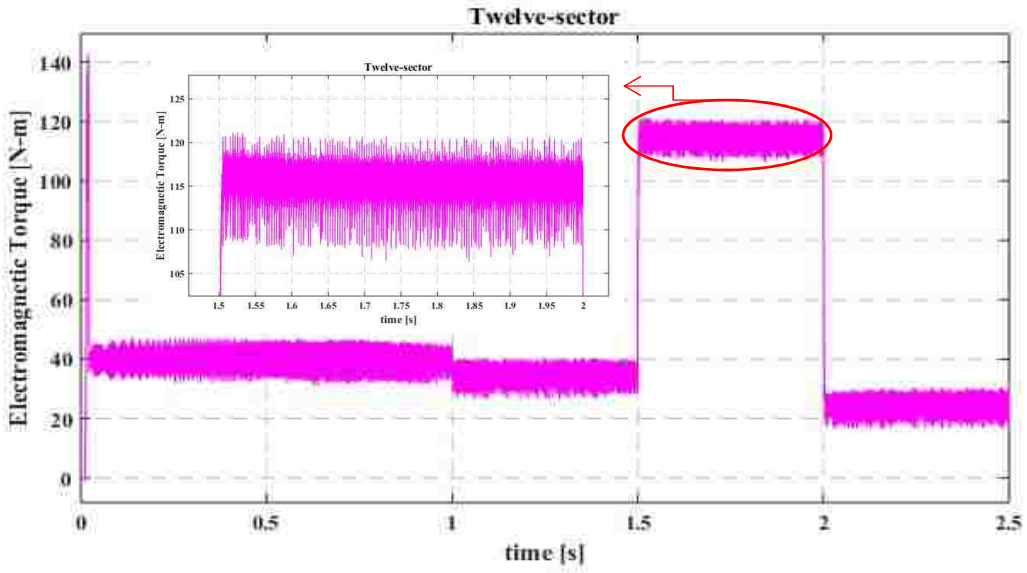

(d)

Figure 5.10 Response comparisons between six-sector and twelve-sector: (a)-(b) Real Power [W], (c)-(d) Electromagnetic torque [N-m], (Method 1)

Fig 5.14 compares real power and electromagnetic torque ripples with six-sector and twelve-sector strategies. Similar to the previous case, twelve-sector strategy results in reduced real power and torque ripples. Comparing at Fig 5.5 (b)-(c) and Fig 5.12 (b)-(c), it can be noticed that the stator current quality improves under the twelve sector strategy as well.

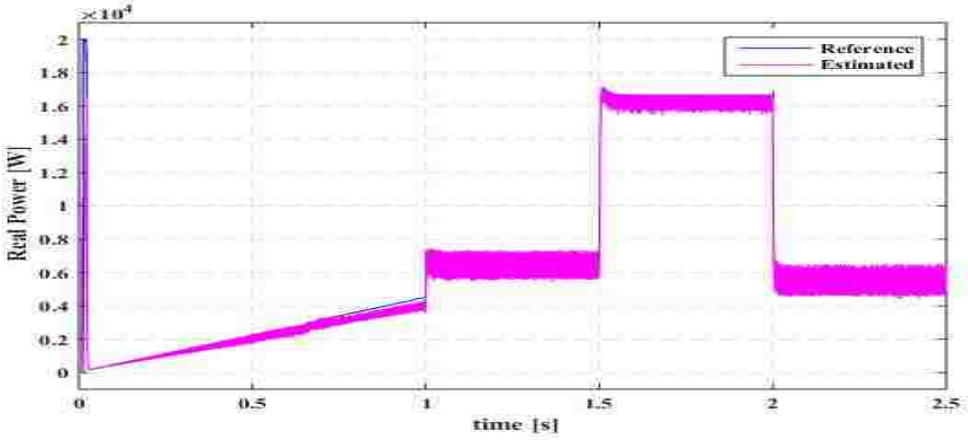

(a)

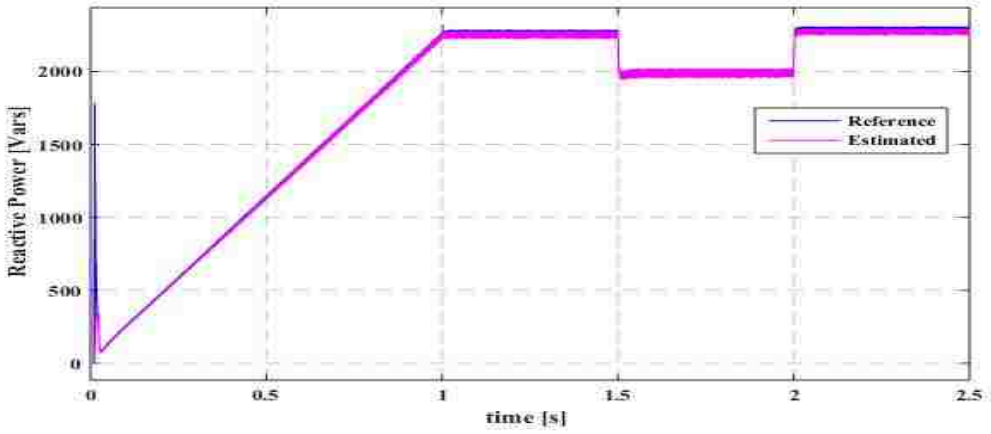

(b)

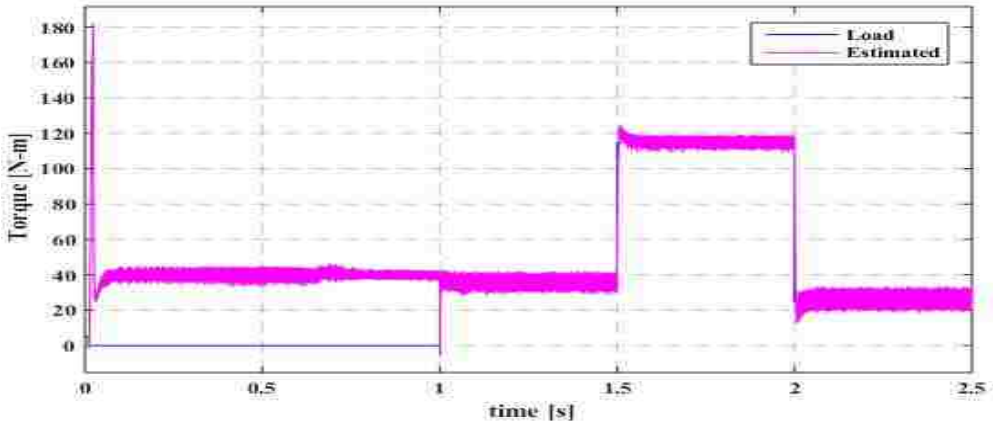

(c)

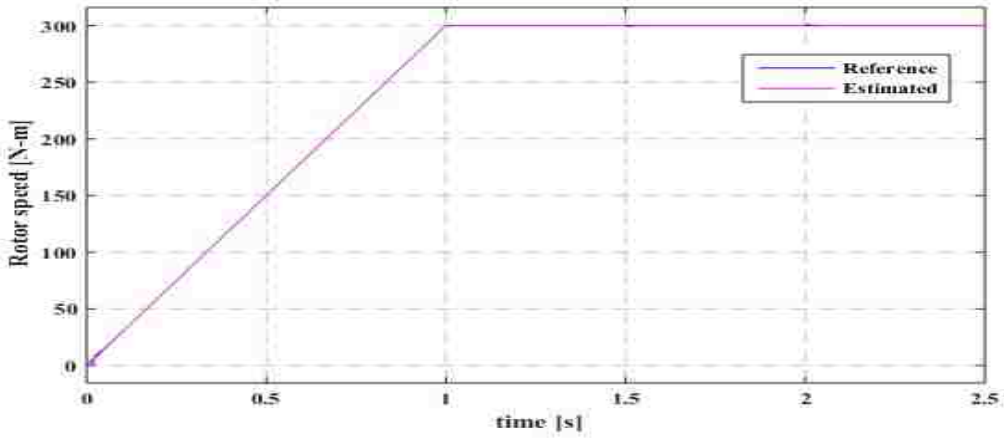

(d)

Figure 5.11 (a) Real Power [W], (b) Reactive Power [Vars], (c) Load and electromagnetic torque [N-m], (d) Rotor speed [rad/s]. (twelve-sector, Method 2)

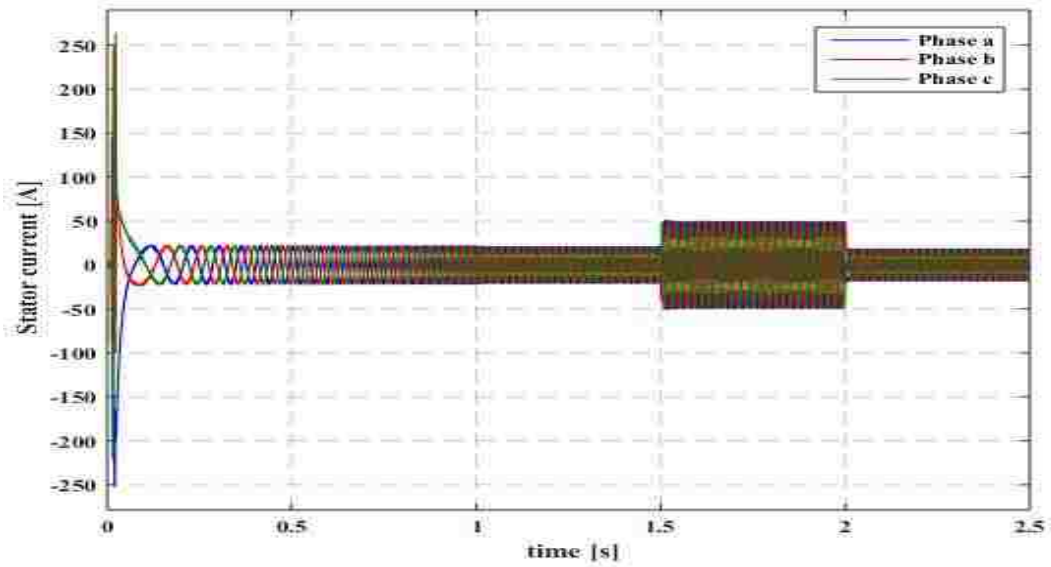
Phase a
Phase b
Phase c
Stator current [A]
time [s]

(a)

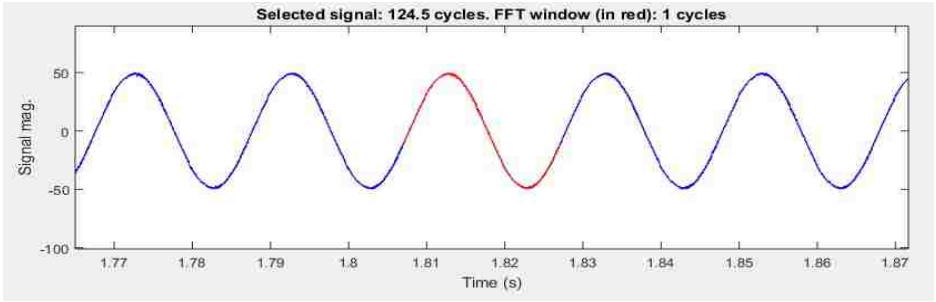
Selected signal: 124.5 cycles. FFT window (in red): 1 cycles
Signal mag.
Time (s)

(b)

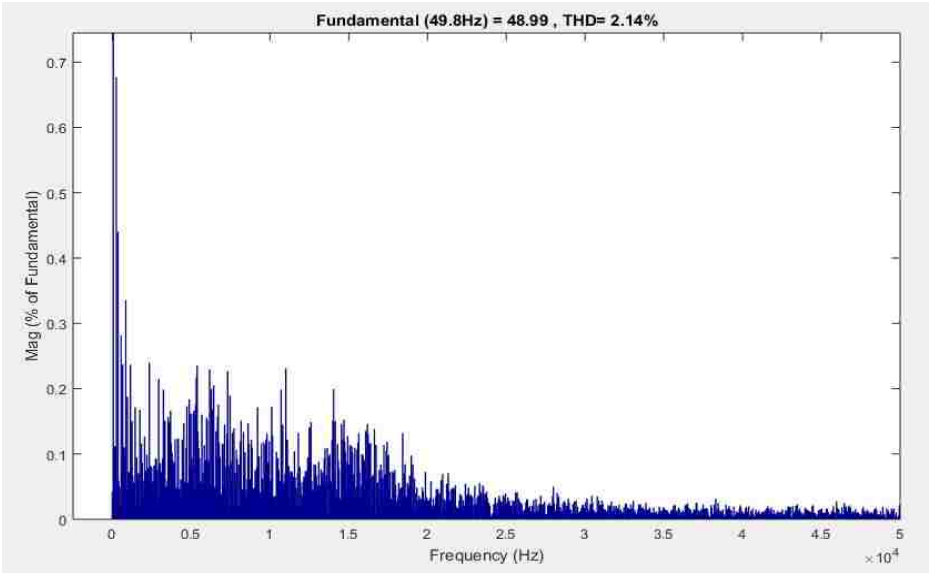
Fundamental (49.8Hz) = 48.99 , THD= 2.14%
Mag (% of Fundamental)
Frequency (Hz)

(c)

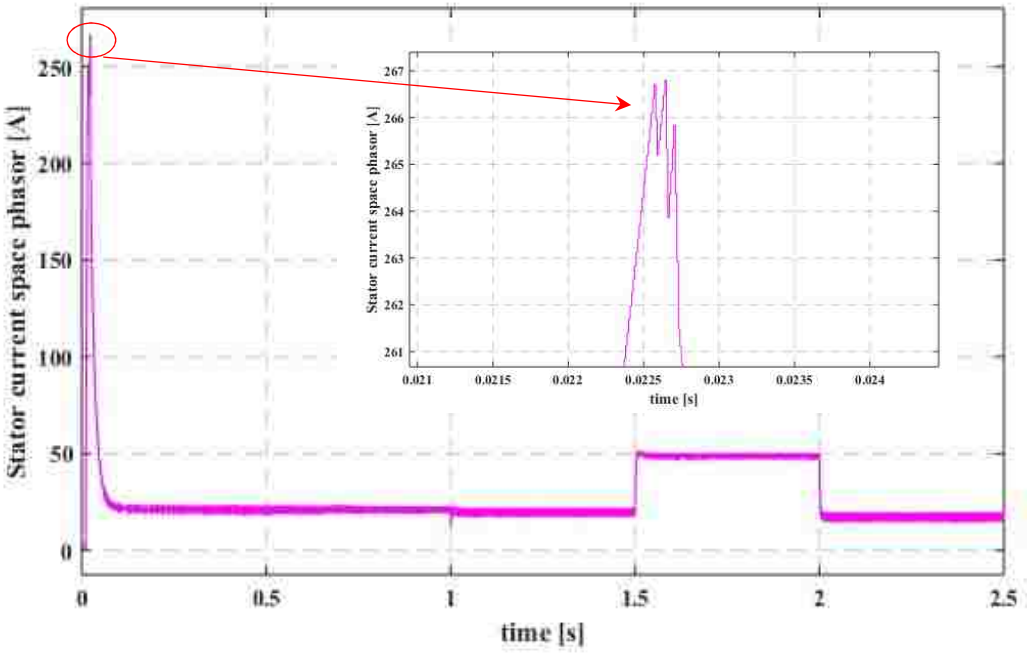

(c)

Figure 5.12 (a) Three-phase stator currents [A], (b)-(c) Harmonic spectrum of phase stator current, (d) Stator current space phasor showing overcurrent during motor start-up period [A]. (twelve-sector, Method 2)

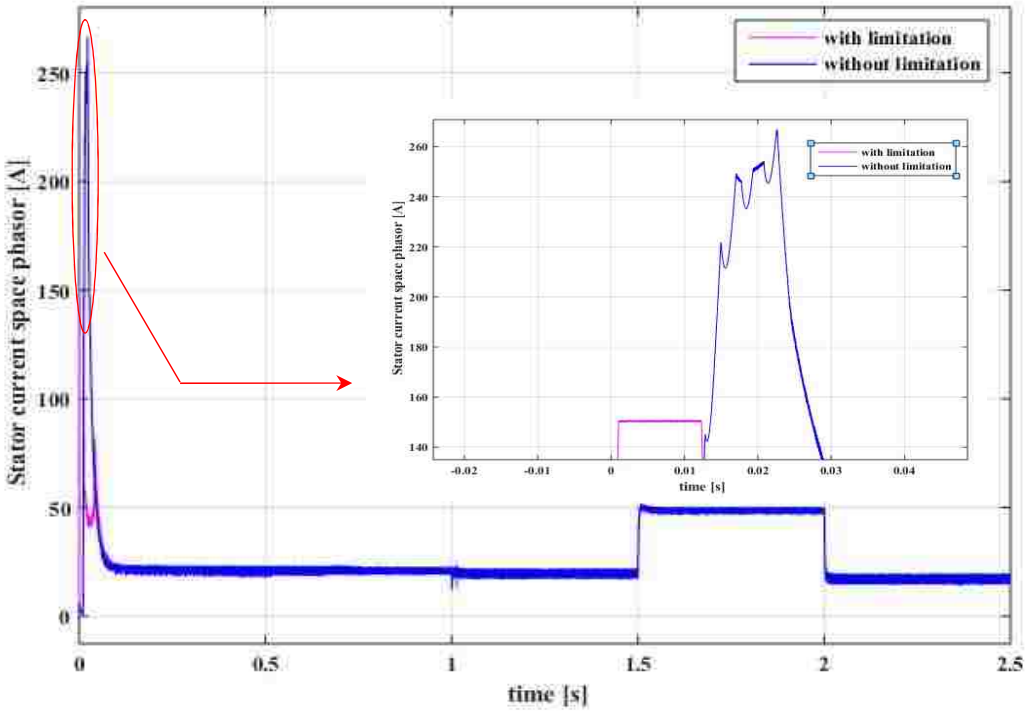

Figure 5.13 Stator current with overcurrent limitation strategy during motor start-up stage. (twelve-sector, Method 2)

5.3 MPPC Strategy

As it can be seen in Fig 5.15, the MPPC control strategy offers fast responses of real power, reactive power, and electromagnetic torque when load torque steps are applied. This outstanding dynamic response is achieved due to lack of inner stator current loops with PI controllers. As a consequence, no bandwidth restrictions are imposed on the power and torque responses. Fig 5.16 shows the stator current and its harmonic spectrum, which presents a low THD content. In addition, the magnitude of the stator current space phasor is shown in Fig 5.16, with maximum value of 276 A. In order to limit the overcurrent during motor start-up period, the current limitation strategy introduced in sub-section 4.5.2 is employed. As in the previous cases, the predefined current limit is 150 A. The effectiveness of overcurrent limitation strategy is shown in Fig. 5.17.

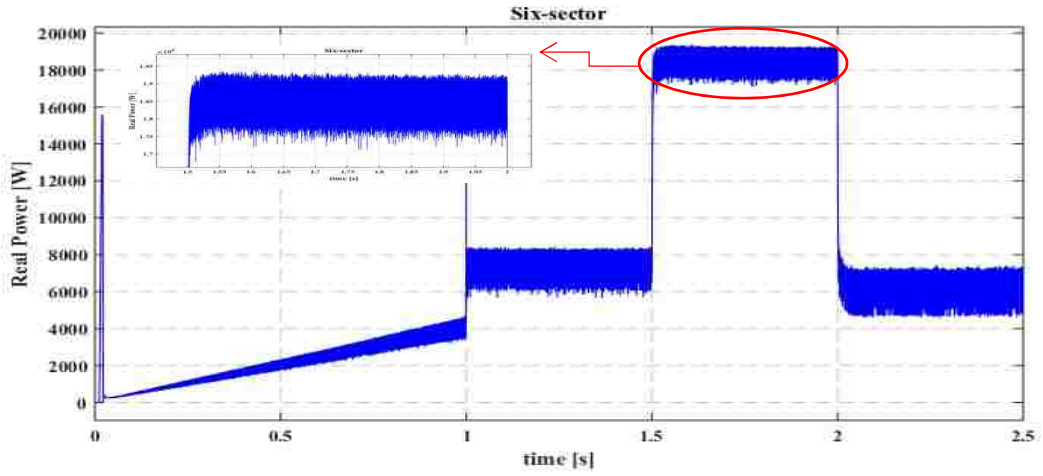

(a)

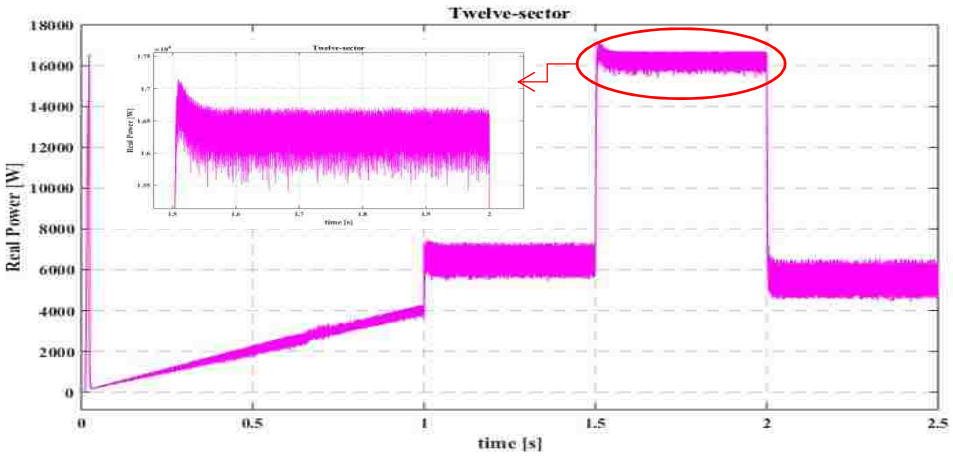

(b)

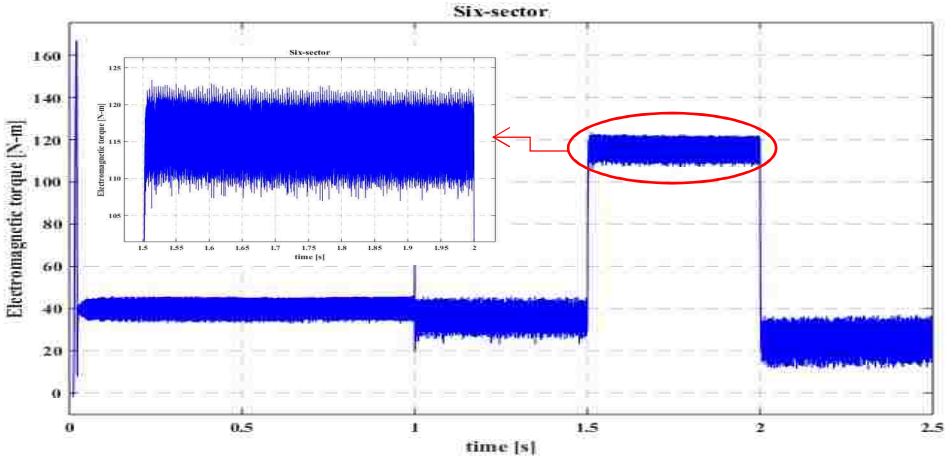

(c)

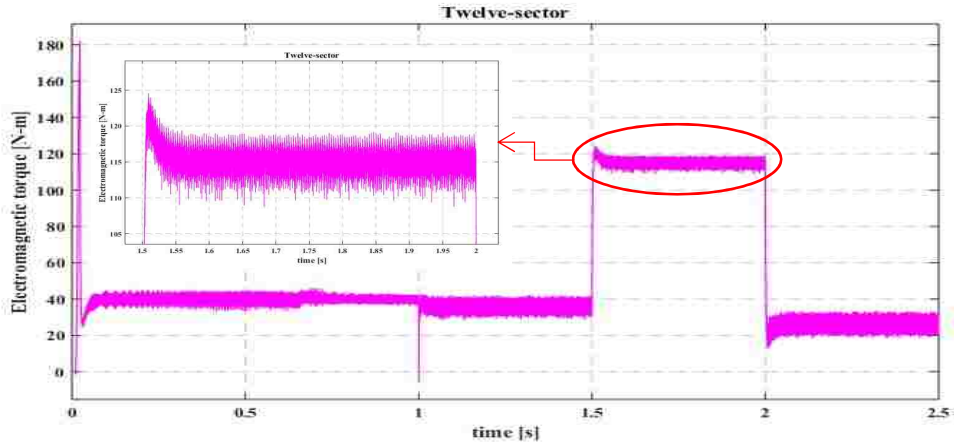

(d)

Figure 5.14 Response comparisons between six-sector and twelve-sector: (a)-(b) Real Power [W], (c)-(d) Electromagnetic torque [N-m], (Method 2)

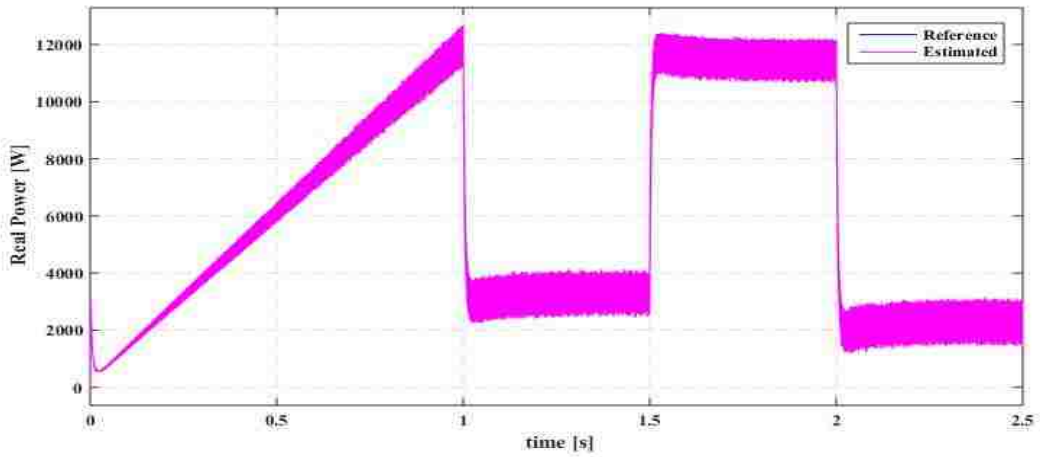
Reference
Estimated
Real Power [W]
12000
10000
8000
6000
4000
2000
0
0
0.5
1
1.5
2
2.5
time [s]

(a)

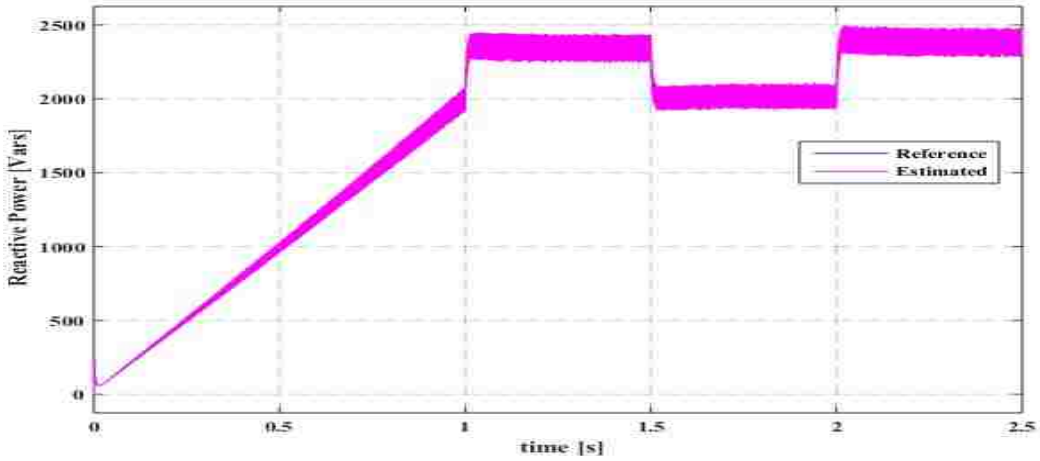
Reference
Estimated
Reactive Power [Vars]
2500
2000
1500
1000
500
0
0
0.5
1
1.5
2
2.5
time [s]

(b)

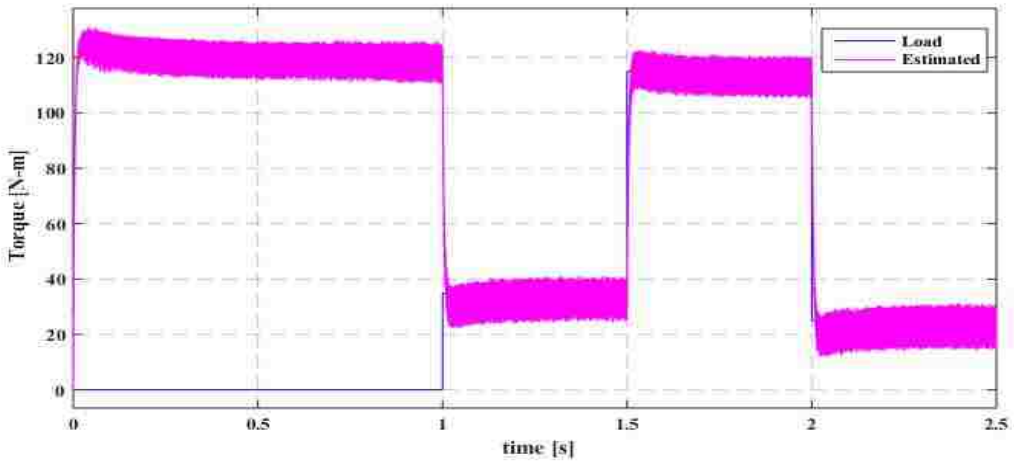
Load
Estimated
Torque [N-m]
120
100
80
60
40
20
0
0
0.5
1
1.5
2
2.5
time [s]

(c)

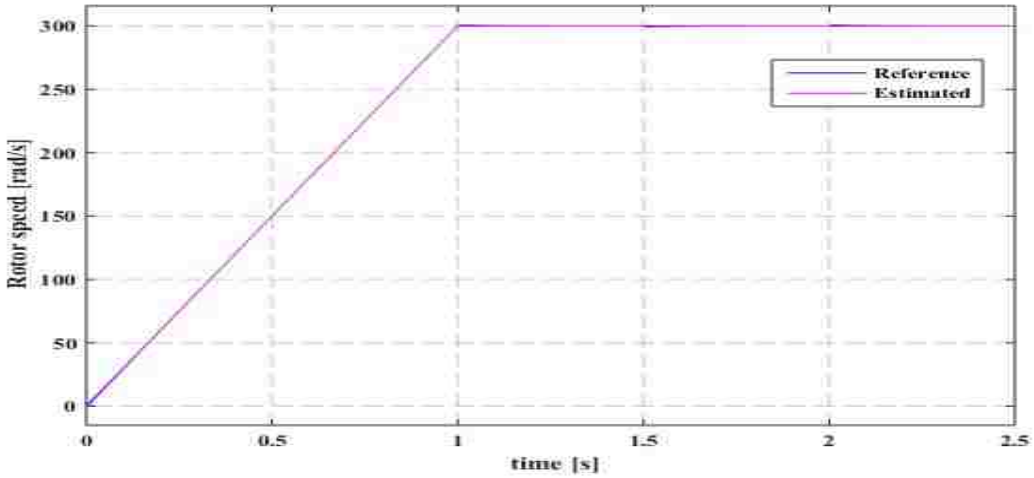

(d)

Figure 5.15 (a) Real Power [W], (b) Reactive Power [Vars], (c) Load and electromagnetic torque [N-m], (d) Rotor speed [rad/s]. (MPPC)

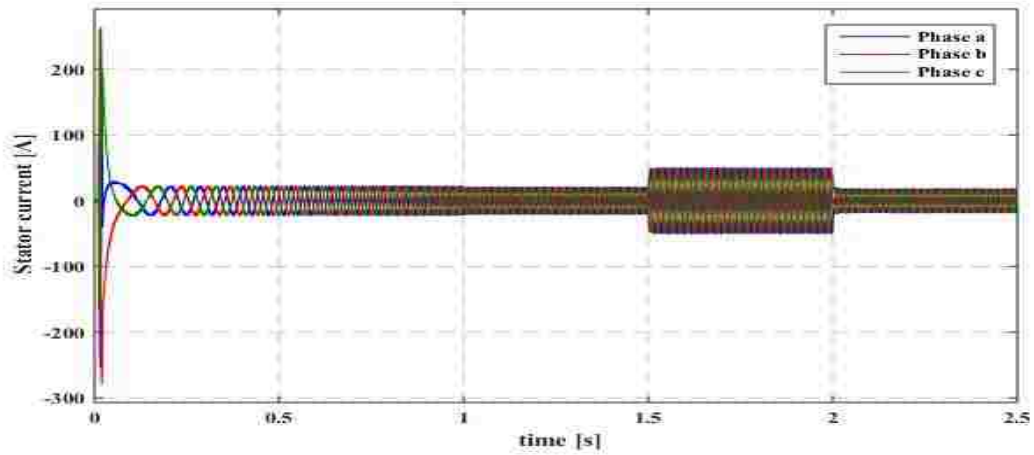

(a)

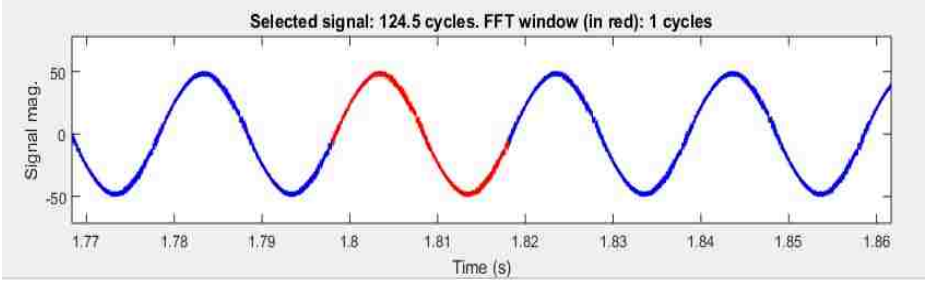

(b)

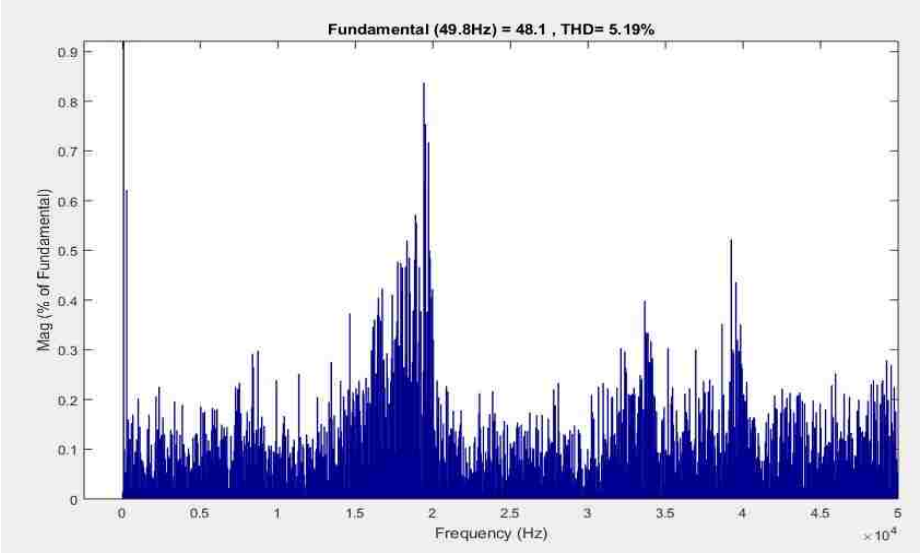

(c)

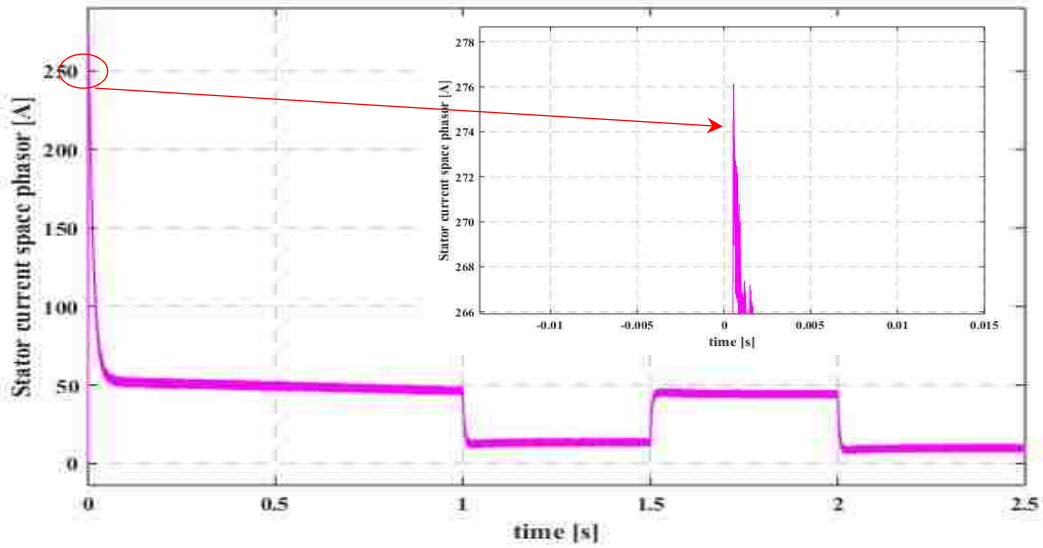

(d)

Figure 5.16 (a) Three-phase stator currents [A], (b)-(c) Harmonic spectrum of phase stator current, (d) Stator current space phasor showing overcurrent during motor start-up period [A]. (MPPC)

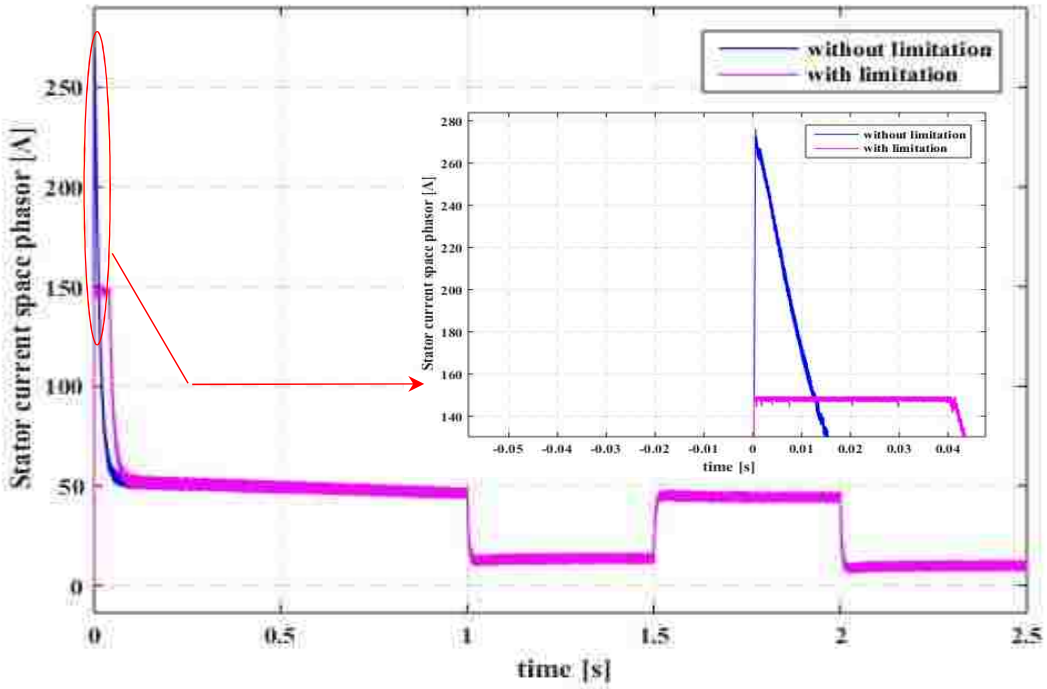

Figure 5.17 Stator current with overcurrent limitation strategy during motor start-up stage. (MPPC)

5.4 Parameter Variations

To study the robustness of the proposed control strategies against motor parameter variations, several studies are carried out. The machine parameters that are prone to variations are: stator resistance and magnetizing inductance. The stator resistance varies with temperature, and as a consequence, accurate estimation of the stator flux-linkage can be adversely affected. The magnetizing inductance changes with iron saturation negatively, affecting reactive power calculation. For the same load and reference speed conditions, value of stator resistance is increased by a factor of 1.5, and magnetizing inductance decreased by a factor of 0.5. The simulations were carried out for the six-sector case (method 1 and 2), twelve sector case (method 1 and 2), and MPPC in presence of these parameter uncertainties.

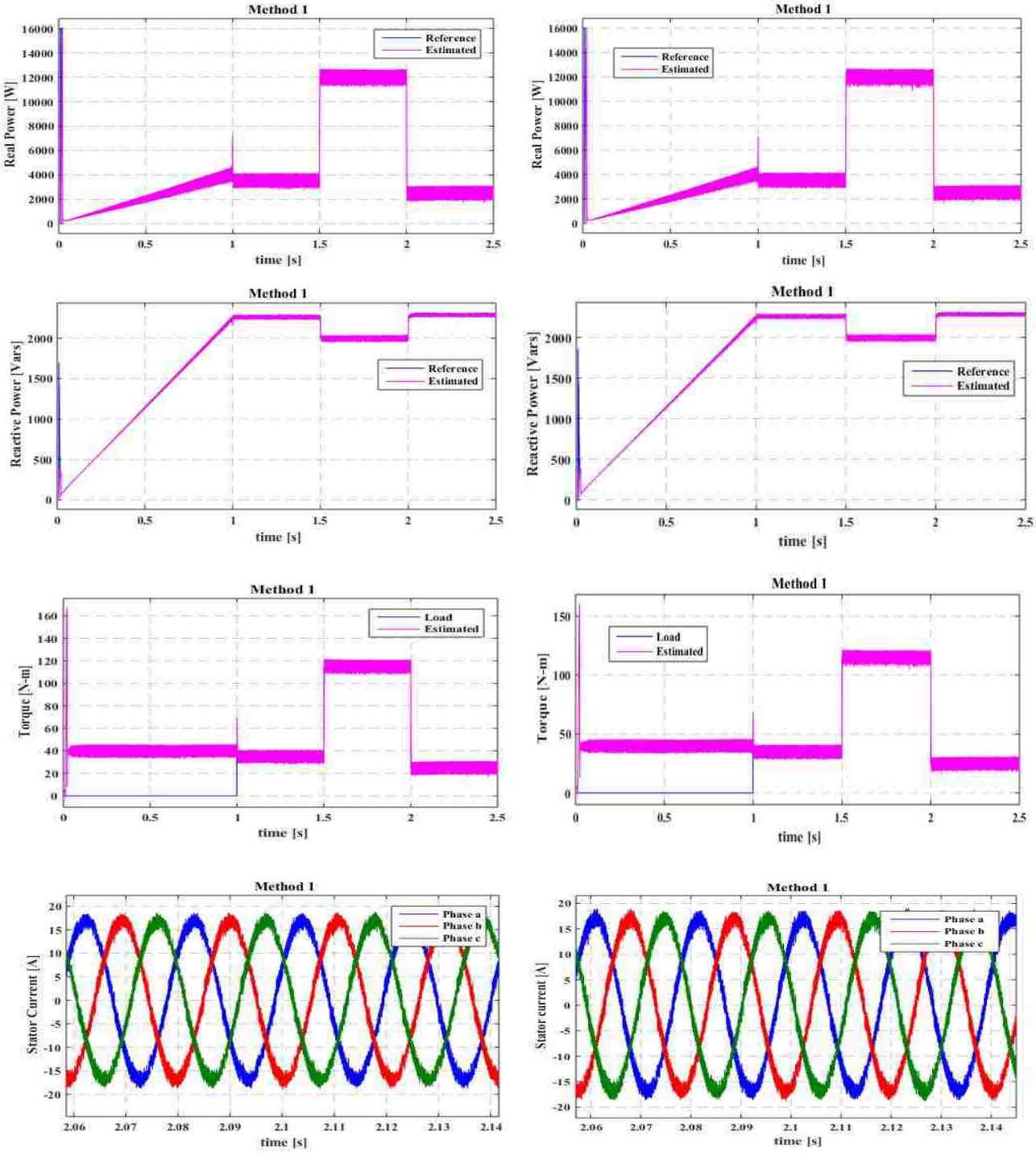

(a) **(b)**

Figure 5.18 Method 1, six-sector. (a) with accurate knowledge of stator resistance, (b) with erroneous knowledge of stator resistance.

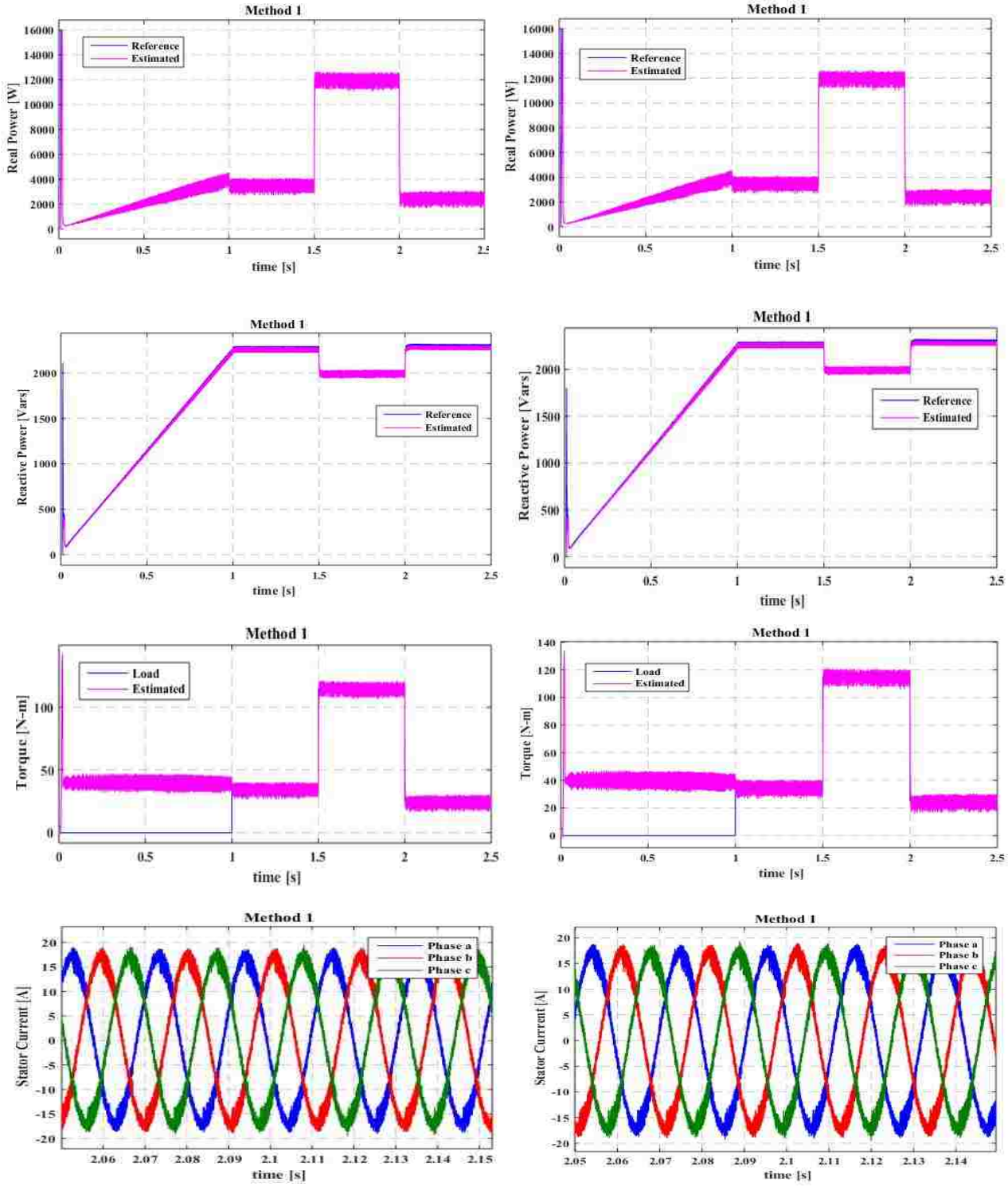

(a) **(b)**

Figure 5.19 Method 1, twelve-sector. (a) with accurate knowledge of stator resistance, (b) with erroneous knowledge of stator resistance.

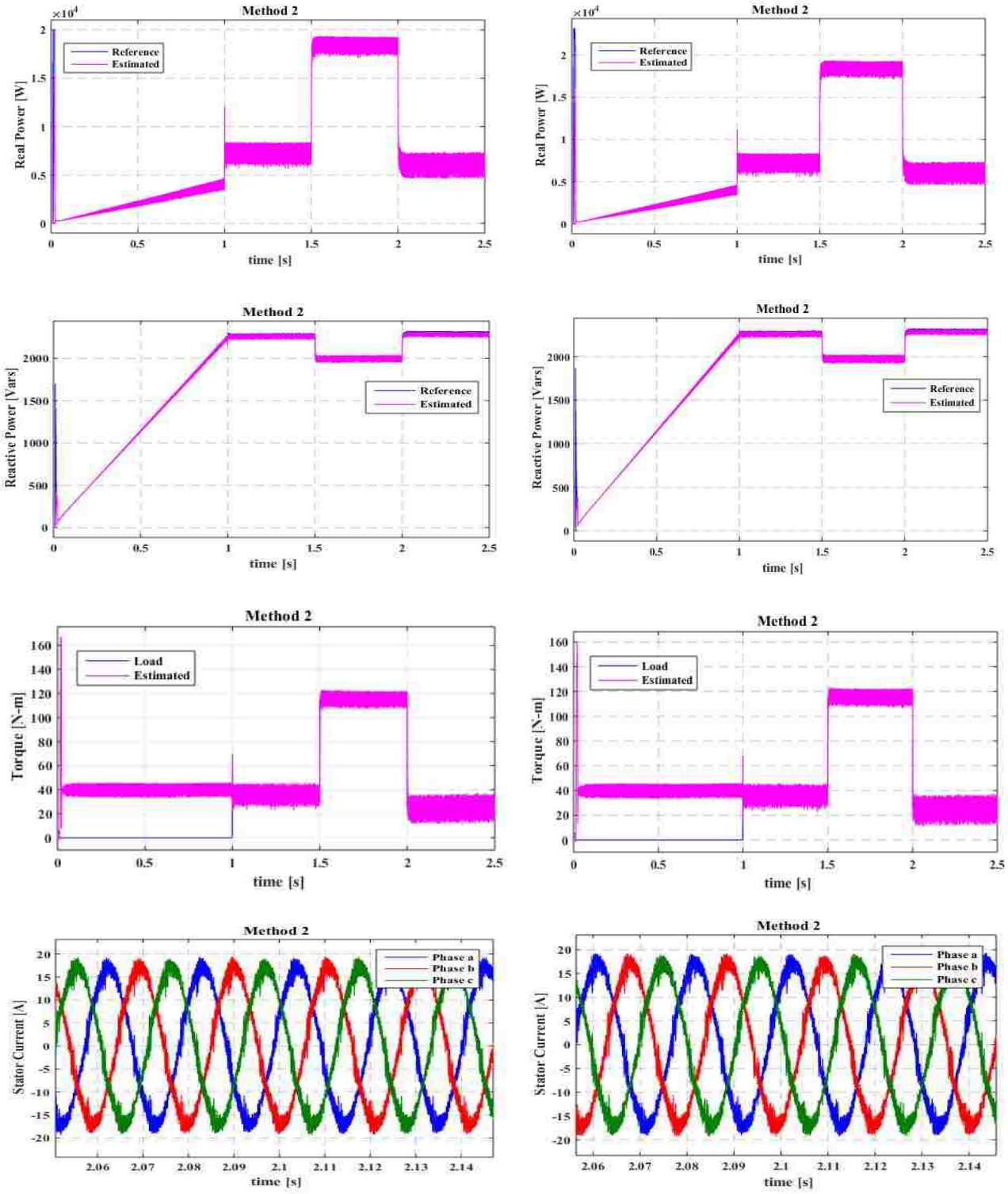

Figure 5.20 Method 2, six-sector. (a) with accurate knowledge of stator resistance, (b) with erroneous knowledge of stator resistance.

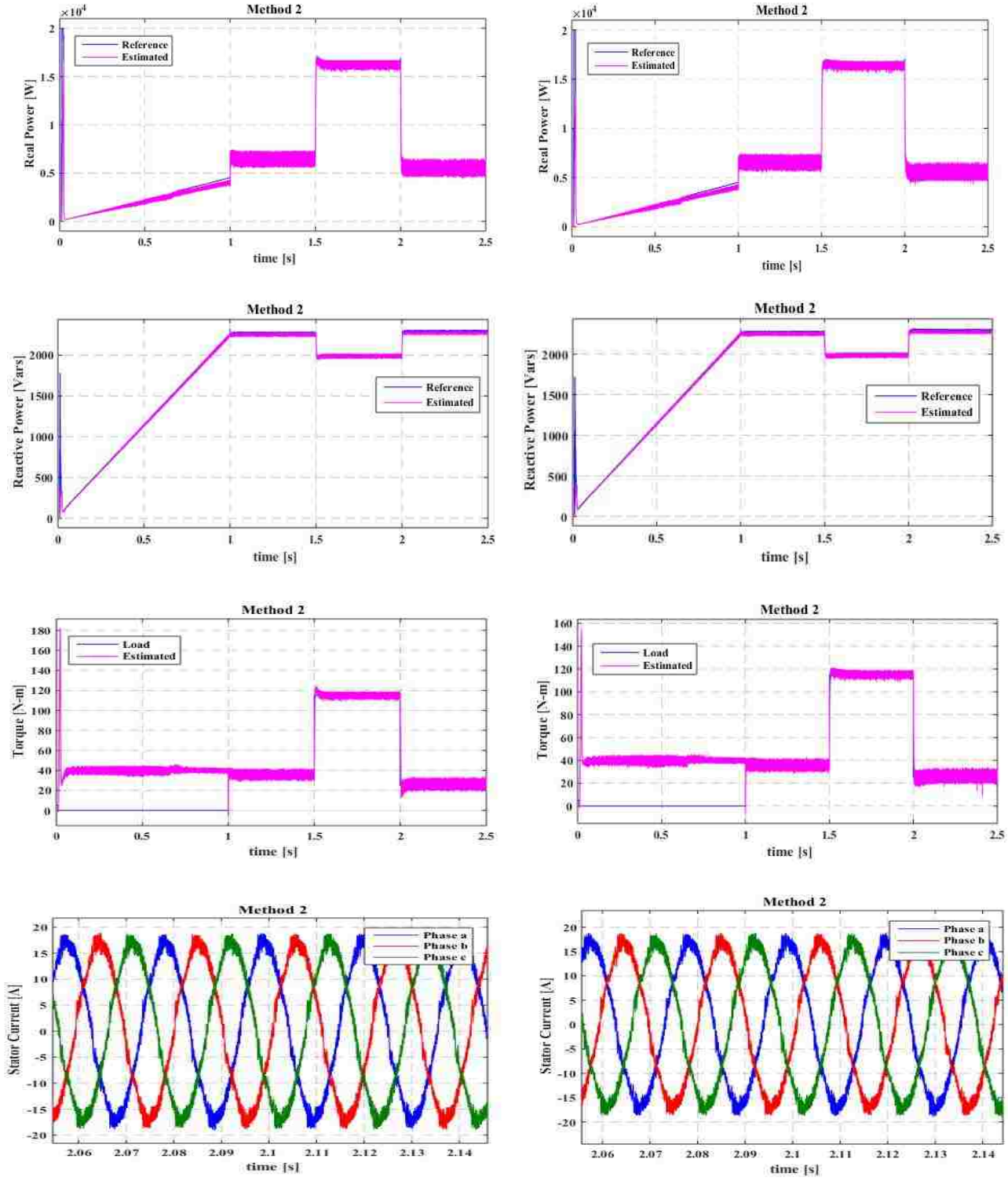

(a) **(b)**

Figure 5.21 Method 2, twelve-sector. (a) with accurate knowledge of stator resistance, (b) with erroneous knowledge of stator resistance.

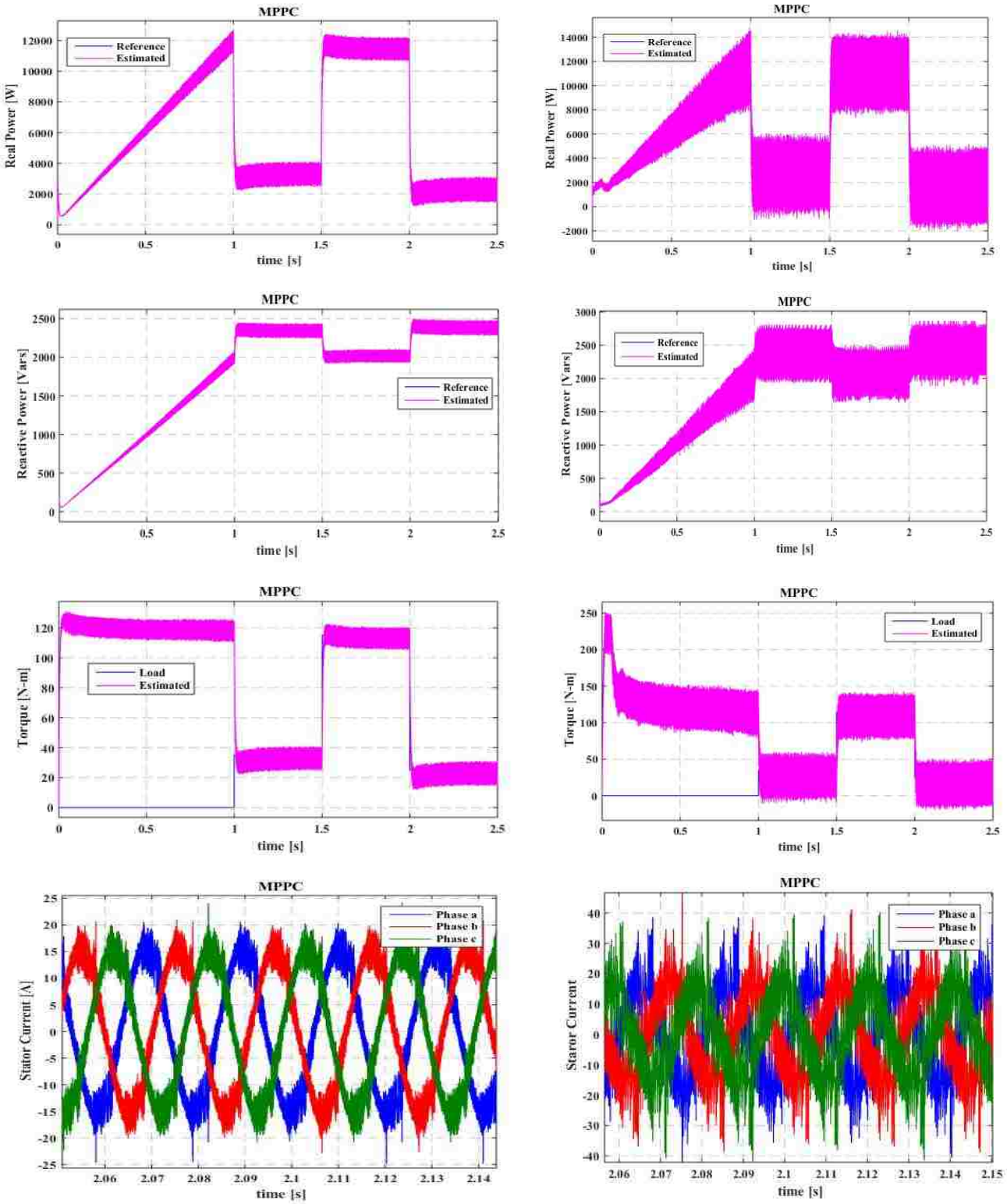

(a) **(b)**

Figure 5.22 MPPC. (a) with accurate knowledge of stator resistance, (b) with erroneous knowledge of stator resistance.

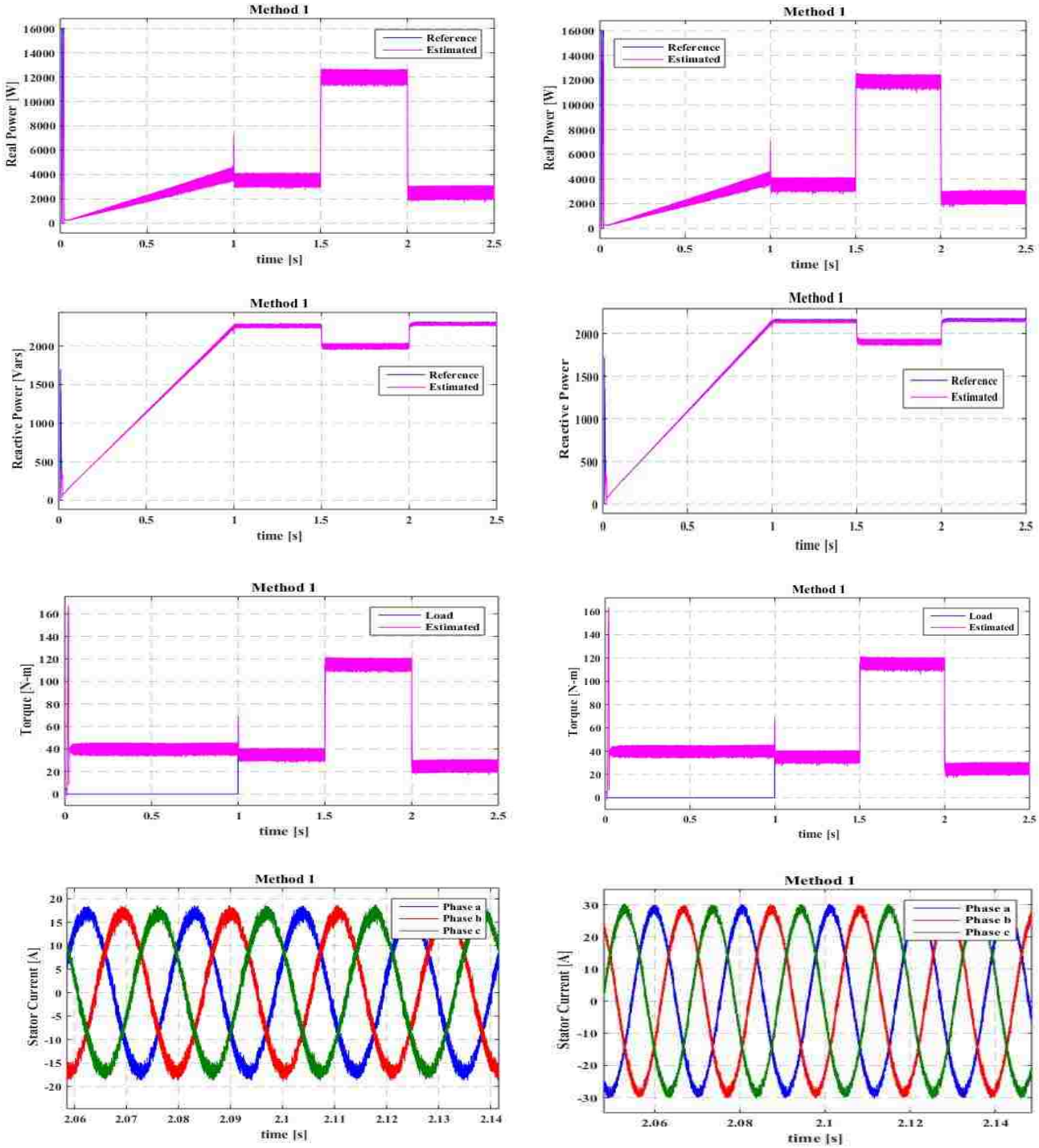

(a) **(b)**

Figure 5.23 Method 1, six-sector. (a) with accurate knowledge of magnetizing inductance, (b) with erroneous knowledge of magnetizing inductance.

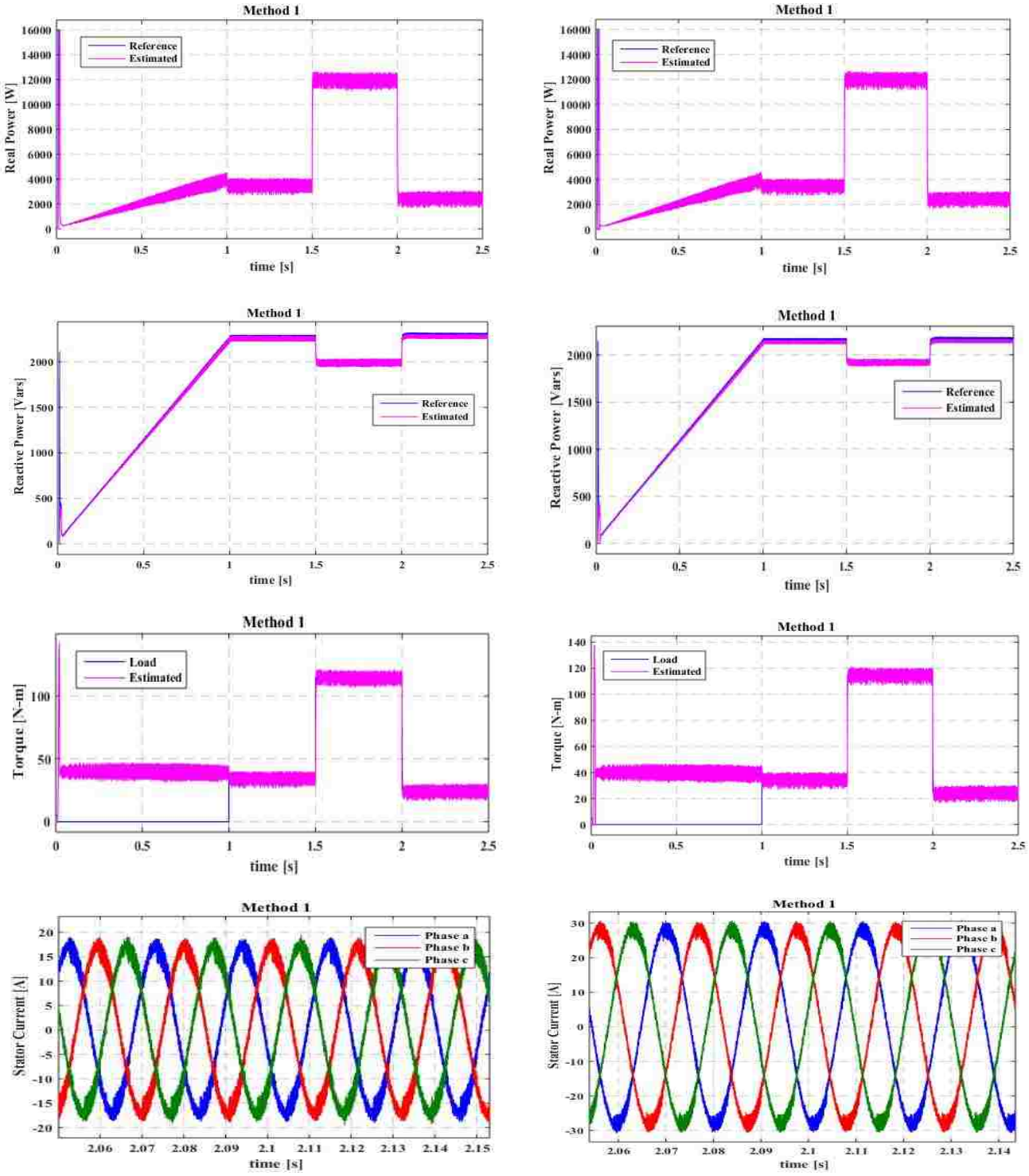

(a) **(b)**

Figure 5.24 Method 1, twelve-sector. (a) with accurate knowledge of magnetizing inductance, (b) with erroneous knowledge of magnetizing inductance.

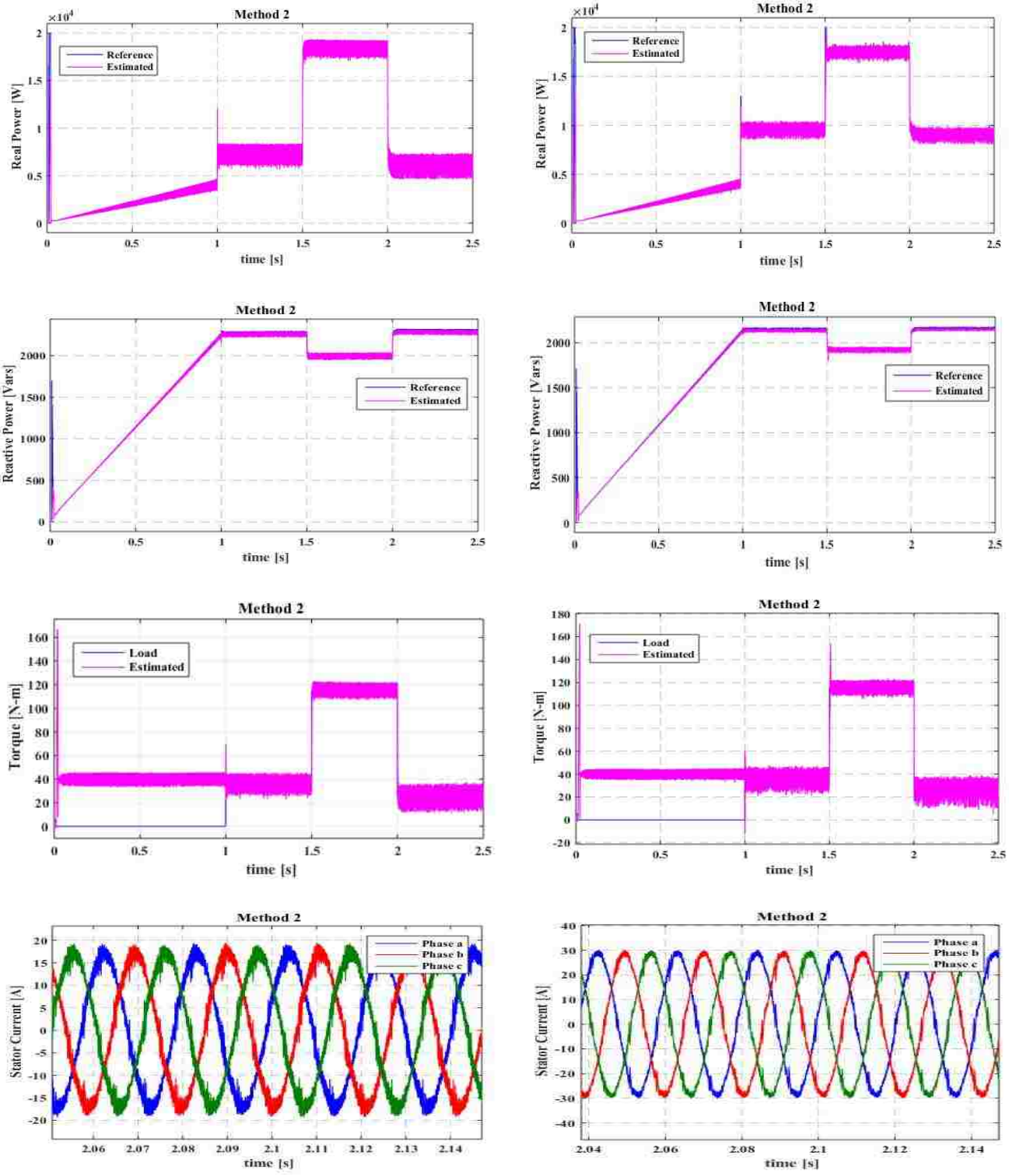

(a) **(b)**

Figure 5.25 Method 2, six-sector. (a) with accurate knowledge of magnetizing inductance, (b) with erroneous knowledge of magnetizing inductance.

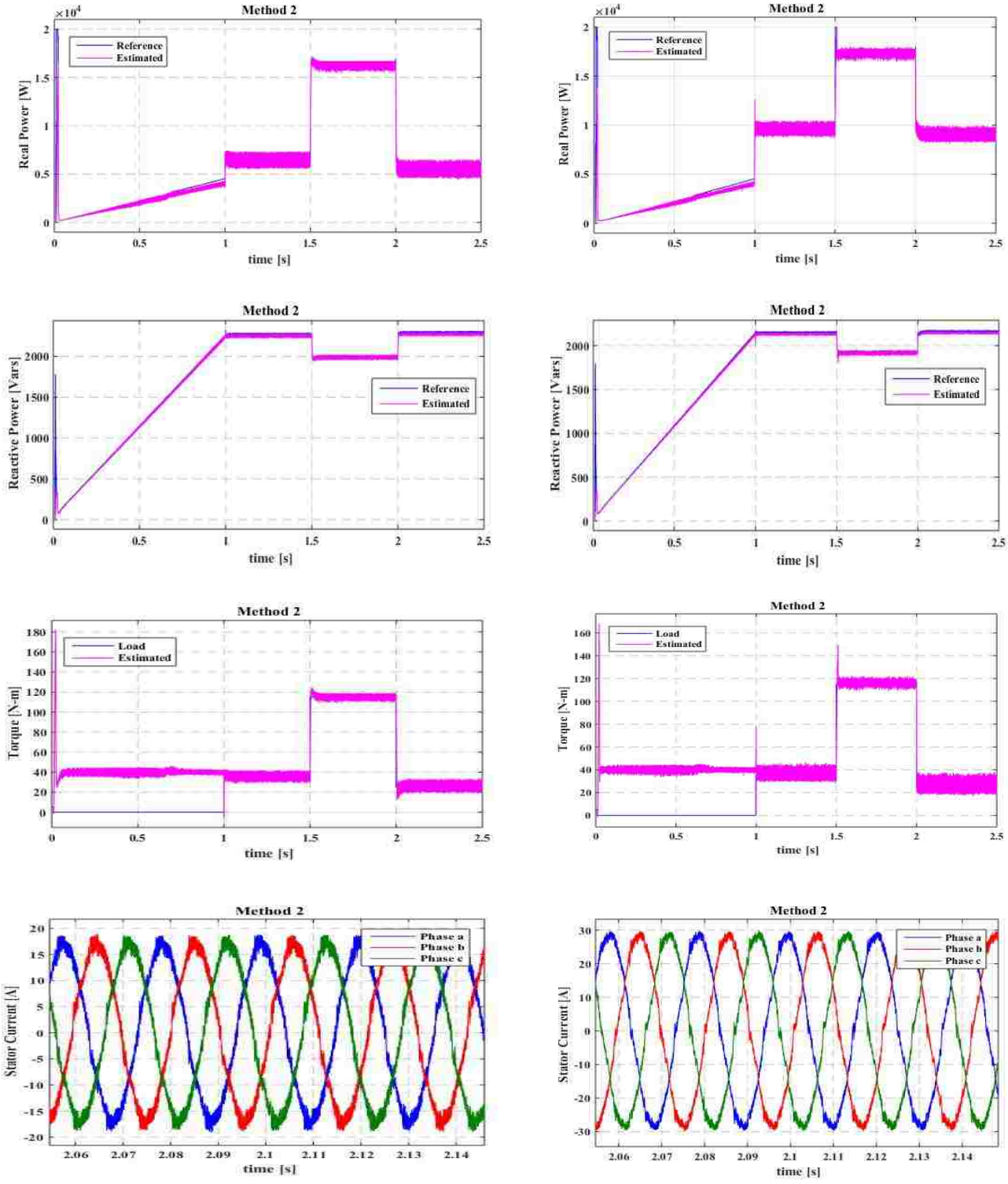

(a) **(b)**

Figure 5.26 Method 2, twelve-sector. (a) with accurate knowledge of magnetizing inductance, (b) with erroneous knowledge of magnetizing inductance.

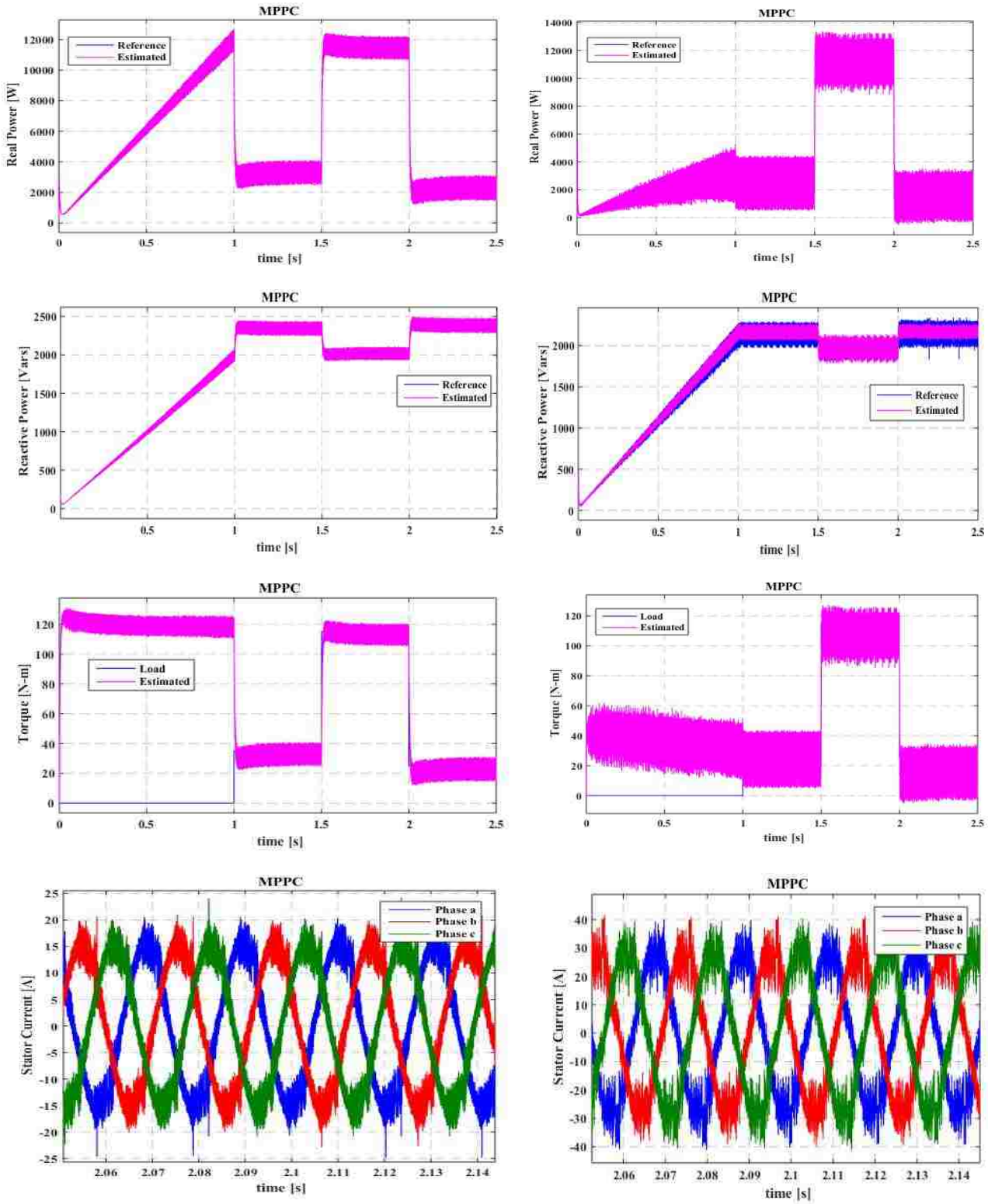

(a) **(b)**

Figure 5.27 MPPC. (a) with accurate knowledge of magnetizing inductance, (b) with erroneous knowledge of magnetizing inductance.

Comparing the obtained results in presence of parameter variations with the ones obtained with accurate knowledge of motor parameters, it can be concluded that the direct power control strategy provides the most robust response. This applies to both six-sector and twelve-sector versions with consumed real power calculated based on either of methods 1 or 2. It should be explained that, the difference between calculated real power and measured stator current is basically the reference torque that in turn is generated by the PI speed controller. Therefore, performance of the direct power control strategy is hardly affected when the machine parameters vary.

For MPPC, motor parameter variations has more significant effects on the responses. Fig 5.21(b) shows that the stator resistance variations results in increased real and reactive power as well as electromagnetic torque and stator current ripple. Furthermore, magnitude of real power and stator currents are increased. The most significant effect is noticed on the stator current quality, as the obtained current THD is very high. Examining the results in presence of inductance variations, shown in Fig 5.26(b), it can be concluded that, as in the case of stator resistance variations, high ripples in real and reactive power as well as the electromagnetic torque and stator current appear. Stator current quality deteriorates with erroneous inductance value. However, the degradation is not as severe as is with the stator resistance variations.

CHAPTER 6:
CONCLUSIONS AND FURTHER WORK

Two high-performance induction motor control strategies, which are based on the idea of controlling real and reactive power flow into/out of the machine, are presented. The proposed control strategies are conceptually similar to classical DTC and MPC strategies.

In the first method, i.e. direct power control, two approaches to calculate consumed real power are introduced. Selection of voltage space phasors to be applied to stator terminals of the machine is analyzed based on two alternatives: six-sector and twelve-sector.

In the second approach, i.e. model predictive power control, real power is mainly calculated using measured voltages and currents. This constitutes the mayor advantage of the second approach over the first one. This is due to the fact that only two quantities, i.e. stator flux and synchronous speed, are required to be stimated. Model predictive power control, showed to be very simple to implement, and flexible to include constrains without major complications.

An overcurrent limitation strategy is introduced to deal with high stator currents that appear during the motor start-up period.

A series of simulation studies are carried out to verify the effectiveness of the porposed methods in controlling the dynamic response of an induction motor with accurate and erroneus knowledge of motor parameters. Six-sector and twelve-sector direct power control provides robust response with low ripples in torque and stator current. However, performance of model predictive power control degrades in presence of motor parameter uncertainties and large ripples appear on stator currents. Overcurrent limitation strategy is embedded in both strategies, resulting in effective current limitation during motor start-up period

Following subjects are proposed for further studies

- Experimental verification of the proposed control strategies,
- Investigating influence of real and reactive power hysteresis bands on switching frequency, real and reactive power ripple, current distortion, and losses,
- Investigating performance of proposed control strategies at very low speeds, and.
- Investigating speed sensorless power control strategies

REFERENCES

[1] P. Krause, O. Wasynczuk, and S. Sudhoff. Analysis of Electric Machinery and Drive Systems. John Wiley and Sons. 2002.

[2] P. Vas. Sensorless Vector and Direct Torque Control. Oxford University Press. July 1998.

[3] D. Gerling. Electrical Machines: Mathematical Fundamentals of Machine Topologies. Springer. 2015.

[4] I. Boldea, L. N. Tutelea. Electric Machines: Steady State, Transients, and Design with MATLAB®. CRC Press. 2009

[5] D. A. Andrade, A. W. F. V. Silveira, P. B. Severino, and T. S. Tavares, "DSP Based Torque Estimation in Three-phase Cage Induction Motors", in Proc. IEEE International Electric Machines & Drives Conference (IEMDC), 2007, pp. 1726-1731.

[6] A. Hughes, B. Drury. Electric Motors and Drives: Fundamentals, Types and Applications. Newnes. 2013.

[7] J. Rodriguez, P. Cortes, R. Kennel, and M. P. Kazrnierkowsk, "Model Predictive Control – a Simple and Powerful Method to Control Power Converters," International Power Electronics and Motion Control Conference (IPEMC), pp. 41-49, 2009.

[8] A. Linder, R. Kennel, "Model Predictive Control for Electrical Drives", in proceedings of the 36th IEEE 2005 Power Electronics Specialists Conference, PESC '05, pp.1793 – 1799.

[9] H. Miranda, P. Cortes, J. I. Yuz, and J. Rodriguez, "Predictive torque control of induction machines based on state-space models," IEEE Trans. Ind. Electron., vol. 56, no. 6, pp. 1916–1924, Jun. 2009.

[10] J. Rodriguez, P. Cortes. Predictive Control of Power Converters and Electrical Drives. Wiley-IEEE Press.2012.

[11] R. E. Betz and B. J. Cook, "Instantaneous power control - an alternative to vector and direct torque control?," Industry Applications Con/, vol. 3, pp. 1640-1647, 2000.

[12] L. Xu and P. Cartwright, “Direct active and reactive power control of DFIG for wind energy generation,” IEEE Trans. Energy Convers., vol. 21, no. 3, pp. 750–758, Sep. 2007.

[13] Prabu, T., Sampathkumar, S., & Gunabalan, R. (2011). Advanced direct torque control of induction motor. In *International conference on process automation, control and computing* (pp. 1–6).

[14] Y. A. Chapuis, D. Roye, “Direct torque control and current limitation method in start up of an induction machine,” Seventh International Conference on power Electronics and Variable Speed Drives, 1998, pp. 451-455.

[15] H. Zhu, X. Sun, “Starting current limitation method of DTC controlled induction machine for EV,” ICEMS 2005, Vol1, pp. 836-838.

[16] A. Trzynadlowski. Control of Induction Motors. Academic Press. October 2000.

[17] M.P. Kazmierkowski, R. Krishnan, F. Blaabjerg, "Control in Power Electronics Selected Problems", Academic Press, 2002.

VITA

Juan Rafael Nunez Forestieri was born in 1980 in Guayaquil, Ecuador. He completed his Bachelor of Science in Electrical Engineering at Escuela Superior Politecnica del Litoral, Guayaquil, Ecuador in 2004. After graduation, he worked in the power industry where he held different engineering roles. In fall 2014 he enrolled as a graduate student in the School of Electrical and Computer Engineering at Louisiana State University, Baton Rouge, LA, where he is currently pursuing the Master's Degree. His current research interests include renewable energies, electric machines, electric drives and power systems.